Peptide functionalised gold nanorods for the selective eradication of target cells using photothermal therapy

Miché Desline Meyer

A thesis submitted in partial fulfilment of the requirements for the degree Magister Scientiae in the Department of Biotechnology, University of the Western Cape.

Supervisor: **Prof. Mervin Meyer**

2019

Abstract

Cancer is one of the leading causes of death, worldwide. Mortality tolls are estimated to reach approximately 13.1 million in 2030. These statistics suggest that current therapeutic strategies are not effective. This is partly due to the fact that the drugs used in the treatment of cancer lack selectivity and specificity, which lead to undesirable side effects and reduced drug efficacy. There is therefore a need for alternative therapeutic approaches. In view of this, the therapeutic goal of chemotherapy has shifted towards targeted drug delivery systems, which have been successfully demonstrated using nanotechnology. The nano-based drug delivery vehicles that specifically target diseased cells are appealing as they could reduce drug toxicity towards healthy tissues and be more effective at lower dosages.

The main aim of this study was to develop gold nanorods (AuNRs) capable of inducing cell death in cancer cells specifically. Selectivity of the AuNRs (denoted as AGK) for cancer cells was achieved by conjugating the AuNRs to a peptide (Adipose Homing Peptide or AHP) that has high affinity and specificity for a cell surface receptor (prohibitin or PHB) that is expressed on some cancer cells. Cell death was achieved through conjugating the AuNRs to a pro-apoptotic peptide, $_{D}(KLAKLAK)_2$. Spherical AuNPs (AuNSs) conjugated with AHP and $_{D}(KLAKLAK)_2$, capable of selectively inducing apoptosis in cancer cells that express PHB, was previously reported. However, in this study the AuNSs were replaced with AuNRs.

AuNRs has the ability to absorb light in the near infrared (NIR) light spectrum and converts this light energy into heat. This property of AuNRs has been used in several studies to demonstrate the application of AuNRs for the treatment of cancer using photothermal therapy (PTT). Consequently, the AuNRs described in this study can also be used for PTT. These AuNRs can induce cell death through the target specific delivery of the pro-apoptotic peptide $_{D}(KLAKLAK)_2$ as well as through PTT. The study showed that three human cancer cell lines (PC-3, Caco-2 and U-87) express PHB. The cytotoxicity testing of AGK AuNPs on PC-3 cells showed that these AuNRs could

induce apoptosis in these cells without exposure to a NIR light source. The study also shows that AuNRs conjugated with the targeting peptide only (denoted as AG) can induce cell death in Caco-2 through PTT. This study demonstrates the potential of the AuNRs described in this study for application in the targeted elimination of cancer cells through the selective induction of PTT and apoptosis.

Keywords

Nanotechnology

Nanomedicine

Cancer

Apoptosis

Selective killing

Bi-conjugation

Prohibitin

Target receptor

Photothermal therapy

Gold nanorods

Near Infrared Region

Declaration

I declare that "***Peptide functionalised gold nanorods for the selective eradication of target cells using photothermal therapy***" is my own work that has not been submitted for any degree or examination in any other university and that all the sources I have used or quoted have been indicated and acknowledged by complete references.

Miché Desline Meyer Date: **December 2018**

Signed.....

Acknowledgements

Lord, how amazing and gracious you have been to me. I cannot express my gratitude for all the blessings bestowed on me. Thank you for giving me the strength and courage to pursue my goals and providing me with the right people who stood by my side and walked this journey with me.

I would like to express my sincere gratitude to all the people and institutions that have made this project possible.

To my mother, Deborah Meyer, thank you for all the sacrifices you have made. You continuously encourage me to do my best and believe in me even when I doubt myself, which I tend to do much too often. To the rest of my closest family, Dimitri Meyer, Abigail Scheepers, Justin Scheepers, Lynthea Stuurman, Lucian Meyer, Jesse Scheepers, Jada Scheepers and Joel Scheepers, I am grateful for all your patience and support, you are my biggest fans and I hope I continue to make you proud. This achievement wouldn't be worth having if I didn't have anyone to share it with.

I will be forever grateful to be granted an amazing opportunity to work under the supervision of Prof Mervin Meyer. Your advice and guidance has taught me so much and your time invested in me has not gone unnoticed. Thank you for believing in me, your encouraging words, your patience and support.

Prof Abram Madiehe, Dr Nicole Sibuyi and Dr Mustafa Drah, you really are a God sent. Words are honestly not enough to express my gratitude. Thank you for your willingness to train me in any technique and trouble shoot any problem I have encountered. It has gotten me through some difficult phases of this work and I have become a better researcher through your mentorship.

A special thanks to Mr Riziki Martin, Miss Taahirah Boltman, Mr Ephraim Maphasa, Mr Mihlali Mlaza, Miss Lauren Swartz and the rest of my lab mates in the Apoptosis, NIC Biolabels groups and Biotechnology Department. You have all been so welcoming and helpful and your support and encouragement is highly appreciated.

To my friends, Mrs Meena Waggie, Miss Shevonne Jemanie, Mr Kyle Davids, Mrs Waseemah Geduld, Miss Danielle Dalton, Mrs Taskeen Simons, Mr Achmat Williams, Mrs Mishka Sedres Kalam, Miss Yo-Neal Bless and Mr Po-An Chen thank you for the laughs, the talks and the motivation. You have shared in my frustrations and my joy and your support is invaluable.

Lastly, thank you to the University of the Western Cape for giving me the opportunity to obtain my Master's degree at this institution. Additionally I would like to express my appreciation to the DST/ Mintek Nanotechnology Innovation Centre (NIC) and the National Research foundation (NRF) for funding this project.

Dedication

To my mother, who instilled in me the
virtues of perseverance and
commitment, and relentlessly
encouraged me to strive for excellence.

" Stay far from timid, only make moves when your heart's in it, and live the phrase 'Sky's the limit' " – Christopher Wallace

Conferences/workshops contributions and publications

Miché Desline Meyer, Nicole Sibuyi, Abram Madiehe, Amanda Skepu and Mervin Meyer. **"**Peptide functionalised gold nanoparticles for the selective induction of apoptosis in target cells" at the 7th NIC workshop, 25-26 January 2017 at the South African Medical Research Council (SA-MRC). **Poster presentation (2nd prize).**

Miché Desline Meyer, Nicole Sibuyi, Abram Madiehe, Amanda Skepu and Mervin Meyer. "Peptide functionalised nanoparticles for the selective induction of apoptosis in target cells" at the University of the Western Cape Science faculty research open day, 3rd August 2017. **Oral presentation.**

Miché Desline Meyer, Nicole Sibuyi, Abram Madiehe, Amanda Skepu and Mervin Meyer. "The selective eradication of target cells using peptide-conjugated gold nanorods and photothermal therapy" at the BioAfrica Convention, 27-29 August 2018 in Durban- South Africa. **Poster presentation**.

Miché Desline Meyer, Nicole Sibuyi, Abram Madiehe, Amanda Skepu and Mervin Meyer. "Peptide functionalised gold nanorods for the selective induction of apoptosis in target cells" at the International Conference On Nanomedicine And Nanobiotechnology – ICONAN, 26-28 September 2018 in Rome – Italy. **Poster presentation**.

Miché Desline Meyer, Nicole Sibuyi, Abram Madiehe, Amanda Skepu and Mervin Meyer. "Peptide functionalised gold nanorods for the selective eradication of cancer cells using photothermal therapy" at the 10th DST/Mintek NIC workshop, 14-16 October 2018 in Pretoria – South Africa. **Oral presentation**.

Sibuyi, N.R.S, Thovhogi, N., Gabuza, K.B., **Meyer, M.D**., Drah, M., Onani, M.O., Skepu, A., Madiehe, A.M. and Meyer, M. (2017). Peptide-functionalised nanoparticles for the selective induction of apoptosis in target cells. *Nanomedicine*, *12*(14), 1631-1645.

TABLE OF CONTENTS

List of abbreviations

~	Approximately
°C	Degree Celsius or degree centigrade
%	Percentage
λ_L	Longitudinal plasmon wavelength
λ_T	Transverse plasmon wavelength
ζ	Zeta
Ag	Silver
$AgNO_3$	Silver nitrate
AHNP	Anti-HER2/neu peptide
AHP	Adipose homing peptide
AIF	Apoptosis-inducing factor
Apaf-1	Apoptotic protease activating factor-1
ATCC	American Type Culture Collection
ATP	Adenosine triphosphate
Au	Gold
AuMBS	AuNRs in protein-shell microbubbles
AuNPs	Gold Nanoparticles
AuNRs	Gold Nanorods
AuNSs	Gold Nanospheres
AuNTs	Gold Nanostars
Bax	Bcl-2 associated protein-X
Bcl-2	B-cell lymphoma 2
Bcl-xL	B-cell lymphoma 2 extra large
BSA	Bovine Serum Albumin
C	Carbon
CAD	Carbamoyl-phosphate synthetase 2, aspartate transcarbamylase, and dihydroorotase
c-FLIP	cellular FLICE-inhibitory protein

Caspases	Cysteine aspartate-specific proteases
cm^2	Square centimetre
CO_2	Carbon dioxide
Cu	Copper
CW	Continuous wave
CTAB	Cetyl trimethylammonium bromide
DAB	3,3'-diaminobenzidine
DAPI	4’,6-diamidino-2-phenylindole
DCs	Dendritic cells
DEVD	Caspase 3 cleavage site
dH_2O	Distilled water
DISC	Death-inducing signal complex
DLL3	Delta-like protein 3
DMEM	Dulbecco’s modified Eagle’s medium
DMSO	Dimethyl sulfoxide
DNA	Deoxyribose nucleic Acid
EDX	Energy Dispersive X-ray Spectroscopy
EGF	Epidermal growth factor
EGFR	Epidermal Growth Factor Receptor
EPR	Enhanced permeability and retention
Fab	Antigen-binding fragment
FADD	Fas-associated protein with death domain
Fas/L/R	Apoptosis stimulating factor/Ligand/Receptor
FBS	Fetal Bovine serum
FCC	Face Centre Cubic
FDA	Food and Drug Administration
FRα	Folate receptor alpha
FTIR	Fourier-transform infrared spectroscopy
GNG	Gold nanogels
$HAuCl_4$	Gold (III) chloride trihydrate
HCl	Hydrochloric acid

HER 2	Human Epidermal growth factor Receptor 2
HNO_3	Nitric acid
HRP	Horseradish peroxidise
Hrs	Hours
HR-TEM	High Resolution-Transmission electron microscopy
IAPs	Inhibitor of apoptosis proteins
IC_{50}	Half maximal inhibitory concentration
ICC	Immunocytochemistry
ICP-OES	Inductively coupled plasma optical emission spectrometry
kDa	kilodalton
M	Molar
mAb	Monoclonal antibody
mg	Milligram
min	Minutes
ml	Millilitre
mm	Millimeter
mM	Millimolar
MOMP	Mitochondrial outer membrane permeabilization
mV	Milli Volts
$NaBH_4$	Sodium Borohydride
NaCl	Sodium Chloride
NCS	Neocarzinostatin
NIR	Near Infrared Region
nm	Nanometer
nM	Nano Molar
NPs	Nanoparticles
NSCLC	Non-Small Cell Lung Cancer
PAA	Poly (acrylic acid)
PAH	Poly (allyamine hydrochloride)
PBS	Phosphate buffered saline
PDGF	Platelet-derived Growth Factor

PEG	Polyethyl glycol
PFA	Paraformaldehyde
PHB	Prohibitin
PMLA	Pro-drug called poly (β-L malic acid)
PS	Phosphatidyl serine
PSMA	Prostate-Specific Membrane Antigen
PTT	Photothermal therapy
rhTNF	Recombinant human tumour necrosis factor
RIP	Receptor-interacting protein
RNA	Ribose Nucleic Acid
ROS	Reactive oxygen species
RPM	Revolutions per minute
RPMI-1640	Roswell Park Memorial Institute medium
ScFV	Single-chain variable fragments
SCLC	Small-Cell Lung Cancer
SELEX	Systemic Evolution of Ligands by Exponential enrichment
SEM	Scanning Electron Microscopy
Si	Silicon
siRNA	short interfering Ribose Nucleic Acid
SMA	styrene maleic acid copolymer
SMAC	Mitochondria-derived activator of caspases
SMANCS	NCS conjugated to SMA
SPR	Surface plasmon resonance
TCGA	The Cancer Genome Atlas
THPA	The Human Protein Atlas
TNF	Tumour Necrosis Factor
TRADD	Tumour necrosis factor receptor type 1-associated DEATH domain protein
Trail/R	TNF-related apoptosis-inducing ligand/ Receptor
µl	Microliter
UV-Vis	Ultraviolet visible

VEGF	Vascular endothelial growth factor
Vol.	Volume
WASF3	Wiskott-Aldrich syndrome protein Family member 3
WRC	WASF Regulatory Complex
WAT	White Adipose Tissue
WHO	World Health Organization
WST-1	Water-soluble tetrazolium-1

List of figures

List of tables

Chapter one: Literature review

1.1. Introduction

Cancer is the second most common cause of death globally, exceeded only by ischaemic heart disease (American Cancer Society, 2016). According to World Health Organization (WHO), annual cancer cases are expected to rise from 14 million in 2012 to 22 million within the next 20 years (World Health Organization, 2015) and surpass heart disease as the leading cause of death (Jemal *et al*., 2010). Cancer is a heterogeneous disease caused by both external and internal factors. External factors include infectious organisms, unhealthy diet, exposure to chemicals/radiation and tobacco. Internal factors include hormones, immune conditions and genetic mutations (İlem-Özdemir *et al*., 2015).

Although conventional cancer therapies such as radiation, chemotherapy, immunotherapy and surgery have improved patients' survival rate, mortality tolls are steadily escalating (Rivankar, 2014). The increased mortality can be largely attributed to drug non-specificity, resulting in inadequate targeting of the drugs to the tumour site as well as the resultant systemic side effects (Kumari *et al*., 2016). Further to non-specific biodistribution, conventional anticancer drugs often have poor solubility, (Le Garrec *et al*., 2004). Minimal interaction between the drug and the tumour is thus associated with reduced drug efficacy (Kumari *et al*., 2016 & Arranja *et al*., 2017). Additionally, cancer cells are known to proliferate autonomously and uncontrollably, due to multiple mutations and acquisition of multidrug resistance (Sioud and Mobergslien, 2012 & Sims *et al*., 2016). There is therefore an urgent need to develop improved cancer therapeutics that can be disease-specific with higher efficacy.

Nanotechnology-based systems were shown to have enhanced efficacy due to their ability to interact with diseased tissues at a cellular level with a great degree of specificity. These nanomedicines employ a strategy known as the enhanced permeability and retention (EPR) effect, which relies on porous vessels in the solid

tumours (Steichen *et al*., 2013). These nanomaterials can be used as vehicles to transport therapeutic payloads to disease sites. Nanoparticles can easily permeate and accumulate within the tumours via the EPR effect, leading to the sustained delivery of their therapeutic payloads (Yu *et al*., 2012 & Steichen *et al*., 2013). In this manner, toxicity could be limited to target cells, reducing side effects and immune response. This can significantly enhance the half-life of the therapy, mask the therapy from attack by phagocytes and reduce early drug clearance from the blood system. To develop the ideal nanotechnology-based cancer targeting system, an in-depth understanding of tumour pathophysiology, growth and mechanisms is required. Herein, prohibitin (PHB)-targeted nanorods are explored for their photothermal effect on cancer cells.

1.2. Cancer development

1.2.1. Tumour physiology

Cancer can be described as a multi-gene and multi-step disease that originates from a single cell with unrepaired DNA damage (Hanahan and Weinberg, 2011). In the lifecycle of normal cells, signals dictate whether a cell will continue to divide, differentiate or die (Hejmadi, 2010). In contrast, during the development of cancer, cells with altered DNA acquire a degree of autonomy from these signals resulting in failure to repair or destroy such cells (Hanahan and Weinberg, 2011). As shown in Figure 1.1, the abnormal cells multiply and grow uncontrollably by escaping physiological functions such as apoptotic signalling (Hejmadi, 2010). The tumour microenvironment also plays a role in cancer development and progression; it promotes tumour growth through angiogenesis, which is the process of new blood vessel formation to sustain the growth of new tissue (Gupta and Zhang, 2005). From this perspective the growth of a tumour is new tissue requiring new blood vessel formation. As the tumour increases in size it develops into a dense population of cells with a poor drainage system. The tumour microenvironment is biochemically

characterized by low levels of oxygen, low pH, and low glucose. Cancer cells are fast growing cells constantly requiring nutrients and oxygen in order to continue cell proliferation and gain metastatic potential (Rieger *et al*., 2016). Without new blood vessel formation, cancer cells will rely solely on diffusion of nutrients through the existing blood vessel network (Steichen *et al*., 2013). New blood vessel formation is therefore essential for the growth of the tumour.

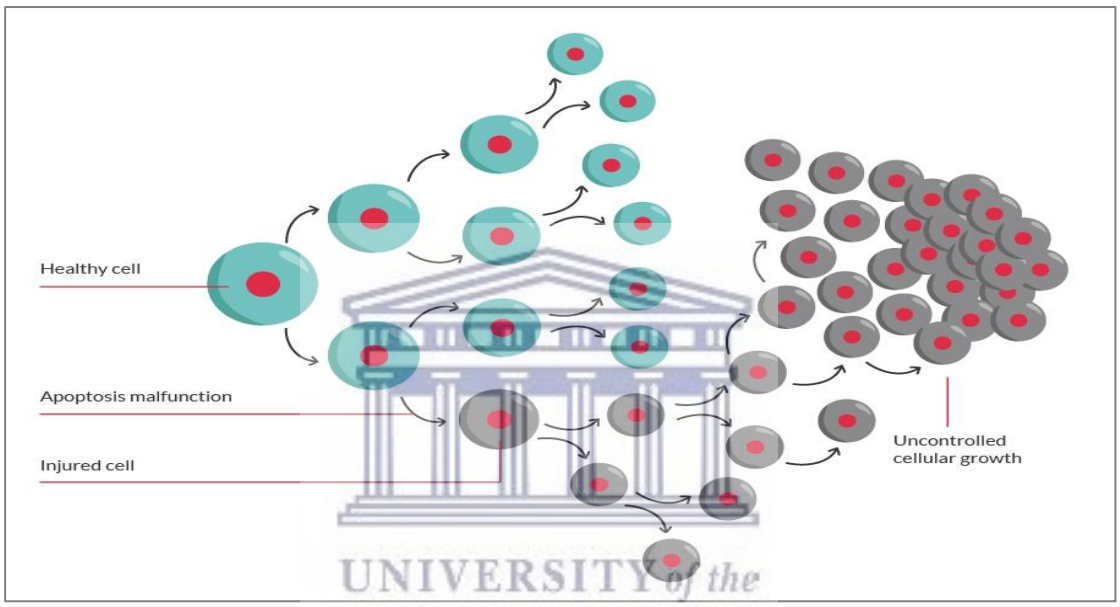

Figure 1.1: Tumour formation from a single cell. Failure to repair damaged DNA results in the malfunctioning of apoptosis. The abnormal cell grows and proliferates uncontrollably and undergoes successive rounds of mutation to form a tumour mass (www.thebraintumourcharity.org, 2016).

1.2.2. Tumour vasculature

Like most cellular mechanisms, angiogenesis is regulated by the stimulation and blocking of cellular signals in a series of discrete steps during tumour development as indicated in Figure 1.2. Once the process is initiated, growing vessels produce a vasculature that is aberrant and unorganized (Haley and Frenkel, 2008). As a result, there are regions within the tumour that have high blood supply due to the presence of an extensive vasculature, while other regions, which are usually at the centre of a tumour mass, have low blood supply with poor vasculature (Byrne *et al*., 2008 & Danhier *et al*., 2010). Consequently, the delivery of anti-cancer drugs through the

blood stream is not effectively delivered to the centre of the tumour (Betof *et al*., 2015). Cancer cells proliferate much quicker than normal cells, resulting in abnormal basement membranes and incomplete endothelial linings and subsequently, leaky blood vessels (Haley and Frenkel, 2008 & Reiger *et al*., 2016). This gives rise to the EPR effect, which is a phenomenon exploited for delivery of conventional anti-cancer drugs (Steichen *et al*., 2013). It is speculated that the EPR effect facilitates the faster growth rate of cancer cells by allowing the passing of larger macromolecules such as bradykinin, nitric oxide / peroxynitrite, prostaglandins, vascular endothelial growth factor (VEGF), tumor necrosis factor (TNF) and others from the blood stream to the surrounding tumour tissue. It is also speculated that this promotes the delivery of anti-cancer drugs to the tumour since the drugs accumulate much faster in the tumour tissue compared to the normal tissues, which do not receive blood supply from leaky vessels.

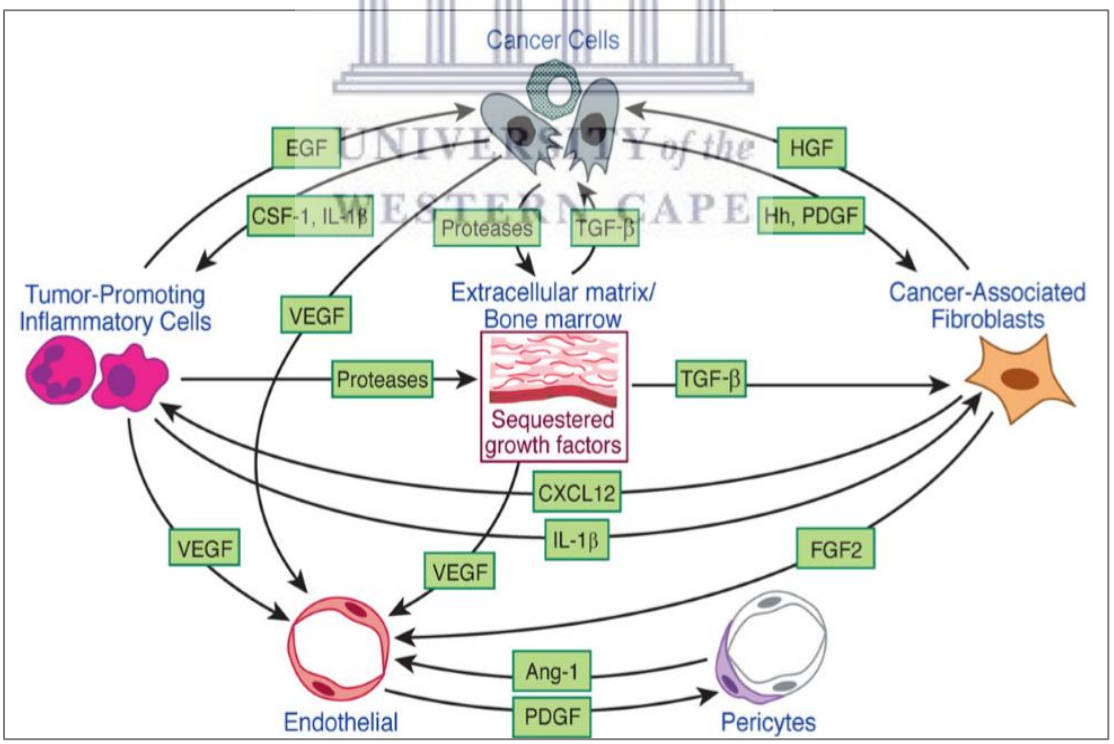

Figure 1.2: Signalling interactions during tumour growth. The tumour microenvironment is regulated by several signals of which only a few are illustrated. During angiogenesis tumour cells release factors such as VEGF which are pro-angiogenic. These factors then bind to and activate receptors present on existing blood vessels. Activated endothelial cells subsequently divide and migrate towards the tumour. A new basement membrane is formed by endothelial cells, which secrete growth factors such as Platelet-derived Growth Factor (PDGF) which stabilizes the new vessels by attracting pericytes. These pericytes form incomplete endothelial linings resulting in leaky vessels (Hanahan and Weinberg, 2011).

1.3. Current cancer therapies and their limitations

Conventional cancer therapies include surgery, radiation, chemotherapy and immunotherapy. The course of treatment depends on the type of cancer, its location, and its state of advancement (Arranja *et al*., 2017). Surgery is one of the oldest forms of cancer therapy. It is, however, only feasible if the tumour is benign and has not metastasized (Durante and Loeffler, 2010). Furthermore, this form of therapy is relatively costly and more invasive and in many cases, the cancer can return.

Radiation makes use of gamma rays, X-rays, or neutrons targeted directly to the tumour, causing the endothelial cells to swell and die (Li *et al*., 2003). Radiation is more harmful to cancerous cells than normal cells as they are unstable due to a faulty cellular repair mechanism and thus, more vulnerable to the damaging radiations (Mandal, 2013). At the beginning of the 20th century, shortly after the initial use of radiation, it was discovered that radiation could cause cancer as well as cure it due to the lack of selectivity towards cancer cells (Mandal, 2013). Martin *et al.* (2014) reported that the rapid breakdown of a tumour could cause a flood of cancerous cells to enter the lymphatic flow and form tumours in healthy organs, a possible mechanism of the formation of therapy-related metastasis. However, in patients with inoperable tumours, radiation therapy is one of the only options (Durante and Loeffler, 2010).

Early in the 20th century, only tumours that were small and localized enough to be completely removed by surgery were curable. Radiation was used after surgery to control residual small tumour growth, this was often followed by chemotherapy to destroy small tumour growths that had spread beyond the reach of the surgeon and radiotherapist (Arranja *et al*., 2017). A number of chemotherapeutic agents that are clinically used for cancer treatment are listed in Table 1.1, and these include anticancer drugs like Adriamycin, Paraplatin, Taxol etc. that are used to destroy cancer cells by inhibiting their cell division (Mandal, 2013 & Mauer *et al*., 2015). Nevertheless, chemotherapeutics have a short half-life, exert adverse side effects such as bone-marrow suppression, neuropathy, cardiotoxicity, hair loss and nausea;

have restricted drug dosage and cause systematic toxicities and multidrug resistance (Massey *et al*., 2014; Truong *et al*., 2014 & Arranja *et al*., 2017). Due to the non-specificity of conventional therapies, tumour cells can continue their uncontrolled proliferation with consequent tumour recurrence and poor prognosis. In view of this, the therapeutic goal has shifted towards selective or targeted eradication of cancer cells whilst preserving healthy cells by using targeted drug delivery systems. In order to design such targeted delivery systems, drugs are incorporated into nanocarrier systems. These systems are developed using nanotechnology (this will be discussed further in Section 1.8) which enable the design of multimodal systems that act as drug carriers, while simultaneously direct the delivery of the drugs to the tumour site. These delivery systems also have other advantages, most notably, increase of the circulation times of drugs (Kim *et al.,* 2010; Chung *et al.,* 2014 & Heinrich *et al.,* 2016).

Table 1.1: Conventional intravenously administered drugs and their side effects.

Chemotherapeutic agent	Cancer type	Possible short-term side effect
Doxorubicin (Adriamycin)	Breast cancer, lymphoma, and multiple myeloma	Decrease in blood cell counts, mouth ulcers, hair loss (reversible), nausea and vomiting, and heart damage
Carboplatin (Paraplatin)	Ovarian, head and neck, and lungs	Decrease in blood cell counts, hair loss (reversible), confusion, nausea, vomiting, diarrhoea
Cisplatin (Platinol, Platinol-AQ)	Bladder, Ovarian, and Testicular	Decrease in blood cell counts, allergic reaction, including a rash and/or laboured breathing, nausea and vomiting that usually occurs for 24 hours or longer, ringing in ears and hearing loss, fluctuations in blood electrolytes, and kidney damage
Fluorouracil (5-FU)	Colon, breast, stomach, and head and neck	Decrease in blood cell counts, diarrhoea, mouth ulcers, photosensitivity, and dry skin.
Paclitaxel (Taxol)	Breast, ovarian, and lung	Decrease in blood cell counts, allergic reaction, nausea and vomiting, loss of appetite, change in taste, thin or brittle hair, joint pain (short term), and numbness or tingling in fingers/toes

(Adapted from Khan *et al*., 2014)

1.4. Targeted drug delivery systems for cancer treatment

For the effective elimination of tumours, three essential dynamics should be considered: enhanced selectivity towards the target; capability of bypassing biological barriers; as well as selectively killing cancerous cells once it reaches the target (Cho *et al*., 2008). There are two modes of action that can be used for targeted drug delivery, passive and active targeting as depicted in Figure 1.3.

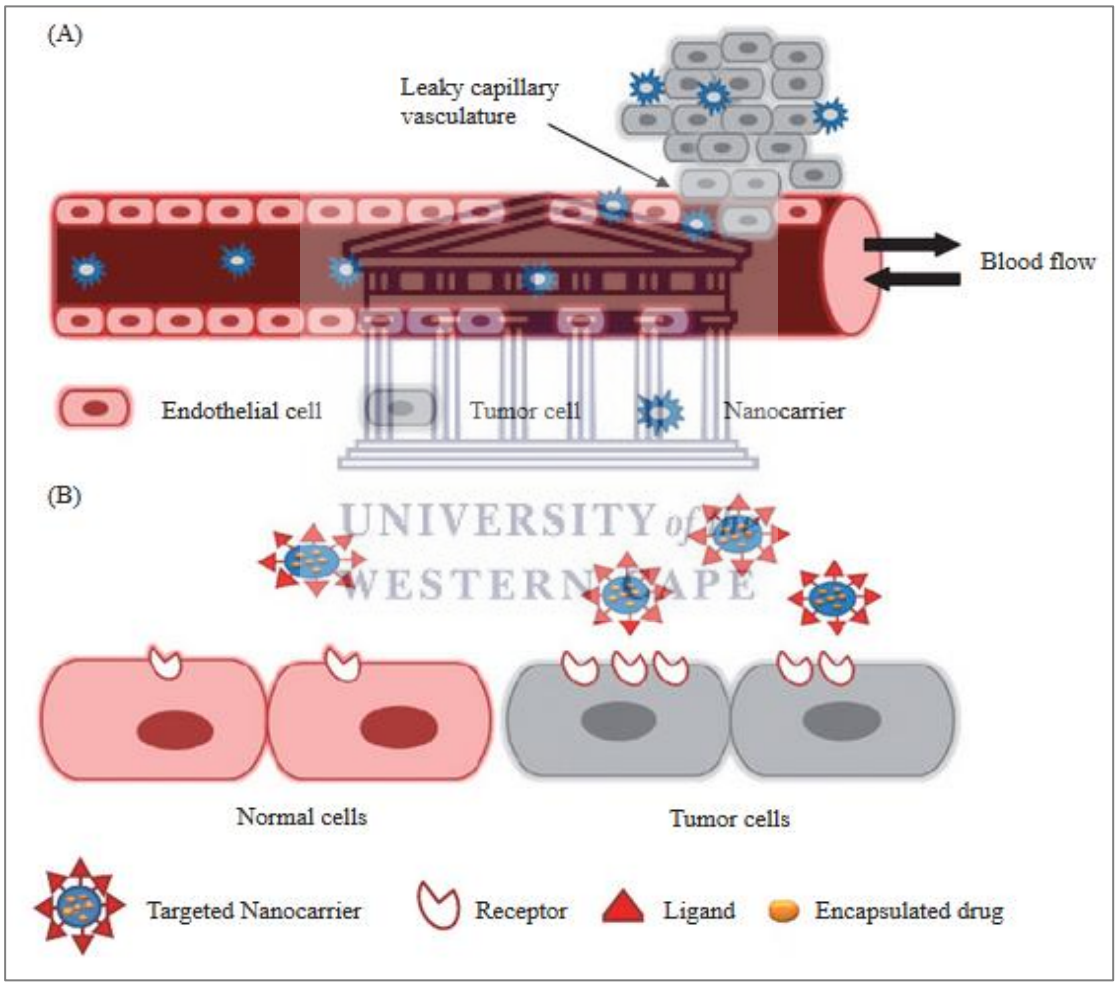

Figure 1.3: Schematic of targeting drug delivery utilizing nanocarriers. (A) Passive targeting that shows the delivery of a nanocarrier containing an encapsulated drug to the tumour site. (B) Active targeting, which makes use of ligands attached to the nanocarrier which binds directly to receptors that are over expressed on tumour cells regardless of leaky vasculature (Kumari *et al*., 2016).

1.4.1. Passive targeting

Passive targeting is the preferential accumulation of anti-cancer drugs at tumour sites and is dependent on the pathophysiology of the tumour mass as a whole and the uniqueness of the tumour microenvironment (Srinivasan *et al*., 2015). The vasculature of tumours consists of leaky blood vessels, which supplies the growing mass of cells with nutrients and oxygen (de Barros *et al*., 2012). Due to decreased lymphatic drainage, the vessels become permeable to anti-cancer drugs and prevent them from leaving the tumour mass (EPR effect), resulting in elevated levels of intra-tumour drug concentration and enhanced tumour cytotoxicity (Matsumura and Maeda, 1986 & Maeda *et al.*, 2000). Neocarzinostatin (NCS) was the first anticancer protein to be conjugated to a polymer (styrene maleic acid copolymer SMA) to form a nanocarrier therapeutic, named SMANCS (Matsumura and Maeda, 1986). SMANCS had a longer circulation time than NCS. Later other anticancer drugs, which showed selective tumour accumulation in mice xenograft models were also developed (Kim *et al*., 2010; Chung *et al*., 2014 & Heinrich *et al*., 2016). Their circulating half-life ranged from hours to days in humans depending on the delivery system. The drug with the longest circulation half-life in humans (~300hrs) was shown to be dextran–camptothecin and has also been shown to be less cytotoxic than the "free camptothecin drug" used in clinical phase II trials (Soepenberg *et al*., 2005).

Although passive targeting appears efficient, specificity remains a challenge, as indicated by the delivery of the drug doxorubicin. The antineoplastic drug, doxorubicin is one of the first drugs that have been encapsulated into a nanocarrier. This led to the development of liposomal doxorubicin or Doxil, which makes use of the EPR effect to deliver doxorubicin to tumour tissues (Barenholz, 2012). Although Doxil has an extended circulation time and reduced cardiotoxicity when compared to free doxorubicin, increased toxicity was observed in other organs such as the skin and there was also no difference between Doxil and free doxorubicin in the amount of drug accumulation in the tumour tissue (Danhier, 2016). This suggests that the use of the EPR effect may not be a beneficial approach in all tumour types since the degree of cell membrane penetrability differs between tumour types and stage (Lammers *et*

al., 2007 & Hansen *et al*., 2015). To overcome this limitation, the use of targeting ligands as an alternative has been studied.

1.4.2. Active targeting

Active targeting makes use of agents that i) specifically recognize and target receptors that are (over-) expressed on cancer cells (transferrin, folate, Epidermal Growth Factor Receptor (EGFR) or Glycoprotein receptors) [Arranja *et al*., 2017] and/or ii) target the endothelial cells of tumour vasculature (VEGF, integrins or matrix metalloproteases) [Danhier, 2016]. Molecules or targeting moieties used to specifically bind to these receptors include antibodies (Davis *et al*., 2010), aptamers (Hrkach *et al*., 2012), small molecules such as folic acid (Park *et al*., 2016) and peptides (Aina *et al*., 2005). The targeting moieties selectively bind to tumour-specific antigens and then trigger receptor-mediated endocytosis for controlled release of payloads to the target cells (Ashley *et al*., 2011 & Lu *et al*., 2011). The drugs can diffuse from target sites and kill neighbouring tumour-associated cells (Chi *et al*., 2017). These targeting systems show an increase in drug efficacy compared to passive targeting systems due to an improved target cell recognition and uptake rather than passive tumour accumulation (Lammers *et al*., 2012 & Danhier, 2016). As shown in Figure 1.4 active targeting can be achieved by using molecules such as antibodies, aptamers as well as ligands, which is discussed below.

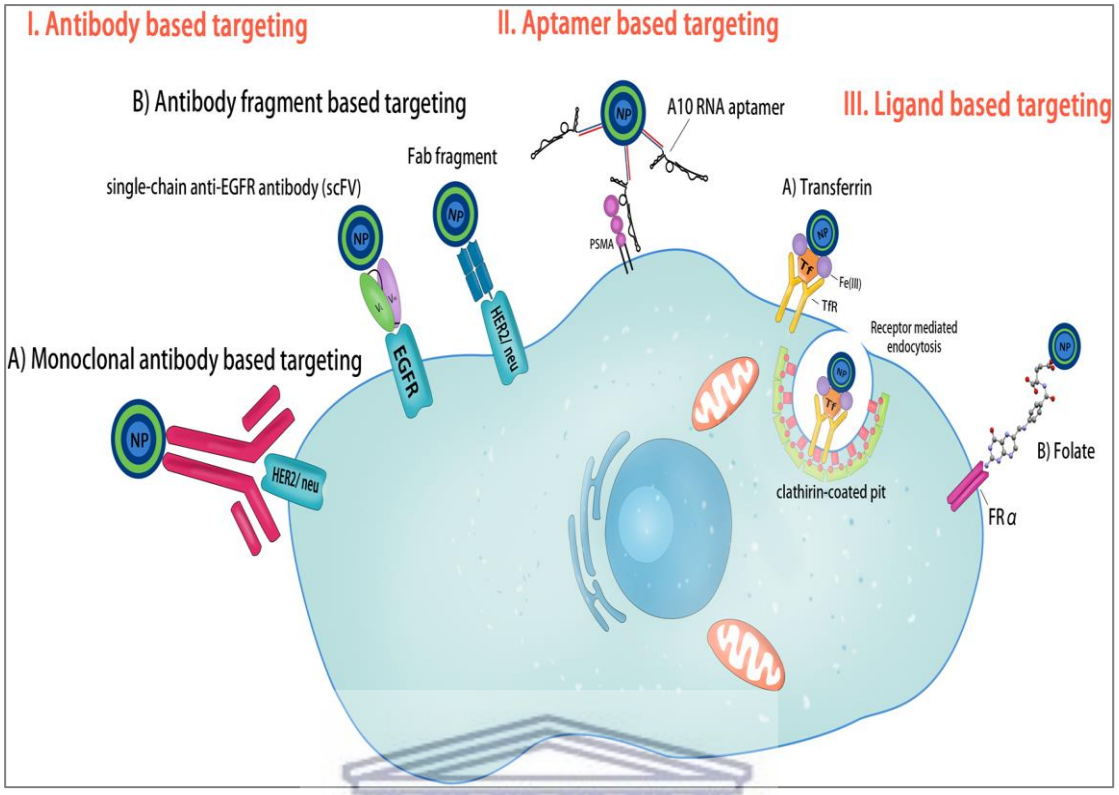

Figure 1.4: Schematic showing methods used for active targeting of cancer cells. I) Antibody-based targeting, which involves the use of **(A)** monoclonal antibodies such as anti-Her2/neu antibody directed toward Her2/neu receptors on the target cell membrane and **(B)** antibody fragments: single-chain variable fragments (scFV) such as single-chain anti-epidermal growth factor receptor (EGFR) antibody directed toward EGFR, or antigen-binding fragment (Fab) such as anti-Her2/neu Fab. **II)** Aptamer-based targeting such as the A10 RNA aptamer directed toward prostate-specific membrane antigen (PSMA) on the surface of the target cells. **III)** Ligand-based targeting such as **(A)** transferrin-based targeting of nanoparticles toward transferrin receptors and **(B)** folate-based targeting using folic acid to target folate receptor alpha (FRα), which is upregulated on the surface of neoplastic cells (Bazak *et al*., 2015).

1.4.2.1. Antibodies as cancer targeting agents

As targeting agents, antibodies have high selectivity and binding affinity by virtue of the presence of two epitope binding sites in a single molecule (Yu *et al*., 2012). The first monoclonal antibody (mAb) able to specifically bind to tumour antigens was developed in 1975 (Köhler and Milstein, 1975), but the potential role of mAbs in cancer treatment was not explored until nearly two decades later (Béduneau *et al*., 2007). The murine mAb Muromonab CD3 (OrthoClone OKT3®) was the first mAb to be approved by the FDA for clinical application (Thistlethwaite *et al*., 1984). Various cancers up regulate proteins such as surface antigens, including fetoprotein, human carcinoembryonic antigen, and human chorionic gonadotropin antigen, as well as

non-surface biomarkers which provide targets for mAb mediated targeting (Sultana *et al*., 2013).

Human Epidermal growth factor Receptor 2 (HER2) cell surface receptor is overexpressed or mutated in a variety of solid tumours including breast (Wolff *et al*., 2013), gastric (Liang *et al*., 2014), lung (Mazieres *et al*., 2013) and ovarian cancers (Cai *et al*., 2015). Treatment with trastuzumab, a humanized mouse mAb directed against HER2, has become the standard of care for HER2-overexpressing breast cancer (Hudis, 2007) and metastatic gastric cancer (Bang *et al*., 2010). The versatility and effectiveness of using mAb as a targeting moiety and therapeutic was demonstrated by delivering short interfering RNA (siRNA) to a solid tumour xenograft model of ovarian cancer using trastuzumab (Palanca-Wessels *et al*., 2016). Independent preclinical investigations and early phase clinical trials have shown the utility of mAb to deliver siRNA for the suppression of genes critical for tumour growth or resistance to chemotherapy (Davis *et al*., 2010 & Tabernero *et al*., 2013). These studies demonstrated the successful *in vitro* and *in vivo* mAb-targeted delivery of siRNA to HER2-overexpressing cancer cells with cleavage of target mRNA verified as the mechanism of gene suppression (Palanca-Wessels *et al*., 2016).

Another novel putative therapeutic target is Delta-like protein 3 (DLL3) which play a role in high-grade neuroendocine carcinomas including Small-Cell Lung Cancer (SCLC) (Saunders *et al*., 2015 & Rudin *et al*., 2017). DLL3 is thought to inhibit the Notch receptor, which is a tumour suppressor (Chapman *et al*., 2010). A first-in-human, open-label, phase I study was conducted to deliver Rovalpituzumab tesirine, a DLL3-targeted antibody-drug conjugate, and investigate the safety, tolerability, pharmacokinetics, and anti-tumour activity of rovalpituzumab tesirine in patients with SCLC or large-cell neuroendocrine tumours (Rudin *et al*., 2017). The study demonstrated encouraging anti-tumour activity with a manageable safety profile, suggesting that DLL3 is a clinically relevant, novel target for SCLC and that rovalpituzumab tesirine mAb-drug conjugate is selective for DLL3-positive SCLC (Rudin *et al*., 2017). Currently, there are several FDA approved mAb therapies with 74

approvals achieved between 19 January 2016 and 1 December 2017 alone (Food and Drug Administration, 2017). Hundreds more are undergoing clinical trials.

1.4.2.2. Aptamers as cancer targeting agents

In oncology, another field that is rapidly expanding is the use of aptamers as targeting agents. Aptamers are short single-stranded DNA or RNA oligonucleotides that are folded into secondary and tertiary three-dimensional structures enabling specific binding to biological targets (Nichols and Bae, 2014). More than 900 aptamers have been generated from an iterative *in vitro* selective process called "systemic evolution of ligands by exponential enrichment" (SELEX), towards a wide range of targets such as inorganic ions, small organic ligands, amino-acids, nucleotides and derivatives, oligonucleotides, antibiotics, peptides, proteins, sugars, parasites, virus, cells and tissues (Lao *et al*., 2015). Aptamers are considered equivalent to mAbs based on their high sensitivity and specificity as targeting agents (Ni *et al*., 2011). Aptamers however, possess several advantages over mAbs such as their simple production methods, low production cost (Zhang *et al*., 2011) and they are more stable as they are resistant to bio–degradation due to resistance to physical and environmental stressors such as heat, pH and organic solvents (Lee *et al*., 2010). They can be transported at ambient temperatures and remain stable during long-term storage (Talekar *et al*., 2011), exhibit slow degradation kinetics and can be denatured and renatured multiple times without significant loss of activity (Liss *et al*., 2002). Unlike mAbs they lack immunogenicity/toxicity (Zhang *et al*., 2011); and due to their small molecular weight (~10 -30 Da) they can penetrate tissues faster and more efficiently than a 150 kDa mAbs (Xiang *et al*., 2015).

Farokhzad *et al.* (2004) first reported the use of the A10 RNA aptamers, which recognizes the extracellular domain of the Prostate-Specific Membrane Antigen (PSMA) for targeted drug delivery of nanoparticle/aptamer bioconjugates. In a follow up study, the authors showed that docetaxel encapsulated nanoparticles functionalised with the PSMA targeted RNA aptamer had significantly enhanced *in vitro* cytotoxicity compared to non-targeted nanoparticles (Farokhzad *et al*., 2006). In

a similar fashion, the PSMA aptamer-conjugated gold nanoparticles loaded with doxorubicin showed significantly more potent cytotoxicity against LnCaP cells than PC-3 cells, which do not express PSMA (Kim *et al*., 2010). More recently, an aptamer named NOX-A12, which neutralizes CXCL12 (a critical chemokine involved in the homing and retention of hematological cancer cells (Marasca and Maffei, 2014), was found to enhance the susceptibility of hematological cancer cells to conventional therapies, and inhibited the growth and metastasis of CXCL12-derived tumours (Hoellenriegel *et al*., 2014 & Liu *et al*., 2013). Clinical trials demonstrated that the combination of NOX-A12 and Bendamustine/Rituximab improved clinical responses in patients with chronic lymphocytic leukemia and multiple myeloma, as opposed to the single agents on its own (clinical trials IDs: NCT01486797 and NCT01521533) (Zhou *et al*., 2016).

1.5. Cancer specific peptide ligands as targeting molecules

1.5.1. Why peptides?

The application of peptides as a targeting agent emerged to circumvent limitations presented by mAbs (Shadidi and Sioud, 2003). Peptides are typically differentiated from their larger counterparts (i.e. proteins) by having amino acid sequences less than 50 residues (Bertrand *et al*., 2014). Although peptides are flexible and have lower affinity to receptors compared to mAbs, their use in theranostics (therapeutics and diagnostics) is advantageous due to their smaller size, reduced immunogenicity, high multivalency, deep tumour penetration, ease of synthesis and conjugation, and lower production costs (Cheng and Allen, 2010 & Bakhtiary *et al*., 2016). Peptides can be chemically modified to alter their affinity, charge, hydrophobicity, stability, and solubility allowing for fine-tuning of their *in vivo* bio-distribution (McGuire *et al*., 2014). These advantages, combined with improved screening techniques to isolate ligand-substrate combinations have contributed to the increased role of peptides as targeting moieties in the past decade (Bertrand *et al*., 2014).

The importance of cancer cell surface receptors as therapeutic targets is exemplified by the successful use of mAbs such as Rituxan, Zevalin, Herceptin, and Mylotarg in the treatment of cancer (Aina *et al*., 2005). Peptides are believed to be better cell surface–targeting agents than mAbs, particularly when used as carriers and targeting moieties for cytotoxic payloads such as chemotherapy or radionuclides (atoms that have excess nuclear energy) (Aina *et al*., 2005). Cancer targeting peptides can be identified using Phage display technology (Arap et al., 1998). Phage display is an *in vitro* screening technique, which makes use of bacteriophages to study protein/protein (Beirnaert *et al*., 2017), protein/peptide (Wu *et al*., 2016), and protein/DNA interactions (Godonoga *et al*., 2016). Phage display has been used successfully to identify several cancer targeting peptides (Che *et al*., 2015 & Lee *et al*., 2016).

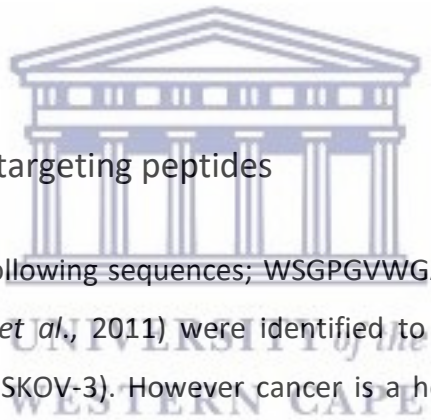

1.5.2. Known cancer targeting peptides

Two peptides with the following sequences; WSGPGVWGASVK (Ma *et al*., 2013) and SVSVGMKPSPRP (Zhang *et al*., 2011) were identified to have high affinity for the ovarian cancer cell line (SKOV-3). However cancer is a heterogeneous disease, and there are various pathological types of ovarian cancer, and not one peptide can be used for all cell types, an indication of specificity. A novel peptide (with the following sequences NPMIRRQ) was shown to target HO-8910 ovarian cancer cells (Wang *et al*., 2016). Eleven peptides were isolated using three phage display peptide libraries on a series of well-defined human Non-Small Cell Lung Cancer (NSCLC) cell lines (McGuire *et al*., 2014). The peptides showed distinct binding profiles across 40 NSCLC cell lines and did not bind normal bronchial epithelial cell lines. Furthermore, both *in vivo* and *ex vivo* studies demonstrated that the peptides home to tumours (McGuire *et al*., 2014). These peptides add to the growing toolbox of tumour targeting agents and their versatility allows for easy incorporation into a variety of imaging and drug delivery systems.

In a recent study, a 12 amino acid trastuzumab-mimetic peptide, named anti-HER2/neu peptide (AHNP) was used to deliver a pro-drug called poly (β-L malic acid) (PMLA) to HER2 + cells using a polymeric nanoparticle (Ding *et al*., 2017). The authors demonstrated that HER2+ cells were inhibited by the nanodrug, which prevented cancer cell proliferation and significantly reduced the tumour size. A protein that plays a vital role in prostate cancer is Wiskott-Aldrich syndrome protein Family member 3 (WASF3) [Teng *et al*., 2010]. Its inactivation leads to suppression of invasion and metastasis regardless of the genetic background of the cancer cell. WASF3 in combination with a series of other proteins make up the WASF Regulatory Complex (WRC). A series of stapled peptides that disrupt protein-protein interactions between members of the WRC was developed (Teng *et al*., 2016). These peptides are capable of suppressing invasion. Stapled peptides are constrained into an alpha-helical formation, which increases proteolytic stability, active uptake into cancer cells, and higher specificity for the intended target due to the large interacting interface (Guerlavais and Sawyer, 2014). The authors developed a stapled peptide that mimicked an alpha-helical interaction between WASF3 and CYFIP1 (a protein that maintains stability of WRC). This peptide suppressed WASF3 phospho-activation and led to the suppression of invasion in breast and prostate cancer cells (Teng *et al*., 2016). Cowell *et al.* (2017) demonstrated that stapled peptides targeting protein-protein interactions that are essential for the maintenance of the WRC can supress lung and liver metastasis *in vivo*.

Although tumour targeting peptides enable the internalization of drugs, certain drugs once internalized, are unable to localise to the mitochondria on their own in order to initiate the apoptotic process. CGKRK is a well-known tumour homing peptide, discovered by phage display technique (Hoffman *et al*., 2003). It mediates the cellular internalization in a p32 receptor-dependent manner, then it localizes to mitochondria in cells (Agemy *et al*., 2013). This cancer targeting peptide has been used to deliver the pro-apoptotic peptide ($_D$(KLAKLAK)$_2$) to cancer cells. This pro-apoptotic peptide is a cationic α-helical amphipathic peptide (Javadpour *et al*., 1996). This peptide was previously shown to have antimicrobial activity by damaging the bacterial cell membrane, but was unable to cross the Eukaryotic plasma membrane (Javadpour *et al*., 1996). To

exploit its cytotoxic activity in the treatment of cancer, the $_D$(KLAKLAK)$_2$ peptide has been coupled to cancer targeting peptides (Ellerby *et al*., 1999).

Mozhi *et al*. (2017) used the CGKRK$_D$(-KLAKLAK)$_2$ fusion peptide to produce pH sensitive polymeric micelle nanoparticles, which also encapsulated the anti-tumour drug docetaxel (Figure 1.5). The mitochondria protein, p32 that is the target for CGKRK, is overexpressed on the surface of various cancer cells (Agemy *et al*., 2013). The CGKRK peptide facilitates the docking of the micelle nanoparticles to cancer cells. Once internalized, the fusion peptide and docetaxel is released via pH sensitive trigger. Docetaxel exert its anti-tumour activity by promoting polymerization of tubules by binding to beta-tubulin and locking the structures in place (Apfel, 1996). The fusion peptide is targeted to the mitochondria via the CGKRK peptide, while the $_D$(KLAKLAK)$_2$ peptide triggers mitochondria-dependent apoptosis (Figure 1.5). The cationic $_D$(KLAKLAK)$_2$ amino acids only disrupt the mitochondrial membrane once they are attached to the head groups of anionic phospholipids in the mitochondrial membrane. The peptide preferentially disrupts the mitochondrial membrane because of their higher anionic phospholipid content than the zwitterionic phospholipids of the cytoplasmic membranes. Thus $_D$(KLAKLAK)$_2$ has minimal toxicity outside of the mammalian cell and only induces mitochondria-dependent apoptosis once internalized (Wang and Huang, 2012). The combination of docetaxel and the therapeutic $_D$(KLAKLAK)$_2$ peptide displayed a synergistic anti-tumour effect in an MCF-7 cell line. The therapeutic mechanism of action of the CGKRK and $_D$(KLAKLAK)$_2$ bi-conjugate to deliver docetaxel is shown in Figure 1.5 (Mozhi *et al*., 2017).

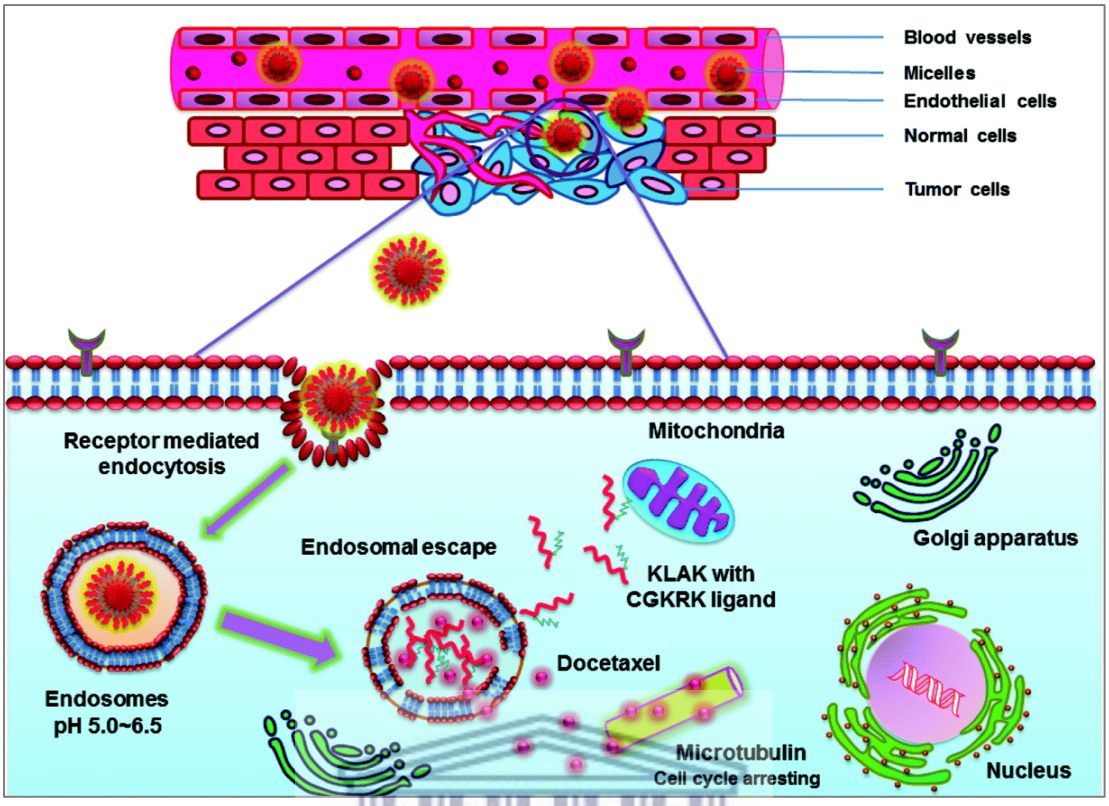

Figure 1.5: Schematic of the drug-loaded polymeric micelles and their cellular uptake mechanism. Delivery of docetaxel and the therapeutic peptide by targeted micelles from the blood circulation into the tumour tissue and internalization of the targeted micelles by tumour cells *via* a receptor-mediated endocytosis pathway (Mozhi *et al.*, 2017).

1.6. Prohibitin as the ideal target for peptides

The prohibitin (PHB) gene was originally isolated and characterized in rat liver cells (McClung *et al.*, 1989) and maps to chromosome 17q21-21 (Sato *et al.*, 1993). PHB belongs to a family of proteins called Band-7, is highly conserved evolutionarily and is ubiquitously expressed in various compartments of eukaryotic cells which include the mitochondria, nucleus, and plasma membrane as shown in Figure 1.6. PHB located in different cellular compartments function in different biological processes, which are involved in multiple diseases such as obesity and cancer.

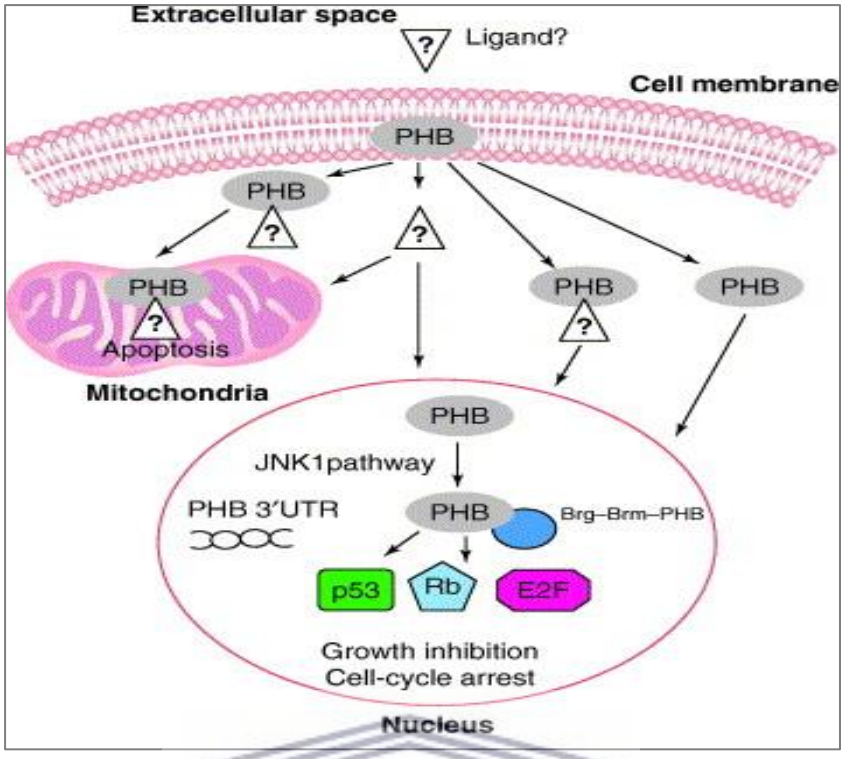

Figure 1.6: The subcellular localization of prohibitin and potential cellular processes PHB is involved in. PHB is present on the cell membrane where it can interact with various targeting ligands. Such ligands could potentially translocate to the mitochondria and disrupt mitochondrial function, resulting in apoptosis. PHB might also translocate from the cell membrane to the nuclear compartment where it might function as a modulator of transcription. The phosphorylation of PHB, possibly by the JNK1 pathway, might be necessary for the anti-proliferative effects of PHB. The latter involves the interaction with Brg–Brm, inhibition of the E2F pathway and both p53- and pRB-dependent and p53- and pRB-independent mechanisms (Mishra *et al*., 2005).

Kolonin *et al.* (2004) used phage display technology to identify a peptide (with amino acid sequence: CKGGRAKDC) that bind to the vasculature of obese tissue. PHB, which is over expressed in the endothelial cells (ECs) of the vasculature of the white adipose tissue (WAT), was identified as the target for this peptide. Consequently the peptide was named Adipose Homing peptide (AHP). Kolonin *et al.* (2004) also demonstrated that when AHP was coupled to the pro-apoptotic peptide $_{D}(KLAKLAK)_2$, it could be used to reverse obesity in mice. The study showed that when the fusion peptide was injected into obese mice, the AHP-conjugate was internalized and localized by the blood vessels of the subcutaneous and peripheral white fat, but not other organs. This led to the death of vascular ECs by apoptosis, subsequent resorption of fat in the WAT, normalization of metabolic processes and weight loss. Due to the specificity of AHP, no systemic or bystander effects were observed. The desired effect of treatment was dependent on the internalization of treatment through the interaction

between the PHB and the AHP-complex (Kolonin *et al*., 2004). On binding to the PHB receptor, the AHP-conjugate gets internalized and released inside the cell and the PHB receptor is then recycled and available for the next cycle, provided the cell is still alive (Kolonin *et al*., 2004).

Several studies using different model organisms suggest that PHB not only plays a role in obesity but in cancer as well. Data from The Cancer Genome Atlas (TCGA) and The Human Protein Atlas (THPA) show that PHB is widely expressed in diverse cancers, at both mRNA and protein levels (Uhlen *et al*., 2017). PHB expression levels are significantly correlated with tumour metastasis and poor prognosis according to literature (Chang *et al.,* 2010; Liao *et al.,* 2013; Cao *et al.,* 2016 & Küçük *et al.,* 2016). In many cancers, the Raf/ERK signalling pathway is constitutively activated, promoting cancer cell metastasis. For example, HeLa cells showed that phosphorylation of PHB in lipid rafts of the plasma membrane is necessary for the activation of Raf/ERK signalling cascades supporting cancer cell metastasis (Chiu *et al*., 2013). A similar mechanism was observed in pancreatic ductal adenocarcinoma (Luan *et al*., 2014) and gall bladder cancer as well (Cao *et al*., 2016). In addition to the Raf ⁄ERK signalling pathway, PHB is implicated in the TGF-β (Ghazy *et al*., 2017) as well as the PI3K ⁄ Akt signalling pathways (Dong *et al*., 2016), which involves the phosphorylation of PHB. All these signalling pathways are involved in cancer and PHB is thus an ideal target for ligands such as AHP to interfere in these signalling pathways with the aim of inhibiting cell proliferation and cancer development by inducing apoptosis.

Similarly and of interest to this study, Sibuyi *et al.* (2017) reported on an *in vitro* anti-proliferative activity of PHB-targeted gold nanoparticles (AuNPs) that used $_D(KLAKLAK)_2$ to induce apoptosis. The targeted nanotherapy was developed by bi-functionalizing spherical AuNPs with the targeting peptide (AHP) and the pro-apoptotic peptide ($_D(KLAKLAK)_2$). Previous studies showed that Caco-2 cells express PHB on the cell surface (Nijtmans *et al*., 2000; Sharma and Qadri, 2004 & Thovhogi *et al*., 2015), while the breast cancer cell line, MCF-7, most likely express PHB in the cytoplasm (Rastogi *et al*., 2006). Caco-2 cells are therefore excellent *in vitro* cell culture models to test the specificity of PHB-targeted

AuNPs. Thovhogi *et al.* (2015) also showed the specific binding of AHP–FITC to Caco-2 cells using competitive binding assays. As further corroboration of this, Sibuyi *et al.* (2017) showed that AHP–FITC is able to bind to Caco-2 cells, but not to the breast cancer cell line MCF-7. This confirms that Caco-2 cells express PHB, the receptor for AHP on the cell surface, while MCF-7 cells do not. The PHB-targeted AuNPs were highly toxic to Caco-2 cells resulting in the induction of apoptosis within these cells, while leaving the viability of MCF-7 cells unaffected. These results demonstrate that the AuNPs specifically only kills cells that express PHB, the receptor for AHP on the cell surface and that the toxicity is likely to be caused by the pro-apoptotic peptide $_{D}(KLAKLAK)_{2}$. This study demonstrates the efficacy and specificity of PHB-targeted nanotherapy *in vitro*, and provides the proof of principle for PHB-targeted therapy.

1.7. The role of apoptosis in cancer progression

Apoptosis, a highly organized and regulated process, is the most investigated and best understood mechanism of programmed cell death (Su *et al*., 2013). It functions as a defence mechanism against cytotoxic agents in order to maintain homeostasis within cell populations (Su *et al*., 2013). Apoptosis can be distinguished from necrosis (traumatic cell injury that is fatal to the surrounding tissue of the target cell) by its unique morphological and biochemical alterations (Rønning *et al*., 2017) as shown in Table 1.2.

Table 1.2: Morphological features of apoptosis and necrosis

Apoptosis	Necrosis
Occurs in single cells or small clusters of cells	Often contiguous cells
Cell shrinkage and convolution	Cell swelling
Pyknosis and karyorrhexis	Karyolysis, pyknosis, and karyorrhexis
Intact cell membrane	Disrupted cell membrane
Cytoplasm retained in apoptotic bodies	Cytoplasm released
No inflammation	Inflammation usually present

(Human Protein Reference Database http://www.hprd.org/).

Apoptosis is triggered by a variety of cellular signals which include DNA replication stress (Gorgoulis *et al*., 2005; Hills and Diffley, 2014 & Desmarais *et al*., 2016), violation of cell-cycle checkpoints (Castedo *et al*., 2004 & Vaish *et al*., 2014), increased intracellular Ca^{2+} concentration (Sergeev and Song, 2014), hypoxia (Shimizu *et al*., 1996 & Liu *et al*., 2013) as well as oxidative damage caused by reactive oxygen species (ROS) [Annunziato *et al*., 2003; Valko *et al*., 2006 & Lu *et al*., 2014]. The evasion of apoptosis (Figure 1.7) is one of the six hallmarks of cancer (Hanahan and Weinberg, 2000), underscoring the important role of this pathway in survival of malignant cells.

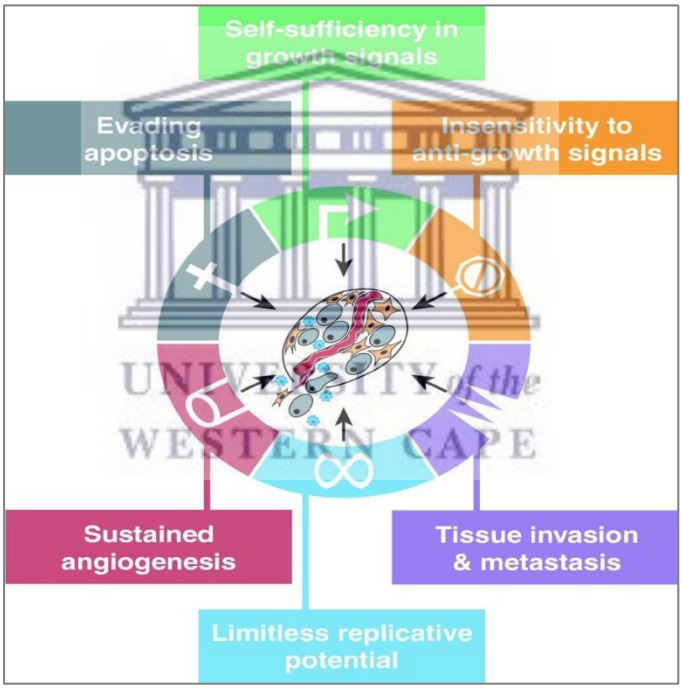

Figure 1.7: The six hallmarks of cancer. The variety of cancer cell genotypes is a manifestation of six essential alterations in cell physiology that collectively dictate malignant growth: self-sufficiency in growth signals, insensitivity to growth-inhibitory (antigrowth) signals, evasion of apoptosis, limitless replicative potential, sustained angiogenesis, and tissue invasion and metastasis (Hanahan and Weinberg, 2000).

1.7.1. Apoptotic pathways

Two different apoptosis pathways have been identified: the intrinsic/mitochondrial pathway and the extrinsic/physiological pathway (Figure 1.8) [Hengartner, 2000]. There is an overlap between these pathways as the extrinsic pathway can also activate the intrinsic pathway. Both pathways result in the recruitment and activation of cysteine-aspartic acid proteases (caspases) [Miura *et al*., 1993 & Yuan *et al*., 1993]. Once caspases are activated, there seems to be an irreversible commitment towards cell death (Elmore, 2007).

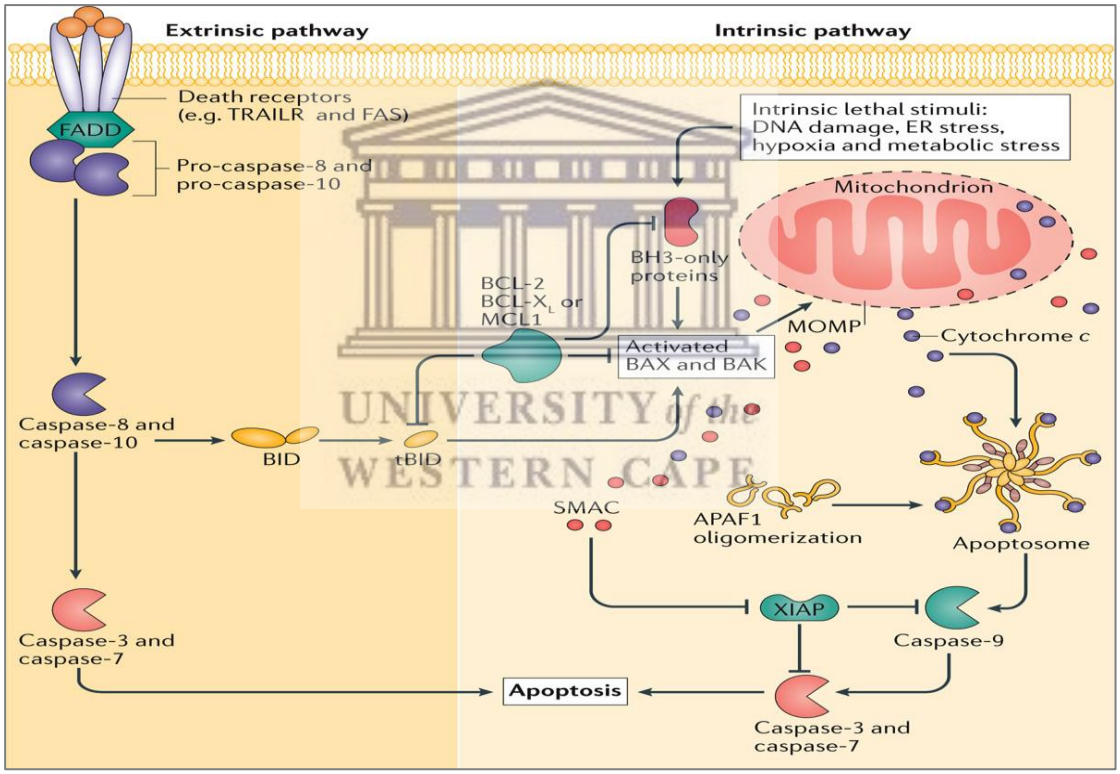

Figure 1.8: The intrinsic and extrinsic apoptotic pathways. In the extrinsic apoptotic pathway is activated by death receptors that recruit death ligands such as tumour necrosis factor (TNF)-related apoptosis-inducing ligand (TRAIL) receptor (TRAILR) and FAS which can activate initiator caspases (caspase-8 and caspase-10), leading to apoptosis. The intrinsic (or mitochondrial) pathway is activated in response to cellular stress and requires mitochondrial outer membrane permeabilization (MOMP), resulting in the release of pro-apoptotic proteins from the mitochondria such as second mitochondria-derived activator of caspases (SMAC) and cytochrome c, which activate downstream caspases (Ichim and Tait, 2016).

1.7.1.1. The extrinsic pathway

The extrinsic pathway involves transmembrane receptor-mediated interactions (Locksley *et al*., 2001). It is activated upon binding and activation of plasma membrane cell death receptors (e.g. apoptosis stimulating factor [Fas], tumour necrosis factor receptor [TNFR], and TNF-related apoptosis-inducing ligand [Trail]) by their specific ligands (Ashkenazi and Dixit, 1998). These death receptors share similar cysteine-rich extracellular domains and have a cytoplasmic domain of about 80 amino acids called the "death domain". This death domain plays a critical role in transmitting the death signal from the cell surface to the intracellular signalling pathways (Elmore, 2007).

The series of events that define the extrinsic pathway of apoptosis are best characterized with the FasL/FasR and TNF-α/TNFR1 models (Ashkenazi and Dixit, 1998). In these models, receptors cluster and bind with their homologous trimeric ligands. Upon ligand binding, cytoplasmic adapter proteins are recruited which exhibit corresponding death domains that bind to the receptors. The binding of the Fas ligand (FasL) to the Fas receptor (FasR) results in trimerization to produce a death-inducing signalling complex (DISC) which includes the Fas-associated protein with death domain (FADD), resulting in the cleavage of effector caspases (caspase-3, -6 and -7) [Peter and Krammer, 2003]. The D-type cyclins (D1, D2 and D3) in the mammalian cell cycle machinery drives cell proliferation, and repress FasL/FasR expression (Choi *et al*., 2014). Thus, the over-expression of D-type cyclins plays a causative role in the development of many cancers (Beroukhim *et al*., 2010). Ablation of all three D-cyclins in the bone marrow of adult mice led to apoptosis via the FasL/FasR pathway (Choi *et al*., 2014).

The binding of the TNF ligand to the TNF receptor results in the binding of the adapter protein, Tumour necrosis factor receptor type 1-associated DEATH domain protein (TRADD) with recruitment of FADD and Receptor-interacting protein (RIP) [Tartaglia *et al*., 1993]. FADD then associates with procaspase-8 via dimerization of the death effector domain (Smith *et al*., 1994). At this point, DISC is formed, resulting

in the auto-catalytic activation of pro-caspase-8. Once caspase-8 is activated, the execution phase of apoptosis is triggered (Ashkenazi and Dixit, 1998). Death receptor mediated apoptosis can be inhibited by a protein called cellular FLICE-inhibitory protein (c-FLIP), which binds to FADD and caspase-8, rendering them ineffective (Kataoka *et al*., 1998). The TNF-related apoptosis-inducing ligand (TRAIL/Apo2L) induces apoptosis in cancer cells by binding to two transmembrane agonistic receptors, DR4 (TRAIL-R1) and DR5 (TRAIL-R2). Even though TRAIL has shown efficacy in a phase II clinical trial of patients with relapsed/refractory non-hodgkin's lymphoma (Goy *et al*., 2005), resistance by several cancers is a major setback. The anti-cancer drug, Azadirone can sensitize cancer cells to TRAIL–induced apoptosis in order to overcome resistance to TRIAL. Azadirone does this by up regulating DR4 and DR5 receptors, downregulating cell survival proteins, and upregulating pro-apoptotic proteins. Thus combinations of azadirone and TRAIL are an effective approach for cancer therapy (Gupta *et al*., 2013).

1.7.1.2. The Intrinsic pathway

The Intrinsic/mitochondrial pathway is initiated by a range of exogenous and endogenous stimuli such as oxidative stress, DNA damage and ischemia (inadequate blood supply to tissues/organs) (Elmore, 2007). It plays an important role in development and elimination of damaged cells (Muñoz-Pinedo, 2012). The pathway is regulated by the Bcl-2 (B-cell lymphoma 2) family which consists of pro- and anti-apoptotic regulatory proteins, such as Bax (bcl-2-associated X) and Bcl-2, respectively (Caltabiano *et al*., 2013). The functional consequence of pro-apoptotic signalling is the opening of the mitochondrial permeability transition (MPT) pore, loss of the mitochondrial transmembrane potential and release of two main groups of pro-apoptotic proteins normally sequestered from the intermembrane space into the cytosol (Saelens *et al*., 2004). The first group consists of cytochrome c, Smac/DIABLO, and the serine protease HtrA2/Omi (Garrido *et al*., 2006). Cytochrome c binds and activates Apaf-1 as well as pro-caspase-9, forming an "apoptosome" (Hill *et al*., 2004). The apoptosome hydrolyzes adenosine triphosphate (ATP) to cleave and activate

caspase-9. The initiator caspase-9 then cleaves and activates executioner caspases-3, -6, and -7, resulting in apoptosis (Loreto *et al*., 2011).

The anti-apoptotic proteins, bcl-2 and bcl-xL inhibit the release of Cytochrome c (Fesik, 2000). The second group of pro-apoptotic proteins, AIF (Apoptosis- inducing factor), endonuclease G and CAD (carbamoyl-phosphate synthetase 2, aspartate transcarbamylase, and dihydroorotase) are released from the mitochondria during apoptosis, but this is a late event that occurs after the cell has committed to die (Elmore, 2007). AIF and endonuclease G both translocate to the nucleus and causes DNA fragmentation in a caspase-independent manner (Li *et al*., 2001). CAD is subsequently released from the mitochondria and translocates to the nucleus where, after cleavage by caspase-3, it leads to oligonucleosomal DNA fragmentation and a more pronounced and advanced chromatin condensation.

1.7.2. Pro-apoptotic agents as anti-cancer drugs

Apoptosis is a complex process with numerous points of regulation, which could be manipulated for therapeutic benefit for the treatment of cancer. A greater understanding of these regulatory pathways and how they are altered in cancer resulting in resistance to apoptosis has been key in the development of pro-apoptotic agents. Interestingly, mutation rates in apoptotic proteins such as death receptors (Lee *et al.*, 2001) or Bcl-2 proteins (Kim *et al.*, 2012) are low, indicating that many cancer cells have apoptotic machinery, but they are being inhibited. If the machinery were to be unblocked, it would efficiently kill tumour cells (Fox and MacFarlane, 2016). The three key points in apoptotic signalling pathways often targeted to overcome the resistance of apoptosis in cancer are discussed below.

1.7.2.1. Current pro-apoptotic molecules used in therapy

Three key points in apoptotic signalling pathways are used as targets for cancer therapeutic strategies. One of which is triggering extrinsic apoptosis via death receptors by the addition of exogenous ligands such as TRAIL, which will initiate DISC formation and cause cell death by apoptosis (Fox and MacFarlane, 2016). TRAIL is a robust and selective tumour suppressor that offers itself as an attractive natural drug target to restore anti-tumour immunity. The TRAIL-inducing compound ONC201/TIC10 induced sustained TRAIL up-regulation and apoptosis in tumour cells *in vitro* and *in vivo* experiments while sparing normal cells (Allen *et al*., 2015). ONC201/TIC10 exclusively activates Foxo3a transcription factor (Ghaffari *et al*., 2003) through inactivation of the Akt/ERK pathway, which results in up-regulation of TRAIL and its pro-apoptotic death receptor DR5 (Allen *et al*., 2015). Another novel class of small molecules named bioymifi are capable of activating the TRAIL death receptor pathway by specifically binding and activating the death receptor DR5, inducing DR5 clustering and aggregation, leading to apoptosis (Wang *et al*., 2013). Although TRAIL can induce apoptosis in several cancer cell lines, it has emerged that most primary cancer cells are resistant to TRAIL monotherapy (Lemke *et al*., 2014).

The second apoptotic signalling pathway that is a target for therapeutic intervention is to initiate apoptosis by targeting anti-apoptotic Bcl-2 family members mainly BCL-2, Bcl-xL and MCL-1 (Fox and MacFarlane, 2016) as well as pro-apoptotic effectors (Bax and Bak) (Korsmeyer, 1992). ABT-737 and its analogue ABT-263 (Navitoclax) bind to and inhibit Bcl-2, Bcl-xL and Bcl-W, but not MCL-1 (Anderson *et al*., 2014). They were the first inhibitors of anti-apoptotic Bcl-2 proteins to be identified. Although Navitoclax showed promising clinical activity, it also induced thrombocytopenia (a condition characterized by abnormally low levels of platelets in blood) as a result of Bcl-xL inhibition (Rudin *et al*., 2012). ABT-199 (Venetoclax) has similar Bcl-2 inhibitory activity as Navitoclax's, but does not have toxicity towards platelets (Souers *et al*., 2013). ABT-199 has recently been approved by the FDA for the treatment of chronic lymphocytic leukaemia patients with an overall response rate of 79% (Roberts *et al*., 2016). A common drug resistance mechanism in cancer cells, which is caused by

elevated MCL-1 expression has been identified for both ABT-263 and ABT-737 (Yecies *et al*., 2010). In a recent study, doxorubicin and dinaciclib showed synergistic effect with ABT-263 through the downregulation of MCL-1, thereby enhancing the pro-apoptotic effect of ABT-737/263 in SCLC (Inoue-Yamauchi *et al*., 2017). Furthermore, combinations of the Bcl-2 inhibitor ABT-199 and either doxorubicin or dinaciclib provided effective therapeutic strategies in mouse xenograft cancer models, validating new potential therapeutic strategies for SCLC.

The third key point involves targeting regulatory pathways, either by increasing caspase activity or inhibiting the inhibitor of apoptosis proteins (IAPs) using compounds that mimic the endogenous IAP antagonist, SMAC (Fox and MacFarlane, 2016). IAPs are a highly conserved family of signalling regulators that play key roles in the promotion of survival signalling (Walczak, 2011). SMAC is an endogenous antagonist of IAPs, it is released from the mitochondria in response to apoptotic stimuli and neutralizes IAPs thus allowing sustained caspase activity and execution of the apoptotic process (Fulda and Vucic, 2012). Smac mimetics have been designed to overcome IAP-mediated apoptosis resistance of cancer cells. Birinapant (TL32711), a bivalent SMAC-mimetic compound activates caspase-8 by binding to the BIR3 domains of IAPs 1 and 2 (cIAP1 and cIAP2), x-linked IAP (XIAP), and the Baculovirus IAP Repeat (BIR) domain of Melanoma-IAP (ML-IAP) *in vitro* to induce apoptosis. Moreover, birinapant displayed antitumor activity at well-tolerated doses in murine xenograft models of ovarian and colorectal cancers and melanoma patient–derived tumours. This data suggests that birinapant targets IAP proteins to trigger an apoptotic response both *in vitro* and *in vivo* and has potential application in multiple tumour malignancies (Benetatos *et al*., 2014). Smac mimetics have demonstrated synergy with other treatment, including cytotoxic agents such as carboplatin (Janzen *et al*., 2015), paclitaxel (Yang *et al*., 2016) and radiation therapy (Matzinger *et al*., 2015). Although these synergies are well defined in pre-clinical models, so far they have been less successful in clinical settings (Parton *et al*., 2015; Noonan *et al*., 2016 & Finlay *et al*., 2017).

1.8. Nanotechnology based drug delivery systems

1.8.1. Nanotechnology

Emerging nanotechnology-based therapeutics are providing solutions to the shortcomings of conventional cancer treatments (Danhier, 2016). Nanotechnology refers to the fabrication, characterization and applications of active substances in nanometer scale dimension (~1-100nm) for various applications (Sridhar *et al*., 2015). The ideal nanotechnology-based drug delivery system for biological application should possess certain characteristics, such as: chemical compatibility (Di Martino *et al*., 2017), selective toxicity (Korrapati *et al*. 2016), biodegradability and biocompatibility (Gagliardi *et al*., 2017), be easy to design and modify (Richards *et al*., 2017), preferably synthesised from natural/biological materials (Korrapati *et al*. 2016), and have an increased drug loading capacity (Gupta *et al*., 2017).

1.8.2. Nanomaterials used for drug delivery

In the last decade, advances in nanotechnology-based drug delivery systems have enabled more effective drug design and development, which has revolutionized conventional cancer therapies (Kanamala *et al*., 2016). According to Wicki *et al.* (2015), a total of 1381 nanomedicines for cancer treatment were registered for clinical trials by December 2014; these include liposomes, polymer-drug conjugates, micelles, carbon nanoparticles and metallic nanoparticles (illustrated in Figure 1.9).

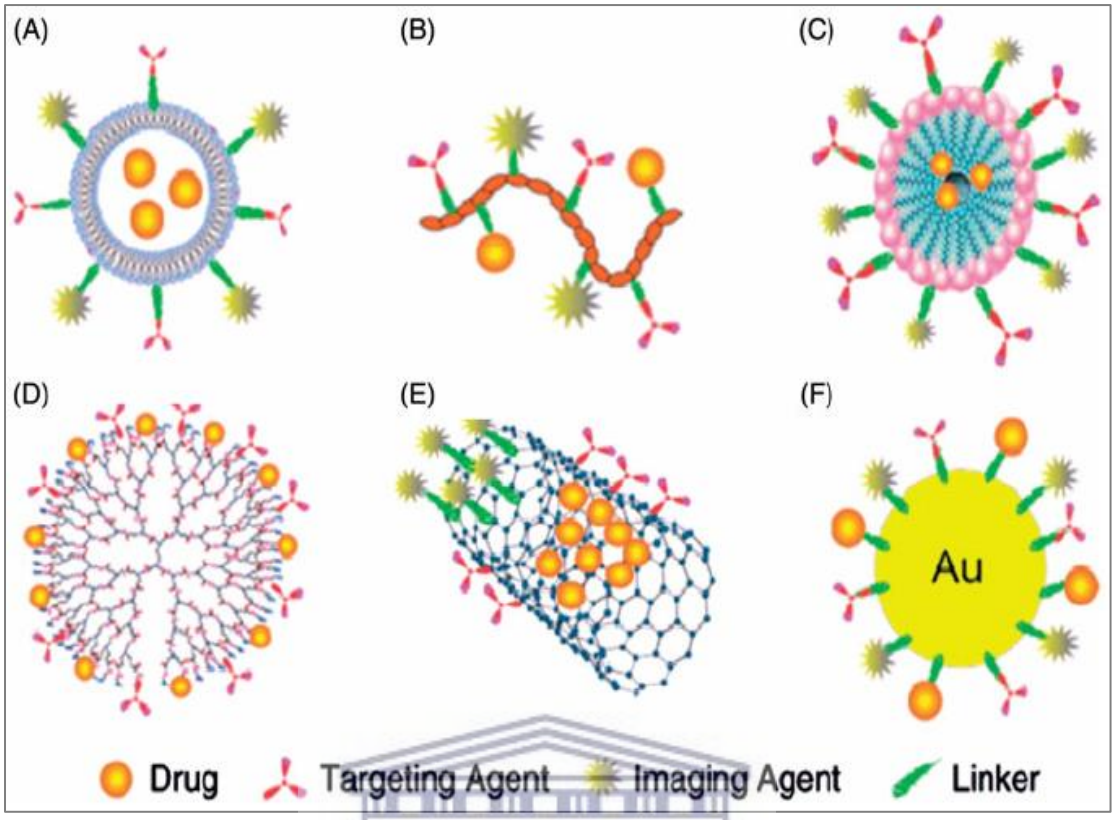

Figure 1.9: Commonly utilized nanomaterials for biomedical applications. (A) Liposomes, (B) Polymer Conjugate, (C) Micelles, (D) Dendrimers, (E) Carbon nanoparticles and (F) Inorganic (gold) nanoparticles (Kumari *et al.*, 2016).

1.8.3. Gold nanoparticles (AuNPs)

One of the most widely studied nanoparticles (NPs) are gold nanoparticles (AuNPs). AuNPs are used as drug carriers, photothermal agents, radiosensitizers, contrast agents and have also shown promise for cancer therapy. There are various types of AuNPs as shown in Figure 1.10 such as gold−silica nanoshells, nanorods, nanocages and nanostars.

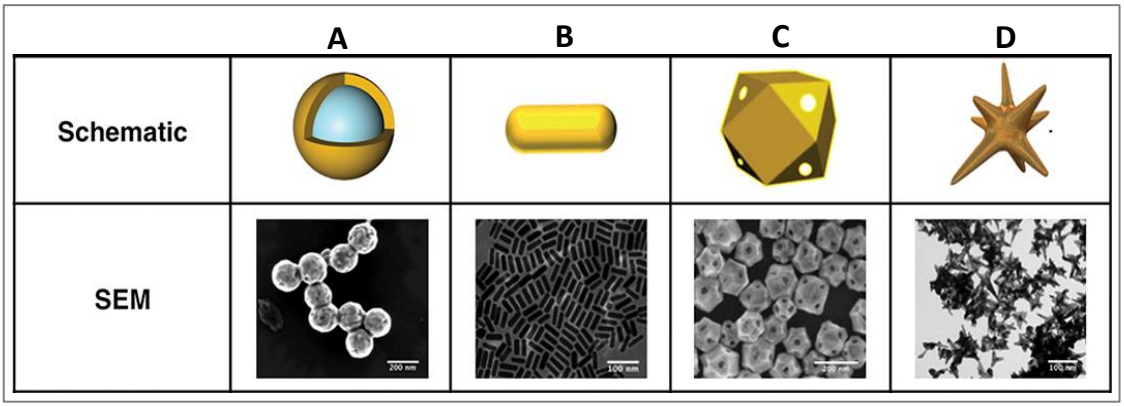

Figure 1.10: Schematic and Scanning Electron Microscopy (SEM) images of AuNPs. Four of the most commonly employed AuNPs include **A**) silica core/gold shell nanoshells, **B**) gold nanorods, **C**) hollow gold nanocages, and **D**) nanostars. (Riley and Day, 2017).

1.8.3.1. Application of AuNPs in targeted drug delivery

The customizable size, shape, and diverse physicochemical properties of AuNPs as well as their potential for surface functionalization with drugs or other molecules, make AuNPs promising tools as drug carriers to disease sites (Niikura *et al*., 2013 & Paul *et al*., 2014). As previously stated, the targeted drug delivery approach could be an alternative to conventional therapy, which will reduce the detrimental side effects caused by off-target drug delivery and high drug doses (Tomuleasa *et al*., 2012). Hepatocellular carcinoma-derived tumour cells treated with AuNP-drug conjugates showed significantly lower cellular proliferation than cells treated with the free drugs alone, supporting surface-functionalised AuNPs as an efficient targeted delivery tool for the treatment of cancer (Tomuleasa *et al*., 2012). The penetration of the blood–brain barrier is a significant problem in the treatment of brain tumours. Ruan *et al.* (2015) demonstrated that functionalised AuNPs loaded with the anti-tumour drug, doxorubicin can target glioma cells in a mouse cancer model. In the study by Ruan *et al.* (2017) the AuNPs were functionalised with angiopep-2, a specific ligand of low-density lipoprotein receptor-related protein-1, which could mediate transfer across the blood–brain barrier. The advantage of this treatment was that doxorubicin could be delivered across the blood brain barrier to glioma cells (Ruan *et al*., 2015).

Various approaches have been used to develop cancer therapies using AuNPs, some of which are currently undergoing clinical trials. In this regard, Li *et al*. (2016) showed that the clinically tested CYT-6091 nanodrug, which is a novel AuNP conjugated to recombinant human tumour necrosis factor (rhTNF) (Libutti *et al*., 2010), may be administered systemically at doses of "free rhTNF" that were previously shown to be toxic. However, although a wide variety of NP treatments have proven to be very successful in clinical trials, only a few nanomedicines, such as Doxil® (Janssen Biotech Inc., Horsham, PA, USA), Myocet® (Sopherion Therapeutics Inc., Princeton, NJ, USA), DaunoXome® (Galen US Inc., Souderton, PA, USA), Depocyt® (Pacira Pharmaceuticals Inc., San Diego, CA, USA), Abraxane® (Celgene Corporation, Inc.,Berkeley Heights, NJ, USA), Genexol-PM® (Samyang Biopharmaceuticals Corporation, Jongno-gu, Seoul, Korea), and Oncaspar® (Enzon Pharmaceuticals Inc., Bridgewater, NJ, USA), are FDA approved for use in the treatment of cancer, none of which consist of AuNPs, indicating a formidable "bottle neck" in translating research from bench to bed-side (Sanna *et al*., 2014). This could be due to the fact that although AuNPs are inert and biocompatible, contradictory results have been obtained regarding their toxicity towards cells.

1.8.3.2. Cytotoxicity of AuNPs

Different AuNP synthesis methods produce AuNPs with different characteristics. The cytotoxicity of the NPs is a common measure for the biocompatibility of materials (Favi *et al*., 2015). The cytotoxicity of AuNPs is directly related to the following characteristics of AuNPs: i) size, ii) surface chemistry, iii) coating materials and iv) shape (Wang *et al*., 2011 & Ahmad *et al*., 2017).

The effect of AuNP size on toxicity has been thoroughly investigated. Tomić *et al*. (2014) showed that smaller AuNPs (10nm) induced low levels of apoptosis (20%) in dendritic cells (DCs), whereas larger AuNPs (50nm) demonstrated no cytotoxic effects on DCs. This observation is in line with the previous studies that demonstrated size dependent cytotoxicity of AuNPs using different cell types (Pan *et al*., 2007 & Yen *et*

al., 2009). Another study showed that smaller AuNP sizes accumulated more readily in cell nuclei and organelles, thus causing DNA damage that lead to adverse effects in the cells (Paino *et al*., 2012). The absence of AuNPs inside the nucleus or organelles has also been reported, despite effective cellular uptake and internalization into DCs. This could be indicative of AuNPs entering cells then exiting the cells once it's performed its function without accumulating in organelles, thus correlating with very low toxicity of AuNPs (Fernández *et al*., 2015; Fytianos *et al*., 2015; le Guével *et al*., 2015). This points out the advantage of AuNPs compared to many other NPs, for example silver NPs, which cause more DNA damage when compared to AuNPs at similar concentrations (Singh *et al*., 2010). These results suggest a stringent size dependency of cytotoxicity, although it remains rather obscure why a particular size is more toxic than another (Fratoddi *et al*., 2015).

Another key feature that functions in controlling cytotoxicity of AuNPs is surface chemistry. AuNPs have a positive effective surface charge (cationic) upon preparation but this changes when the AuNPs are in biological buffers and fluids (Lynch *et al*., 2008). When AuNPs are in blood for example, plasma proteins adsorb on the surface spontaneously, and the surface chemistry of the AuNPs is thus not the same as the originally synthesised preparation (Lynch *et al*., 2008). Instead, the AuNPs adopt the physicochemical properties of the adsorbed proteins. The adsorbed protein layer can influence cellular uptake and particle bio-distribution, ultimately affecting particle cytotoxicity. Surface functionalization with various agents should therefore be carefully studied as it changes the particle charge and function (Fratoddi *et al*., 2015). Positively charged-polymer-coated-AuNPs showed a significant decrease in apoptosis when used to treat DCs, further demonstrating that surface functionalization of AuNPs could be safely applied in a clinical setting. In addition, the synthesis of AuNPs often requires toxic chemical reagents as reducing and stabilizing agents such as citrate and Cetyl trimethylammonium bromide (CTAB). Following synthesis the free chemical reagents need to be properly removed from the AuNP suspension as these reagents have been shown to be extremely toxic even at low concentrations (Alkilany and Murphy, 2010).

The geometric shapes of metallic NPs can significantly influence their optical properties, which can be exploited for applications in diagnostics such as cellular tracking for example. AuNP of different shapes can be synthesised by changing the synthesis conditions. Figure 1.10 shows some of the possible AuNP shapes (Li *et al*., 2014 & Nie *et al*., 2014). Altering the shape of AuNPs can influence their cytotoxicity and optical properties (Zhang *et al*., 2014). For instance, gold nanoparticle spheres (AuNSs) showed greater toxicity compared with gold nanostars (AuNSTs) on human skin fibroblasts and rat fat pad endothelial cells (Favi *et al*., 2015). The AuNSs were lethal at 40µg/mL for both cell lines, whereas the AuNSTs were less toxic at higher concentrations (400µg/mL), indicating that the AuNSs have a greater toxicity to ECs. Although AuNSs are reported to be more toxic than AuNSTs, gold nanorods (AuNRs) have been reported to demonstrate more toxicity than their spherical counterparts (Yah, 2013) due to the use of toxic chemical reagents such as CTAB for their preparation (Fratoddi *et al*., 2015). Alkilany *et al.* (2009) showed that cells treated with CTAB – coated AuNRs had a viability of 30%. When substituting CTAB with poly (acrylic acid) [PAA] or poly (allyamine hydrochloride) [PAH] polymers, the cell viability increased to more than 90% and 80% respectively (Alkilany *et al*., 2009). Of note, the three AuNRs presented approximately the same effective surface charge and size, indicating that the cytotoxicity is in fact caused by the surface functionalization with CTAB. Although deemed the more cytotoxic than its counterparts, AuNRs possess several advantages including large absorption cross sections, tunable longitudinal plasmon wavelengths, high chemical stability, and efficient photothermal conversion; enabling their applications as optically active agents for various biomedical applications, such as photothermal therapy (PTT) [Alkilany *et al*., 2012; Mooney *et al*., 2014 & Park *et al*., 2014].

1.8.3.3. Photothermal (PTT) potential of AuNPs

Photothermal therapy (PTT) is defined as the ability of NPs to effectively convert absorbed Near Infrared (NIR) light into heat (Pattani *et al*., 2015). PTT induces cell death via necrosis or apoptosis (Pattani *et al*., 2015). During necrosis, heat disrupts the plasma membrane, causing the cellular components to leak out with resultant inflammation and harm to surrounding normal tissues (Pattani *et al*., 2015). As previously stated in Section 1.7, apoptosis attenuates inflammatory activities, therefore skewing the PTT response towards apoptotic cell death rather than necrotic death which can be more favourable in clinical settings (Ali *et al*., 2016).

Different shapes of AuNPs such as nanospheres (AuNSs) and nanorods (AuNRs) have been reported to have potential PTT capability, which can be attributed to their optical properties (Nakamura *et al*., 2010; Tsai *et al*., 2013; Mooney *et al*., 2014 & Abadeer and Murphy, 2016). These NPs can effectively convert NIR light into heat that will in turn eliminate cells by either necrosis or apoptosis. NP-induced PTT therefore holds a great promise for cancer therapy (Tsai *et al*., 2013; Mooney *et al*., 2014 & Abadeer and Murphy, 2016). The PTT mechanism of action using ligand-conjugated nanogels to selectively target cancer cells and deliver AuNPs is shown in Figure 1.11 (Nakamura *et al*., 2010). Once the pegylated gold nanogel (GNG) is internalized, PTT can be initiated by exposing the cells to a NIR light source.

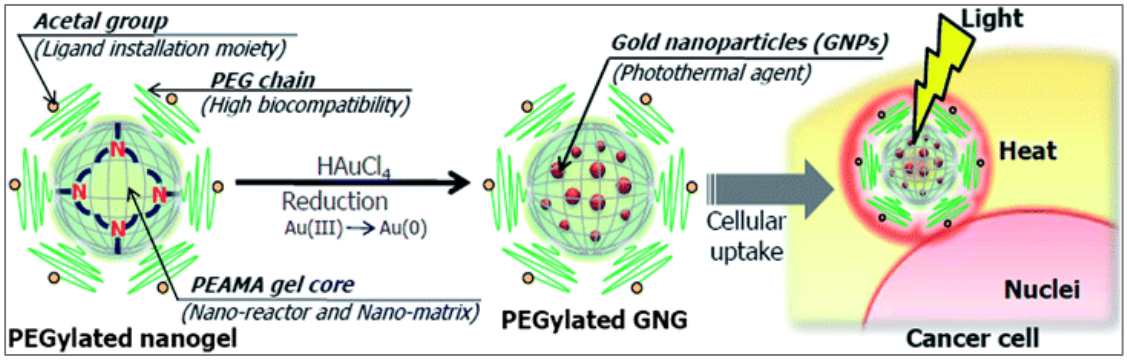

Figure 1.11: Schematic illustration of the preparation of PEGylated gold nanogels (GNGs) for PTT application in cancer. Pegylated nanogels are made up of a nano-matrix, is functionalised with PEG which has affinity for ligand attachment via acetal groups. $HAuCL_4$ is then reduced to Au (0) and AuNPs bind to the gel core. Upon selective targeting and cell internalization, PTT is initiated via heat causing cell death (Nakamura *et al*., 2010).

1.8.3.3.1. Au nanosphere-based PTT

PTT using AuNSs can be achieved with pulsed or continuous wave (CW) visible light spectrum lasers due to the Surface Plasmon Resonance (SPR) absorption in the visible light region of the electromagnetic spectrum (Huang and El-Sayed, 2010). AuNSs can therefore be used for the treatment of shallow cancers (e.g. skin cancer). The first comprehensive study using pulsed laser and AuNSs was performed for the selective and highly localized photothermolysis of lymphocytes cells (Pitsillides *et al*., 2003). The study by Pitsillides *et al.* (2003) showed that lymphocytes exposed to mAb-conjugated AuNSs and nanosecond laser pulses showed cell death whereas adjacent cells remained viable. Cell death is attributed mainly to cavitation damage caused by the generation of micro-scale bubbles around the AuNSs (Huang and El-Sayed, 2010). Similar *in vitro* studies have been performed for the treatment of cervical and breast cancer using the laser induced-bubbles produced by nanosecond laser pulses (Zharov *et al*., 2004, 2005). The treatment modality has since been demonstrated for *in vivo* tumour ablation in a rat cancer model (Hleb *et al*., 2008). Although visible light is successful in destroying cells labelled with spherical-shaped AuNPs, for a more practical application of PTT, deep tissue penetration is required. Near-infrared (NIR) external radiation is capable of achieving this, such that it can penetrate up to 10cm in soft tissues at the NIR tissue transmission window, 650–900nm (Weissleder, 2001).

1.8.3.3.2. Au nanorod-based PTT

The increase of PTT nanosystems in recent years is largely attributed to the emergence of the AuNRs. Due to their non-spherical geometry, AuNRs have both transverse and longitudinal plasmon (Pérez-Juste *et al*., 2005). Their absorption profile includes two absorption bands: one due to light absorbed along the short axis (transverse) and the other due to absorption along the long axis (longitudinal). As the rod length increases, so does the longitudinal band red shift together with an increase in the extinction coefficient (Fratoddi *et al*., 2015). The longitudinal plasmon wavelength is approximately linearly dependent on the length-to-diameter ratio,

which is usually called the aspect ratio (Ni *et al*., 2008). The aspect ratio of the AuNRs can be varied from low to high in order to tune their peak optical absorption wavelength. By changing the shape and composition of the nanoparticle to rod-shaped, the surface plasmon absorption can be shifted into the NIR transmission window (Chen *et al*., 2007 & Wiley *et al*., 2007).

AuNR-based PTT was first reported in 2006, where mAb-conjugated AuNRs were applied to selectively eliminate cancer cells through efficient photothermal conversion (Huang *et al*., 2006). Since then, great efforts have been expended on this aspect, including both *in vitro* and *in vivo* photothermal heating and theoretical modelling to study the PTT performance and the design of more effective PTT agents (Huang *et al*., 2010 & Zhang *et al*., 2014). For example, a computationally guided photothermal tumour therapeutic method that combined the quantitative bio-distribution data of AuNRs with computational modelling enabled photothermal temperature gradients in three-dimensional tissues (von Maltzahn *et al*., 2009). In addition, owing to the advantage of conjugation with cancer targeting moieties, AuNRs have been widely used in the precise control of drug delivery in cells. A controlled delivery was demonstrated by encapsulating AuNRs in protein-shell microbubbles (AuMBs) and then modifying the AuMBs with anti-VEGFR2 to target angiogenesis markers (Wang *et al*., 2014). The AuMBs were destroyed by ultrasound to release the AuNRs and then PTT was activated. The ultrasound-induced MB disruption enhanced the cellular delivery and therapeutic effects of AuNRs (Wang *et al*., 2014).

Initially, several reports concerning the mechanism of PTT were only conducted *in vitro* and focus on a single protein or pathway. To better understand the cellular responses to PTT, systematic *in vivo* studies have been conducted. One such study showed that rifampicin (RF)-targeting enhanced entry of AuNRs into cells and a decrease in exocytosis from the cells (Ali *et al*., 2014). Enhanced PTT effect of RF-conjugated AuNRs in xenograft mice was due to cytochrome c and p53-related apoptosis mechanisms (Ali *et al*., 2017). There was no long-term (15-month) toxicity of the AuNRs *in vivo*. Together, these data demonstrate that the AuNRs-PTT platform

is effective and safe for cancer therapy in mouse models. These studies provide a strong framework for the translation of PTT to clinical studies.

1.9. Aim(s) and objectives of the study

1.9.1. Aim(s)

The aim of the study was to develop a nanoparticle-based targeted drug delivery system using peptide-directed AuNRs as a delivery vehicle and to evaluate whether photothermal therapy could enhance the therapeutic effect of the AuNRs on cancer cells.

1.9.2. Objectives

- To synthesise, functionalise and characterise AuNRs via the seed-mediated method.
- To identify PHB-expressing cells via immunocytochemistry.
- To evaluate the cytotoxic effects of the PHB-targeted-nanotherapy on PHB expressing cancer cells
- To investigate whether laser treatment would enhance the PTT effect of the PHB-targeted AuNRs.

Chapter Two: Materials and methods

2.1. Reagents, Equipment and Suppliers

Table 2.1 Reagents and suppliers

Supplier	Reagent
Anaspec	Adipose Homing Peptide Sequence: $_D$(CKGGRAKDC)
Gibco	Foetal bovine serum (FBS) Penicillin/streptomycin Trypan blue stain (0.4%) Trypsin (2.5%)
GL Biochem	$_D$(KLAKKLAK)$_2$ peptide Sequence: $_D$(KLAKLAK)$_2$-DEVD-SH
BioLegend®	Purified rabbit anti-prohibitin antibody
Kimix	Nitric acid (HNO_3)
Life Technologies	Alexa-Fluor-488 secondary antibody
Lonza	Dulbecco's Modified Eagle's Medium (DMEM) DMEM: F12 Media Phosphate buffered saline (PBS)
Merck	Hydrochloric acid (HCl)
Prochimia Surfaces	PEG-OH, 2-{2-[2-(2-{2-[2-(1-mercaptoundec-11-yloxy) ethoxy]-ethoxy}-ethoxy)-ethoxy]-ethoxy}-ethanol [$C_{23}H_{48}O_7S$] PEG-biotin, N-(2-{2-[2-(2-{2-[2-(1-mercaptoundec-11-yloxy)-ethoxy]-ethoxy}-ethoxy)-ethoxy]-ethoxy}-ethyl) biotinamide [$C_{33}H_{63}N_3O_8S_2$]
Roche	Bovine serum albumin (BSA) Insulin Water-soluble Tetrazolium, 2-(4-Iodophenyl)-3-(4-nitrophenyl)-5-(2,4disulfophenyl)-2H-tetrazolium [WST-1]
Sigma-Aldrich	L-Ascorbic acid

	Streptavidin Cetyl trimethylammonium bromide Sodium borohydride Gold (III)chloride trihydrate Dimethyl sulphoxide (DMSO) Hydrocortisone Flouroshield^{TM} with Dapi Paraformaldehyde Human *Epidermal growth factor* (EGF) Silver nitrate ($AgNO_3$)

Table 2.2: Equipment used

Supplier	Instrument
American Instrument Exchange, Inc.	Sorvall TC6 centrifuge H 400
Carl Zeiss	TEC NAI F20 TEM microscope LSM 780 Confocal microscope
Lasec	BASIC 20 pH-Meter
BMG LABTECH	POLAR star Omega Microplate reader
BD Biosciences	BD CSampler™ Flow Cytometer
Eppendorf	Eppendorf 5417 R microcentrifuge with rotor F45-3011
Invitrogen	Countess™ Automated cell counter
Labnet international Inc.	Vortex Mixer
Leica	Leica Bond Autostainer
Malvern	Zeta Sizer Nano Series
Nikon TMS-F	Inverted light Microscope
Qianbaihe Trading (Wuhan) Co., Ltd.	780nm (100mW) Infrared Laser Diode Module Dot
Thermo Fisher Scientific	Water Jacked CO_2 incubator
Varian	Varian 710-ES ICP Optical Emission Spectrometer

2.2. Research methodology

2.2.1. Synthesis of AuNRs

AuNRs were prepared by the seed-mediated growth method in aqueous solutions through changing the seed-to-Au (III) ions ratio in the growth solution, following a method adapted from Jia *et al*. (2015). Cetyltrimethylammonium bromide (CTAB) was employed as the stabilizing surfactant. CTAB was dissolved by heating to 50°C while stirring and then cooling the solution to 25°C prior to use.

2.2.1.1. Preparation of the seeding solution

The seed solution was made by adding 0.6ml of ice cold freshly prepared Sodium borohydride ($NaBH_4$) (0.01M) (Sigma – Aldrich) to a solution composed of 0.25ml Gold (III) chloride trihydrate ($HAuCl_4$) (0.01M) (Sigma – Aldrich) and 9.75ml of CTAB (0.1M) (Sigma – Aldrich). The resultant solution was stirred vigorously for 2min then left undisturbed at room temperature for 2-4hrs, until solution changed colour from yellow to pinkish/brown (Figure 2.1).

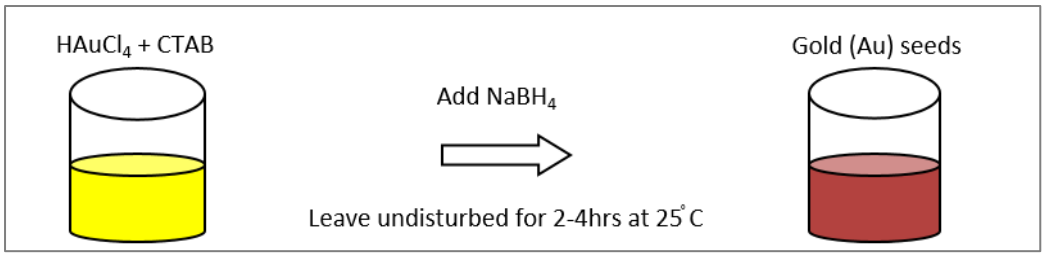

Figure 2.1: Schematic for preparation of AuNR seeds.

Note: The seeding solution was always freshly prepared before every AuNR synthesis.

2.2.1.2. Preparation of the growth solution

The growth solution was prepared by the sequential addition of 0.5ml $HAuCl_4$ (0.01M), 0.1ml Silver nitrate ($AgNO_3$) (0.01M) (Sigma – Aldrich) and 0.2ml Hydrochloric acid (HCl) (1M) (Merck) to CTAB (0.1M) as depicted in Table 2.3. The volume of CTAB varied depending on the seed-to-Au (III) ions ratio in the growth solution. The ratios are named GmSn, where G denotes the growth solution, S refers to the seed solution, m is the volume of the surfactant solution i.e. CTAB used in preparing the growth solution with the volumes of the other ingredient solutions kept unchanged, and n is the volume of the seed solution (Jia *et al*., 2015). The units of m and n are both ml. Three ratios were used in this study i.e. G6S4, G8S2 and G9S1. A freshly prepared 0.08ml ascorbic acid solution (0.1M) (Sigma – Aldrich) was added while stirring the solution rapidly. Once the solution became colourless, seed solution was added while the mixture was vigorously stirred. The resultant solution was stirred for 2min and left undisturbed at 25°C overnight. The appearance of a wine red colour after 24hrs indicated the formation of AuNPs as shown in Figure 2.2.

Table 2.3: The volumes (ml) of solutions used for the preparation of the AuNR growth solution

Solutions use for the preparation of the growth solution	AuNR preparations		
	G6S4	**G8S2**	**G9S1**
$HAuCl_4$ (0.01M),	0.5	0.5	0.5
$AgNO_3$ (0.01M)	0.1	0.1	0.1
HCl (1M)	0.2	0.2	0.2
Ascorbic acid (0.1M)	0.08	0.08	0.08
CTAB (0.1M)	6	8	9
Au Seed	4	2	1

Note: G = growth solution, S = the seed solution, m = volume of CTAB (ml) and n = volume of the seed solution (ml)

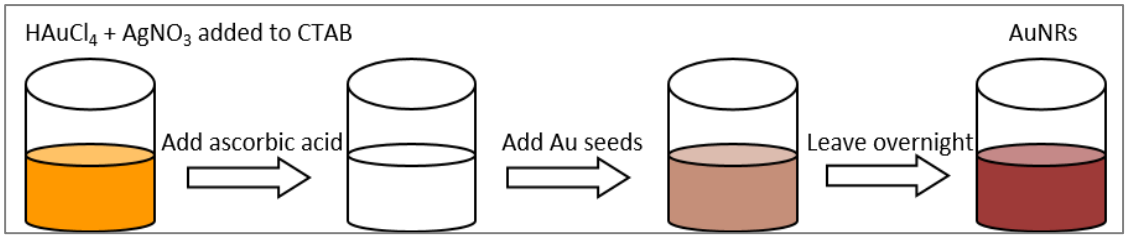

Figure 2.2: Schematic for the preparation of CTAB-capped AuNRs.

The final reaction mixture for AuNR synthesis contains the desired AuNRs as well as a variety of AuNPs of different shapes (spherical, cubic, *etc.*) as shown in Figure 2.3. To obtain a homogeneous population of AuNRs, two cycles of centrifugation were carried out. After the synthesis, all reaction products (spheres, cubes, and rods) were first isolated and purified from the excess CTAB through centrifugation at high rpm (10600 rpm) using a bench top centrifuge (Eppendorf 5417 R microcentrifuge with rotor F45-30-11). Then, AuNR separation was afforded through a second cycle of centrifugation (6000 rpm)(Eppendorf 5417 R microcentrifuge with rotor F45-30-11) adapted from the method reported by Scaletti *et al.* (2014).

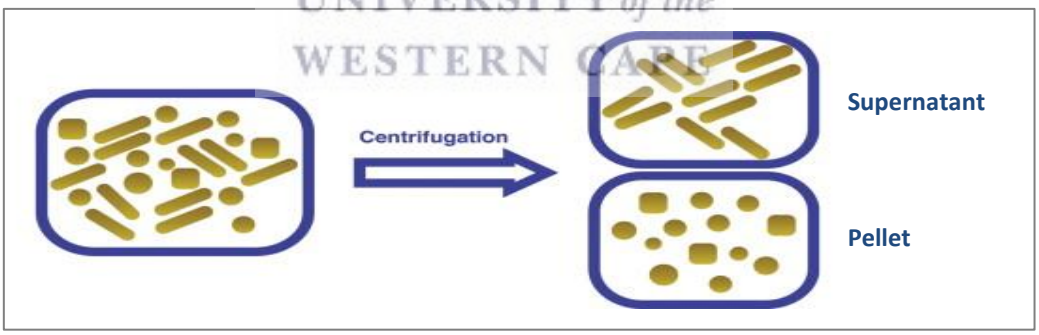

Figure 2.3: Separation of AuNR from other shapes by differential centrifugation.

2.2.2. Functionalization of AuNRs

The CTAB stabilized AuNRs were bi-functionalised by conjugating the targeting (AHP) peptide, sequence: $_{D}$(CKGGRAKDC) (Anaspec) and therapeutic $_{D}$(KLAKLAK)$_2$ peptide, sequence: $_{D}$(KLAKLAK)$_2$-DEVD-SH (GL Biochem) to the NP through ligand exchange.

An aqueous solution containing AuNRs, PEG–OH (2-{2-[2-(2-{2-[2-(1-mercaptoundec-11-yloxy) ethoxy]-ethoxy}-ethoxy)-ethoxy]-ethoxy}-ethanol [$C_{23}H_{48}O_7S$] (Prochimia Surfaces), PEG–biotin (N-(2-{2-[2-(2-{2-[2-(1-mercaptoundec-11-yloxy)-ethoxy]-ethoxy}-ethoxy) ethoxy]-ethoxy}-ethyl) biotinamide [$C_{33}H_{63}N_3O_8S_2$](Prochimia Surfaces) and the KLAK peptides were stirred at 4°C for 24hrs. The ingredients were combined in the molar ratio of 9 ([PEG]–OH): 1 (PEG–biotin): 1 (peptide) according to Sibuyi *et al.* (2017) with slight modifications. A free thiol group in the cysteine residue at the C-terminal of the peptides (KLAK peptide and PEG–OH) facilitated its covalent attachment to the AuNR surface. The functionalised AuNRs were washed twice with dH_2O. The AHP peptide was conjugated to the AuNRs through biotin–streptavidin linkage. The biotinylated peptides and streptavidin (Sigma- Aldrich) were added to the AuNRs in a 1:1 molar ratio and stirred at 25°C for 1hr. The AuNRs were washed and re-suspended in dH_2O. The resulting AuNRs and acronyms used are shown in Table 2.4 and the expected AuNR designs are schematically shown in Figure 2.4.

Table 2.4: Description and characteristics of various gold nanorods.

AuNR conjugates	Acronym	Attached molecules			
		PEG-OH	PEG-Biotin	Biotin–AHP	KLA-DEVD-SH
AuNR-CTAB	G	-	-	-	-
AuNR-PEG	GP	+	+	-	-
AuNR-AHP	AG	+	+	+	-
AuNR-KLAK	GK	+	+	-	+
AuNR-AHP-KLAK	AGK	+	+	+	+

Note: AHP = $_D$(CKGGRAKDC) targeting peptide; KLAK = $_D$(KLAKLAK)$_2$-DEVD-SH therapeutic peptide; peptide, - = absence; + = presence. AuNR-CTAB = CTAB-coated AuNRs; AuNR-PEG = PEG-coated AuNRs; AuNR–AHP = AuNP with a targeting peptide; AuNP–KLAK = Nontargeted AuNP with therapeutic peptide; AuNP–AHP–KLAK = AuNP with AHP and therapeutic peptide (PHB-targeted nanotherapy).

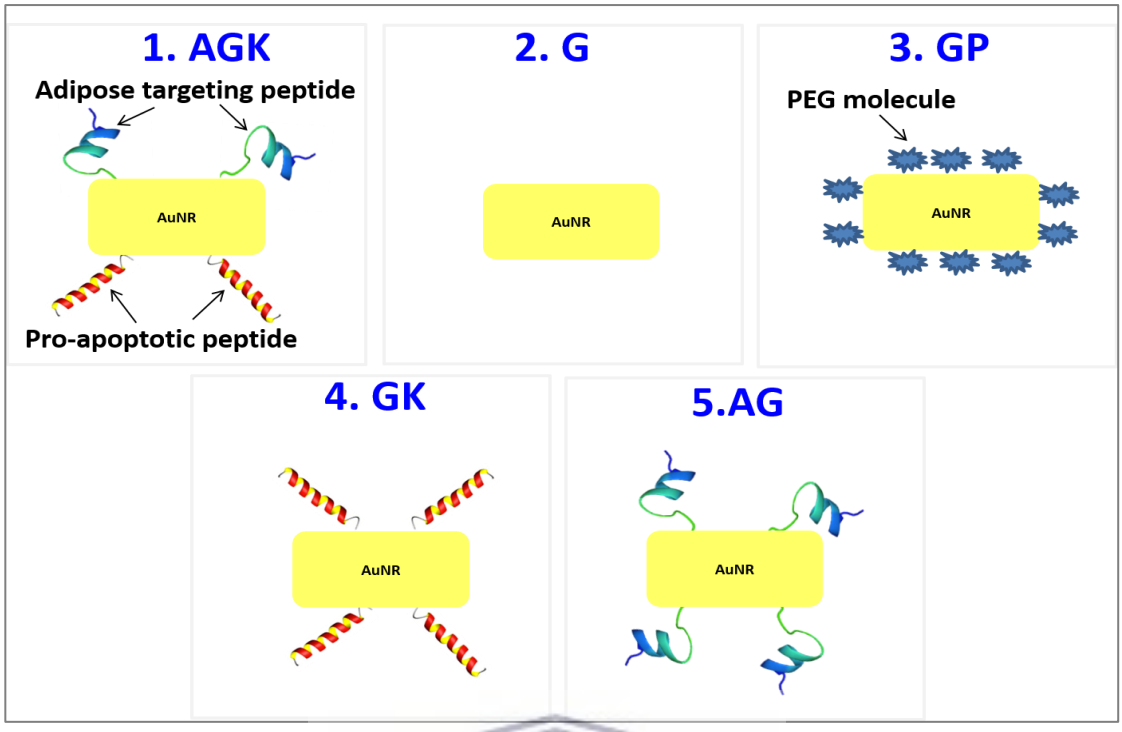

Figure 2.4: Schematic of the expected AuNP design. AGK = AuNRs has both targeting and therapeutic peptides, G = CTAB coated AuNRs, GP = pegylated AuNRs, GK = AuNRs with therapeutic peptide, and AG = targeted pegylated AuNRs.

2.2.3. Characterisation of AuNRs

2.2.3.1. Optical properties: UV-Vis spectroscopy

The resulting AuNRs were characterized after modification by UV-Vis absorption spectroscopy using a POLAR star Omega Microplate reader (BMG LABTECH) to study the peak absorption band (SPR) in a wavelength range of 350-1000nm.

2.2.3.2. Stability of AuNRs

The *in vitro* stability of the AuNRs in different buffer solutions was measured according to a protocol reported by Elbagory *et al.* (2016), with slight modifications. The AuNRs were incubated with six different buffer solutions i.e. 0.5% Bovine Serum Albumin (BSA) (Roche); 1X Phosphate buffered saline (PBS) [Lonza]; Dulbecco's Modified Eagle's Medium (DMEM) [Lonza]; 10% Foetal bovine serum (FBS) [Gibco];

DMEM [complete, containing 10% (FBS) and 0.1% Pen/Strep (Gibco)] and dH_2O. The pegylated AuNRs were centrifuged at 10000rpm using a bench top centrifuge (Eppendorf 5417 R microcentrifuge with rotor F45-30-11) for 15min. The pellets were washed three times with autoclaved dH_2O. The AuNRs were then re-suspended in 1ml dH_2O. The AuNRs and the buffer solutions were mixed in a 6:4 ratio in a 96-well plate and the stability of the AuNPs was evaluated by measuring the changes in UV-Vis spectra after 3, 6, 12 and 24hrs. The SPR of the AuNRs were measured using the POLAR star Omega Microplate reader.

2.2.3.3. Electrochemical charge of AuNRs

Zeta potential measurements of the AuNR conjugates were performed immediately after synthesis using a Malvern Zetasizer Nano ZS operating with a variable power (5–50mW) He-Ne laser at 633nm.

2.2.3.4. Size and morphology: High Resolution-Transmission Electron Microscopy (HR-TEM) and Energy Dispersive X-ray Spectroscopy (EDX) Analysis

To study the morphology of the AuNRs, HR-TEM micrographs were obtained on a field emission TEC NAI F20 TEM microscope (Carl Zeiss) [Physics Department, UWC]. Samples were prepared by drop-coating each test sample solution onto a copper (Cu) grid, supported by a thin film of amorphous carbon. This was then dried under a Xenon lamp for 10min and the samples were analysed under the microscope. Transmission electron micrographs were obtained in a bright field mode at an accelerating voltage of 200kV.

Energy Dispersive X-ray Spectroscopy (EDX) measures the elemental and chemical analysis of the nanomaterial being probed (Rao and Biswas, 2009). EDX was measured from the same samples used for HR-TEM. Energy dispersive X-ray spectra

were measured using an EDAX liquid nitrogen cooled Lithium doped Silicon detector connected to the TEM.

2.2.4. Cell culture

The cell lines (Table 2.5) used in this study were obtained from the American Type Culture Collection (ATCC). Vials containing the frozen cells were removed from the -120˚C freezer and allowed to thaw at 25˚C. The cells were transferred into a 15ml tube containing complete media (pre-warmed to 25˚C) with respective supplements (Table 2.5) and centrifuged at 3000rpm in a bench top Sorvall TC6 centrifuge H400 for 5min. The supernatant was discarded and the cell pellet was re-suspended in their respective supplemented media. The cells were cultured in 25cm^2 cell culture flasks (SPL Life Sciences) which were incubated in a water-jacketed CO_2 incubator (Thermo Fisher Scientific) at 37˚C and 5% CO_2. The cell culture medium was changed every third day until the cells reached 70-90% confluency. The procedures were performed in the Biological Safety Cabinet (Laminar flow) using aseptic techniques.

Table 2.5: Human cell cultures used in this study.

Tissue origin	Acronym	Disease	Growth media	Supplements
Colon	Caco-2	Colorectal Adenocarcinoma	DMEM	1% pen/strep 10% FBS
Lung	A549	carcinoma	DMEM-F12	1% pen/strep 10% FBS
Ovary	Caov-3	Adenocarcinoma	DMEM	1% pen/strep 10% FBS
Ovary	SKOV-3	Adenocarcinoma	RPMI	1% pen/strep 10% FBS
Cervix	Ca Ski	Epidermoid Carcinoma	RPMI	1% pen/strep 10% FBS

Liver	Hep G2	Hepatocellular carcinoma	DMEM	1% pen/strep 10 % FBS
Prostate	LNCaP	Carcinoma	RPMI	1% pen/strep 10 % FBS
Breast	MCF7	Adenocarcinoma	DMEM	1% pen/strep 10 % FBS
Prostate	PC-3	Grade IV adenocarcinoma	RPMI	1% pen/strep 10% FBS
Breast	MCF-12A	Epithelial spontaneous immortalization	DMEM-F12	1% pen/strep, 10% FBS, 10µg/ml Insulin, 500ng/ml Hydrocortisone and 20ng/ml EGF
Kidney	HEK-293	Spontaneous transformation with adenovirus 5 DNA	DMEM	1% pen/strep 10% FBS
Brain	U87	Glioblastoma	DMEM	1% pen/strep 10% FBS
Lung	H157	Squamous cell carcinoma	RPMI	1% pen/strep 10% FBS

2.2.4.1. Sub-culturing of cells

Once the cells had reached 70-80% confluency, the medium in the flask was decanted. Thereafter, the cells were washed with PBS. The PBS was then discarded and the cells were trypsinized by adding 3ml 2X trypsin (Gibco) to the flask, which was then incubated at 37˚C for 1-3min. The detachment of the cells from the flask was periodically inspected using a Nikon TMS-F light microscope. As soon as the cells

start to round up, the detachment was facilitated by gently tapping of the flask on a hard surface to dislodge the cells. Twice the volume (6ml) of medium was added to the flask to inactivate the trypsin. The cells were then transferred to pre-labelled 15ml conical tubes and centrifuged at 3000rpm in a bench top Sorvall TC6 centrifuge H400 for 5min. The supernatant was discarded and the cells were re-suspended in 1-5ml complete media.

2.2.4.2. Cell count: Trypan Blue Exclusion Assay

Cell count was determined using the trypan blue exclusion assay following the manufacturer's instructions. Briefly, a 10µl aliquot of the cell suspension was mixed with an equal volume of 0.4% trypan blue dye (Gibco). The mixture was loaded into a Countess™ chamber slide (Life technologies). The number of viable cells was assessed using the Countess® Automated Cell Counter (Invitrogen), as described by the manufacturer.

2.2.4.3. Storage of cells

The cells were trypsinized as described in Section 2.2.4.1. The cells were recovered by centrifugation and re-suspended in complete medium containing 10% Dimethyl sulphoxide (DMSO) (Sigma-Aldrich). The cell suspension was aliquoted into 2ml cryo-vials and stored at -120˚C until further use.

2.2.5. Localization of PHB expression using immunocytochemistry (ICC)

2.2.5.1. Chromogenic staining

2.2.5.1.1. *Cell fixation*

The cells were cultured on glass slides (76mm x 26mm; 1.0mm to 1.2mm thick) at 37°C until 80% confluency was reached. The cells were washed three times (3min for each wash) with 1X PBS. The cells were then fixed in 4% paraformaldehyde (PFA) (Sigma – Aldrich) at 25°C for 20min. Following fixation, the cells were washed three times (3min for each wash) with 1X PBS.

2.2.5.1.2. *Immunocytochemical Staining*

Immunocytochemical (ICC) staining was performed at The National Health Laboratory Services at Tygerberg Hospital. The cancer cells (Caco-2, PC-3, U-87, A549, Ca0v-3, Caski, H157, Hek-293, Hep-G2, LnCap, MCF-7 and SKOV-3) were stained with purified rabbit anti-prohibitin antibody (1:100 dilution) (Biolegend). All staining, washing and antibody incubations were performed in a Leica Bond Autostainer (Leica), following the steps shown in Table 2.6.

Table 2.6: The ICC staining protocol.

Step	Type	Incubation Time (min)	Temperature	Dispense Type
1	Peroxide Block	5	Ambient	Selected vol.
2	Bond Wash Soln	0	Ambient	Selected vol.
3	Bond Wash Soln	0	Ambient	Open
4	Bond Wash Soln	15	Ambient	Selected vol.
5	Primary Antibody	0	Ambient	Selected vol.
6	Bond Wash Soln	0	Ambient	Selected vol.
7	Bond Wash Soln	0	Ambient	Selected vol.
8	Bond Wash Soln	8	Ambient	Selected vol.
9	Post Primary	2	Ambient	Selected vol.
10	Bond Wash Soln	2	Ambient	Selected vol.
11	Bond Wash Soln	2	Ambient	Selected vol.

12	Bond Wash Soln	8	Ambient	Selected vol.
13	Polymer	2	Ambient	Selected vol.
14	Bond Wash Soln	2	Ambient	Selected vol.
15	Bond Wash Soln	0	Ambient	Selected vol.
16	Deionized water	10	Ambient	Selected vol.
17	Deionized water	0	Ambient	Selected vol.
18	Mixed DAB refine	0	Ambient	Selected vol.
19	Deionized water	0	Ambient	Selected vol.
20	Deionized water	5	Ambient	Selected vol.
21	Deionized water	0	Ambient	Selected vol.
22	Hematoxylin	0	Ambient	Selected vol.
23	Deionized water	0	Ambient	Selected vol.

2.2.5.1.3. *Rehydration*

After the staining procedure, the samples were rehydrated and cleared manually using the steps outlined in Table 2.7. Images were then taken at the Department Medical Biosciences (UWC) with an inverted light microscope (Nikon TMS-F) at 40X magnification.

Table 2.7: The rehydration protocol

Step	Solution	Duration
1	70% Alcohol	5 Dips
2	70% Alcohol	5 Dips
3	70% Alcohol	5 Dips
4	70% Alcohol	5 Dips
5	70% Alcohol	5 Dips
6	Xylene	Dip for 1min
7	Xylene	Dip for 1min

2.2.5.2. Immunofluorescence

2.2.5.2.1. *Fixing of cells*

The cancer cells (Caco-2, PC-3 and U-87) were cultured onto sterilised coverslips in 6-well plates at a cell density of 2 x 10^5 cells/ml. The plates were placed in a water-jacketed CO_2 incubator at 37˚C and the cells were cultured until they reached 50–60% confluency. The media was removed from the cells and washed twice with 1X PBS. The PBS was then discarded and the cells were fixed with 4% PFA for 10min at 25˚C. The cells were washed twice with 1X PBS.

2.2.5.2.2. *Antibody binding and microscopy*

The coverslips containing the fixed cells were incubated at 4˚C for 1hr in blocking buffer (1X PBS, containing 0.5% BSA). The cells were washed thrice with 1X PBS. The cells were incubated in purified rabbit anti-prohibitin antibody (diluted 1:100 in blocking buffer) at 4°C overnight. The cells were washed thrice in 1X PBS for 5min and then incubated in anti-rabbit Alexa Fluor-488–secondary antibody (diluted 1:1000 in blocking buffer) (Life technologies) at 4°C for 2hrs. The cells were washed thrice with 1X PBS. The coverslips were transferred onto the microscope slides containing Fluoroshield DAPI mounting media (Sigma – Aldrich). The images were captured at 60X magnification under oil immersion using the fluorescent Carl Zeiss LSM 780 Confocal microscope with Elyra S.1 super resolution platform (Carl Zeiss) at the Central Analytical Facility Imaging Unit at Stellenbosch University.

2.2.6. Therapeutic potential of the targeted nanotherapy

2.2.6.1. Effect of the AuNRs on cell proliferation: WST-1 Assay

The cytotoxicity of the AuNRs was evaluated using water-soluble tetrazolium salts (WST) -1 cell proliferation reagent as described by the manufacturer (Roche). The cells (Caco-2, PC-3, U-87 and MCF-12A) were seeded at a density of $1x10^5$ cells/well in a 96 well plate (100µl/well). The cells were incubated at in a water-jacketed CO_2 incubator at 37˚C and 5% CO_2. After 24hrs, the media was removed from each well and replaced with 100µl fresh media containing increasing concentrations of the AuNR conjugates ranging from 3µg/ml to 1000µg/ml. All treatments were done for 24hrs in triplicate. The untreated cells served as negative controls, while cells treated with 6% DMSO served as a positive control as DMSO above 4% has a toxic effect on mammalian cells according to literature (Vergara *et al*., 2014 & Siddiqui *et al*., 2016). After 24hrs, 10µl WST-1 cell proliferation reagent was added to all the wells. Additional wells containing the same range of AuNR concentrations was used to determine if there was interference of the AuNR with the assay. The plate was covered in foil and the cells were incubated at 37°C for 3hrs and then placed on a shaker for 1min.

The absorbance of the formazan product formed was measured at 440nm using a PolarSTAR Omega plate reader. Absorbance readings at 630nm were measured and used to eliminate background. The percentage of cell viability was calculated as shown using the formula below.

$$\text{Cell viability (\%)} = \frac{\text{Test absorbance at 440nm - Absorbance at 630nm}}{\text{Negative control absorbance at 440nm - Absorbance at 630nm}} \text{ X 100}$$

2.2.6.2. Quantification of cellular uptake of AuNR

The amount of AuNRs taken up by cells was quantified by Inductively Coupled Plasma Optical Emission Spectroscopy (ICP-OES). Caco-2 cells were seeded in 12 well cell culture plates (Sigma). After reaching 80% confluence, the cells were treated with 500µl of 200µg/ml of pegylated NRs (GP) and NRs functionalised with targeting and therapeutic peptides (AGK). The untreated cells and cells treated with 6% DMSO were included as negative and positive controls, respectively. After 24hrs, the cells were detached using 2X trypsin and transferred into the corresponding 15ml tubes. The cells were centrifuged at 3000rpm in a bench top Sorvall TC6 centrifuge for 3min, the pellet was washed once with 2ml 1X PBS. The samples were digested by incubation at 90°C for 2hrs in 2ml Aqua Regia solution (3:1 HCl: HNO_3 (Kimix)). Thereafter the samples were diluted to 10ml with 2% HCl. In order to calculate the percentage of AuNRs taken up by cells, the concentration of Au present in a 500µl of 200µg/ml preparation of AGK and PG needed to be established. This was done by centrifuging a 500µl aliquot (at a concentration of 200µg/ml) of the AGK and PG AuNPs at 10 000rpm using a bench top centrifuge (Eppendorf 5417 R microcentrifuge with rotor F45-30-11). The pellet was also digested by incubation at 90°C for 2hrs in 2ml aqua regia solution, which was then diluted to 10ml with 2% HCl. At this stage, the cell suspension could be stored at −20°C until analysis. These samples were analysed for total gold content by a Varian 710-ES ICP Optical Emission Spectrometer (Varian) at the Chemistry Department (University of the Western Cape). The measurement was repeated 3 times for each sample submitted, the values reported were based on a calibration curve using a gold ICP standard (Sigma - Aldrich). The formula below was used to calculate the percentage of gold internalized by the cells:

$$\text{Particles internalized by cells (\%)} = \frac{\text{Gold detected in the treated cells}}{\text{Gold detected in 500µl aliquot}} \times 100$$

2.2.6.3. Analysis of apoptotic cell death using the APOPercentage™ Assay

The APOPercentage™ apoptosis assay (Biocolor, UK) was used to quantify the percentage apoptotic cells using the protocol described by Meyer *et al*. (2008). The cells were seeded in 12 well cell culture plates at a density of $2x10^5$ cells/ml. The cells were incubated for 24hrs at 37°C. The culture media was then removed and replaced with media containing 200µg/ml of the AuNRs. The cells were incubated for 24hrs at 37°C. Untreated and cells treated with 6% DMSO served as negative and positive controls, respectively. The cells were detached using 2X trypsin and transferred to their corresponding tubes. Cells were harvested by centrifugation at 3000rpm in a bench top Sorvall TC6 centrifuge H400 for 5min at 25°C. The supernatant was discarded and the pellet was gently re-suspended in 250µl APOP*ercentage*™ dye (diluted 1:160 in growth medium). The cells were incubated for further 30min at 37°C. PBS (2ml of 1X concentration) was then added to each tube, which was centrifuged at 3000rpm in a bench top Sorvall TC6 centrifuge H400 for 5min at 25°C. The supernatant was discarded and the cell pellets were re-suspended in 300µl of 1X PBS. Cell staining was measured using the BD Accuri flow cytometer (BD Biosciences). Acquisition was done in log mode and a maximum of 10000 to 30000 events per sample were acquired and analysed using the BD CSampler software.

2.2.6.4. Photothermal therapy

Caco-2 cells were seeded in 96-well cell culture plates at a density of $1x10^5$ cells/ml and incubated for 24hrs at 37°C. The culture media was then removed and replaced with media containing 500µg/ml of the AuNRs containing the targeting peptide (AG). The cells were then incubated for 30min at 37°C to allow for uptake of the AuNR. The negative (untreated) and positive (6% DMSO) controls were included. Following incubation, the cells were washed with 1X PBS and HAMS-F12 media was added to the cells to avoid interference of phenol red in DMEM. Two areas of the wells were exposed to a 780nm (100mW) Infrared Laser Diode Module Dot with Adapter,

6x68mm Focusable (Qianbaihe Trading (Wuhan) Co., Ltd.), with an exposure time of 30sec to 15min. Following exposure, the media was replaced with DMEM and incubated at 37°C for further 24hrs. Following incubation, cell viability was assessed by the WST-1 assay as described in Section 2.2.6.1.

2.2.6.5. Statistical analysis

Statistical and multiple-comparison analyses were performed within each group of cell viability assays performed in this study. Data were expressed as the mean ± standard deviation of the three replicates. Statistical analysis was conducted using the GraphPad Prism 6 and two-tailed Student's *t*-test. Differences among three or more groups were analyzed by two-way analysis of variance. Differences with $p < 0.05$ were considered to be statistically significant.

Chapter Three: Synthesis and characterization of peptide functionalised gold nanorods

3.1. Introduction

AuNPs have been applied in several industrial and biomedical procedures in the recent past. The versatility of AuNPs depends on their physicochemical properties that can be fine-tuned in order to facilitate their applications in diagnostics and therapeutics (Elder *et al*., 2007 & Dykman and Khlebtsov, 2011). The usefulness of AuNPs depends on their physical, chemical, electronic and optical properties, which hinges on the synthetic design which require considerable control of their composition, size, shape, stability and dispersion properties (Sosibo *et al*., 2015).

Although some studies suggest that gold is biologically inert (Brown *et al*., 2008), the physicochemical properties of AuNPs have been associated with undesirable adverse effects on biological systems (Smolkova *et al*., 2015). Several independent *in vitro* and *in vivo* studies have demonstrated the toxicity of AuNPs (Söderstjerna *et al*., 2014 & Wan *et al*., 2015). However this toxicity can be exploited if channelled to specific cells by modifying the AuNP surface with biomolecules to facilitate their target specific uptake through targeted delivery (Kumar *et al*., 2012). The use of AuNPs as drug delivery vehicles has shown great potential in pre-clinical studies, which have demonstrated that AuNP/biomolecule or AuNP/drug conjugates are more efficient than the biomolecules or drugs on their own (Tomuleasa *et al*., 2012 & Li *et al*., 2016).

In the current study a PHB-targeted nanotherapy was developed by conjugating a pro-apoptotic $_{D}(KLAKLAK)_{2)}$ and a PHB-targeting (AHP) peptide to AuNRs. A recent study by Sibuyi *et al*. (2017) showed that gold nanospheres (AuNSs) functionalised with these two peptides successfully induced apoptosis in Caco-2 cells, which express AHP, the target for PHB. The same strategy was used in this study. However, the shape of the AuNP was changed from AuNSs to gold nanorods (AuNR) in order to

exploit the photothermal (PTT) potential of nanorods for the elimination of cancer cells. The unique plasmonic properties of AuNRs can be exploited in PTT by coherently photo-exciting their conduction electrons to induce surface plasmon oscillations. Upon surface plasmon formation, nonradiative relaxation occurs where the electrons return to a less active state, and the energy is released as a phonon that then generates localized heat that can be transferred to the surrounding environment (Hartland, 2011). AuNRs exhibit better NIR absorption cross-section than any other AuNPs (Hu *et al*., 2006) and demonstrate extremely efficient NIR induced PTT heat conversion (von Maltzahn *et al*., 2009). AuNRs with a length of 40nm, a diameter of 10nm and a longitudinal plasmon resonance of approximately 800nm is most commonly used for PTT (Ni *et al*., 2008; Chen *et al*., 2010).

This chapter reports on the synthesis of AuNRs that were functionalised with two peptides [a targeting peptide, AHP, and a pro-apoptotic peptide, $_{D}(KLAKLAK)_2$. The design (Figure 3.1) of the AuNRs was based on two previous studies (Sosibo *et al*., 2015 & Sibuyi *et al*., 2017). AuNR were synthesised using the seed-mediated growth method. Naked AuNRs tend to be unstable in organic solvents, therefore, to prevent aggregation in solution PEG molecules were used as a stabilizer and emulsifying agent. Encapsulation of the metal core with PEG creates a dielectric shell around the metal core, this provides means of protection for the AuNRs from the surrounding environment or opsonisation when used in biological systems. The AuNRs were stabilised by pegylation using a mixture of SH-PEG-OH and SH-PEG-Biotin as described by Sosibo *et al*. (2015). The thiol (SH) group on SH-PEG-OH and SH-PEG-Biotin facilitated the conjugation of PEG to the AuNR surface. The $_{D}(KLAKLAK)_2$ peptide was similarly thiolated to facilitate conjugation to the AuNR surface as described by Sibuyi *et al*. (2017), while AHP contained a streptavidin tag to facilitate binding of the peptide to PEG-Biotin. Using this design strategy, four different types of AuNRs samples (GP, AGK, GK and AG) were synthesised as shown in Figure 3.1.

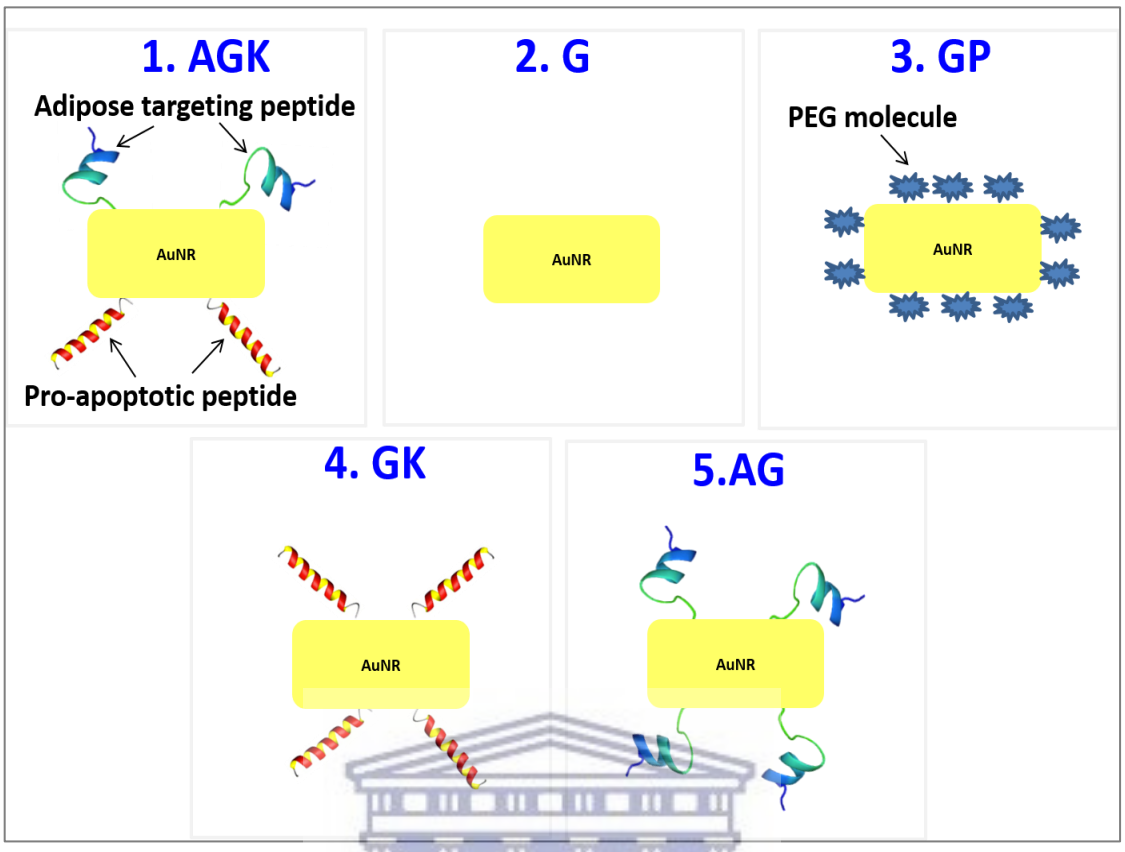

Figure 3.1: Schematic of the AuNP design. AGK = AuNRs functionalised with both targeting (AHP) and therapeutic ($_D$(KLAKLAK)$_2$) peptides, G = AuNRs before functionalization, GP = pegylated AuNRs, GK = AuNRs functionalised with the $_D$(KLAKLAK)$_2$ peptide only and AG = AuNRs functionalised with the AHP peptide only.

3.2. Results and Discussion

3.2.1. Synthesis of AuNRs

AuNR samples were prepared by the seed-mediated growth method using CTAB as the stabilizing surfactant as described in Chapter 2 (Section 2.2.1). The seed-mediated growth method consists of two steps, i) symmetry breaking of Au which involves nucleation, growth and the development of facets and ii) binding of the surfactant (i.e CTAB) to the facets as depicted in Figure 3.2. Briefly, during the first step, gold salt ($HAuCl_4$) is reduced using a strong reducing agent, such as sodium borohydride ($NaBH_4$) to form faceted AuNSs with an average diameter of 3nm (Figure 3.2). The final step involves placing the AuNS seeds in $HAuCl_4$ solution and a mild reducing agent (ascorbic acid) to grow into AuNRs. The CTAB surfactant (capping

agent) and Ag (shape directing agent) selectively adsorb on the side facets of the AuNRs (Abtahi, 2013). CTAB forms a micellar bi-layer around side facets of AuNRs (Nikoobakht and El-Sayed, 2001). This bilayer formation blocks and slows down the growth of side facets in the transverse axis while tip facets are not covered and can grow rapidly in the longitudinal axis (Abtahi, 2013).

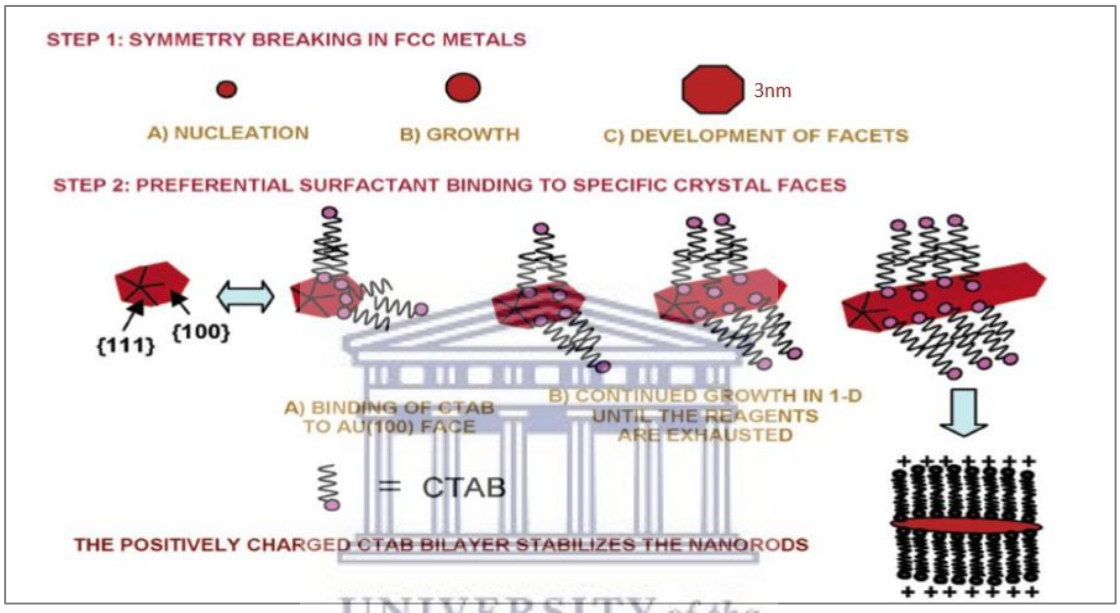

Figure 3.2: AuNR formation using the seed-mediated technique. Seeds of Face Centre Cubic (FCC) metals such as Au, undergo a process of nucleation, growth and develop facets before forming rod-shapes. Once the basic structure is formed, CTAB and ascorbic acid bind to the surface, enabling AuNR stability and growth along the longitudinal axis (Murphy et al., 2005).

3.2.2. Tuning of AuNR size

A fascinating feature of AuNRs is that their plasmonic properties can be tailored by synthetically tuning their size. Of all parameters involved in the synthesis process, the seed-to-Au (III) ions ratio in the growth solution has the most significant effect on the size of the AuNRs (Sau and Murphy, 2004 & Jia *et al*., 2015). Since the ultimate goal of this study is to produce AuNRs that can be used for PTT, it was crucial to synthesise AuNRs that can efficiently absorb NIR light. Previous studies have shown that AuNRs become absorption-dominant if their diameters are less than 10nm (Ni *et al*., 2008 &

Chen *et al*., 2010). Jia *et al*. (2015) demonstrated the size of the synthesised AuNRs usually decreases as the seed concentration is increased at a given concentration of Au (III) ions. This is because of a decreased number of available Au (III) ions per seed particle.

3.2.2.1. Characterisation of AuNRs

3.2.2.1.1. Optical properties of AuNRs

UV-Vis absorbance spectroscopy is one of the most widely used techniques for the characterization of AuNPs. In this technique light with different wavelengths is passed through the sample and its incident and transmitted intensities are measured (Mehta, 2012). For the purpose of this study, the UV-Vis absorbance of AuNRs produced at different seed-to-Au (III) ion ratios were studied at an incident wavelength spectrum of 200 to 1100nm. The UV-Vis absorption spectrum of a typical AuNR suspension shows two absorption peaks whereas only one peak is generated for a suspension for AuNS (Haiss *et al*., 2007). The first peak (at the lower wavelength) is called the transverse plasmon wavelength (λ_T) and the second peak (at the higher wavelength) is called the longitudinal plasmon wavelength (λ_L). The aspect ratio (nanorod length divided by its width) is a function of the λ_L peak of AuNRs. Narrow NRs, which produce the λ_T peak at a short wavelength and a λ_L peak that is shifted far into the NIR region of the electromagnetic spectrum will have a higher aspect ratio (Haiss *et al*., 2007). The standard aspect ratio for AuNRs is 3 to 5. AuNRs with a higher aspect ratio will absorb NIR more efficiently.

AuNP synthesis was done at three different seed-to-Au (III) ion ratios to produce three different AuNR preparations (G6S4, G8S2 and G9S1) as described in Chapter 2 (Section 2.2.1). They are named based on GmSn, where G denotes the growth solution, S refers to the seed solution, m is the volume (ml) of CTAB used in preparing the growth solution and n is the volume (ml) of the seed solution. Figure 3.3 shows the normalized extinction spectra of the AuNR samples prepared with CTAB and all

three samples clearly exhibit two plasmon resonance peaks. The three AuNR preparations produced a similar traverse band at 505nm, while the λ_L bands differed between the AuNR preparations. G6S4, G8S2 and G9S1 produced λ_L peaks at 705, 730 and 800nm, respectively. The peak intensity of the absorbance for the λ_L peak (which was approximately 0.3units) for G6S4 AuNPs was not much different from the peak intensity of the absorbance for the λ_T peak. Conversely, the peak intensity of the absorbance for the λ_L peak for G8S2 and G9S1 was higher (0.7 and 1.12units, respectively) than the absorbance for the λ_T peak. These properties are summarised in Table 3.1.

Figure 3.3 indicates that as the amount of seed in the growth solution is increased, the λ_L peak of the AuNR samples is gradually shortened from 800nm (G9S1) to 730nm (G8S2) to 705nm (G6S4). Jia *et al*. (2015) explained that this essentially means that the λ_L peak blue shifts (shifts to the left) as the seed amount is increased. Theoretically, adding more seeds to the growth solution should mean there are more seeds present in the system for growth, resulting in more nanorods grown. However, there is a limiting $HAuCl_4$ concentration for rod growth (Sau and Murphy, 2004). Once all the Au (III) ions in the growth solution is depleted by ascorbic acid, the nanorod growth process stops. As a result, the excess seeds in the growth solution grow into large spheres instead of rods, causing a drastic blue shift of the λ_L peak (Ward *et al*., 2014). The λ_T peak however, is insensitive to the amount of seed solution added, which is indicated by the consistent absorbance peak at 505nm for all three samples. Furthermore, the larger λ_L peak for G9S1, compared to the other two samples, suggests that the yield of AuNRs in this sample is higher as a result of complete Au (III) ion reduction and thus the majority of the seeds were grown into rods (Figure 3.3). In order to confirm successful synthesis of AuNRs, their size, shape and uniformity, HR-TEM imaging was performed on these AuNR samples.

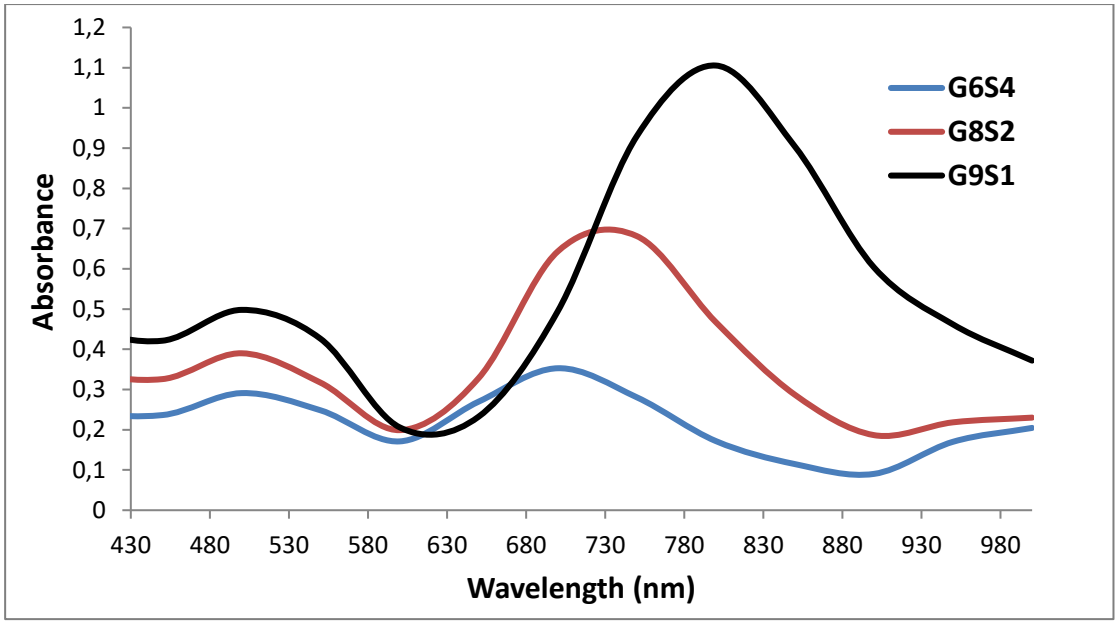

Figure 3.3: UV-Vis spectra of AuNR samples synthesised by varying the seed-to-Au (III) ion ratio in the growth solution. They are named based on GmSn, where G = growth solution; S = seed solution; m = volume of CTAB used in preparing the growth solution and n = volume of the seed solution. The seed solution was incubated for 3hrs before it was added to the growth solution. The resulting mixture was left undisturbed overnight at 25°C, after which the colour changed from colourless to deep purple.

3.2.2.1.2. EDX chemical analysis

Energy-dispersive X-ray (EDX) spectroscopy was performed on the AuNRs in order to determine elemental and chemical composition. All samples were prepared using the drop cast technique as described in Chapter 2 (Section 2.2.3.4). EDX relies on the unique atomic structure ascribed to every element, in such a way that the X-ray spectrum emitted for the different atomic structures, are clearly discernible from one element to another (Rao and Biswas, 2009). The spectrum is formed by excitation of electrons in the inner shell (lower energies). The excited electrons move to a higher energy state, subsequently creating vacant shells in the electronic structure of the atoms being probed. Electrons from the outer shells (higher energies) replenish the vacant shells; and the difference in energy between the higher and lower energy shells are emitted as x-rays (Rao and Biswas, 2009). Based on the EDX analysis of the AuNR samples, it is evident that Au was present in all three samples (Figure 3.4). In their paper Rodríguez-León *et al*. (2013) indicate that the presence of strong peaks for Copper (Cu) and Carbon (C) and Silicon (Si) in some samples can be attributed to the copper TEM grid and detector window.

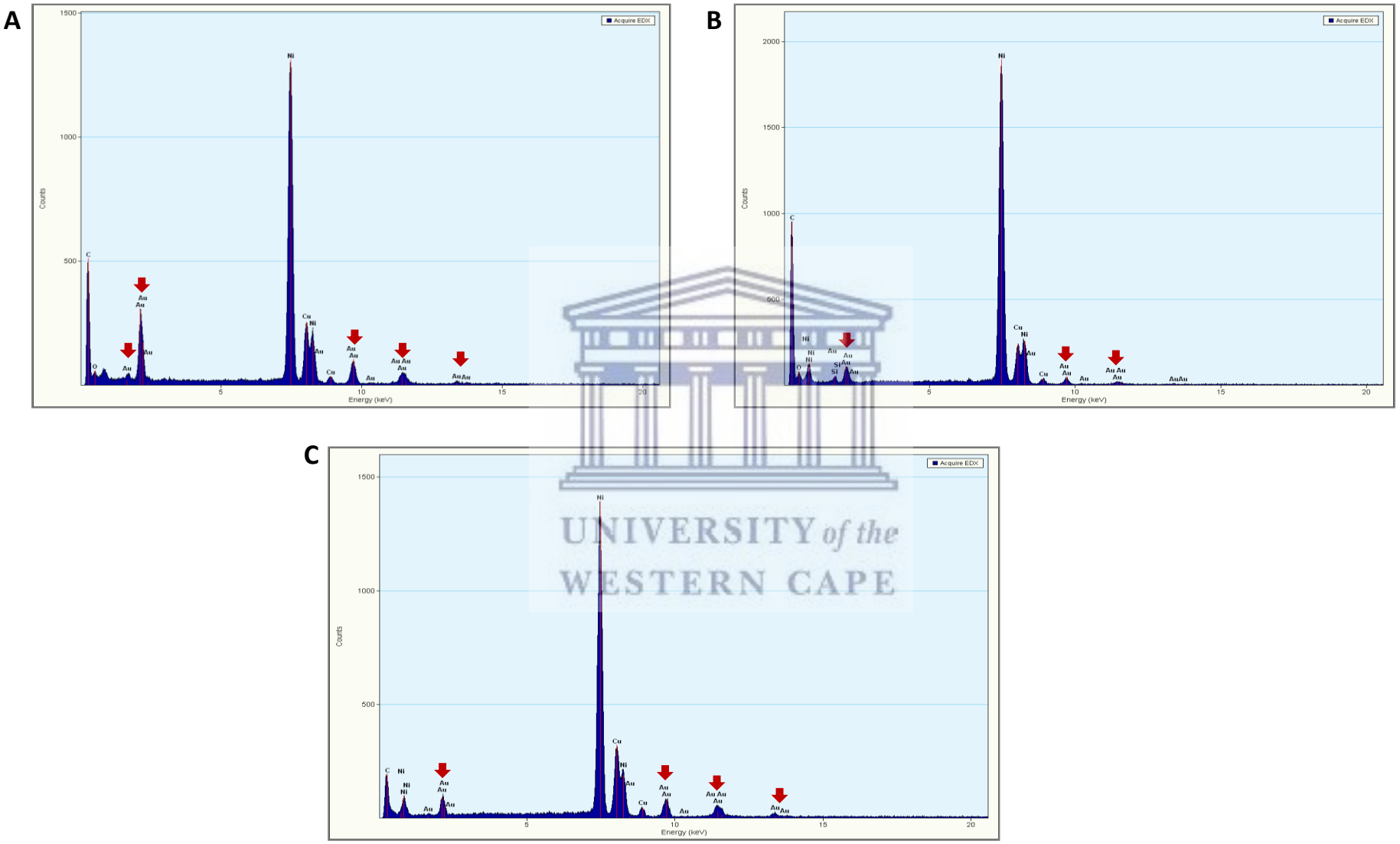

Figure 3.4: EDX spectrum of the AuNR samples. A, B and C shows the spectrum for G6S4, G8S2 and G9S1, respectively. The individual peaks are labelled with the symbols for the different elements that was detected in the samples. The red arrows point to the peaks representing Au.

3.2.2.1.3. HR-TEM analysis

High Resolution (HR)- Transmission Electron Microscopy (TEM) is the one of the most common characterization techniques for NPs. AuNR suspensions were loaded onto copper grids as described in Chapter 2 (Section 2.2.3.4) and changes in the electron beam due to scattering discharged by the sample were then measured. The interaction between the electrons and the sample, at that point, produced an image. The difference in contrast between the sample and the background Cu grid provides direct information about the NP morphology (Qi *et al*., 2001 & Rao and Biswas, 2009). TEM images contain a variety of information regarding shape and size distribution, as well as crystallographic structure of the NPs. The HR-TEM micrograph for the AuNR samples is shown in Figure 3.5. These images suggests that during synthesis, in all three samples, not only were there a very low yield of rod-shaped particles produced, but NPs with various morphologies, which includes spheres, prisms, and cubes were also formed. The majority of the AuNPs produced were in fact high-index-faceted Au nanocrystals, which according to Ming *et al*. (2009) can be produced when the seed amount is much smaller than that used for the preparation of larger AuNRs (>10nm). The TEM images (Figure 3.4) corroborate the UV-Vis data (Figure 3.3) which indicates that a blue shift of the λ_L peak from the NIR region (700-1100nm) to the visible region (200-500nm) occurs when the seed solution is increased, resulting in a decrease in rod formation. The blue shift of the λ_L peaks of the G8S2 and G6S4 samples closer to the visible region indicates the presence of NPs with various morphologies (Figure 3.3). In addition, the TEM images confirm that the higher absorbance peak of the G9S1 sample observed in the UV-Vis data is due to a significantly higher yield of AuNPs in the G9S1 sample compared to G8S2 and G6S4. Furthermore, even though various morphologies of NPs were present in the G9S1 sample, there was a significant red shift of the λ_L peak towards the NIR region, indicating that there was an increase in the abundance of rods in the G9S1 sample (Figure 3.3 and 3.4).

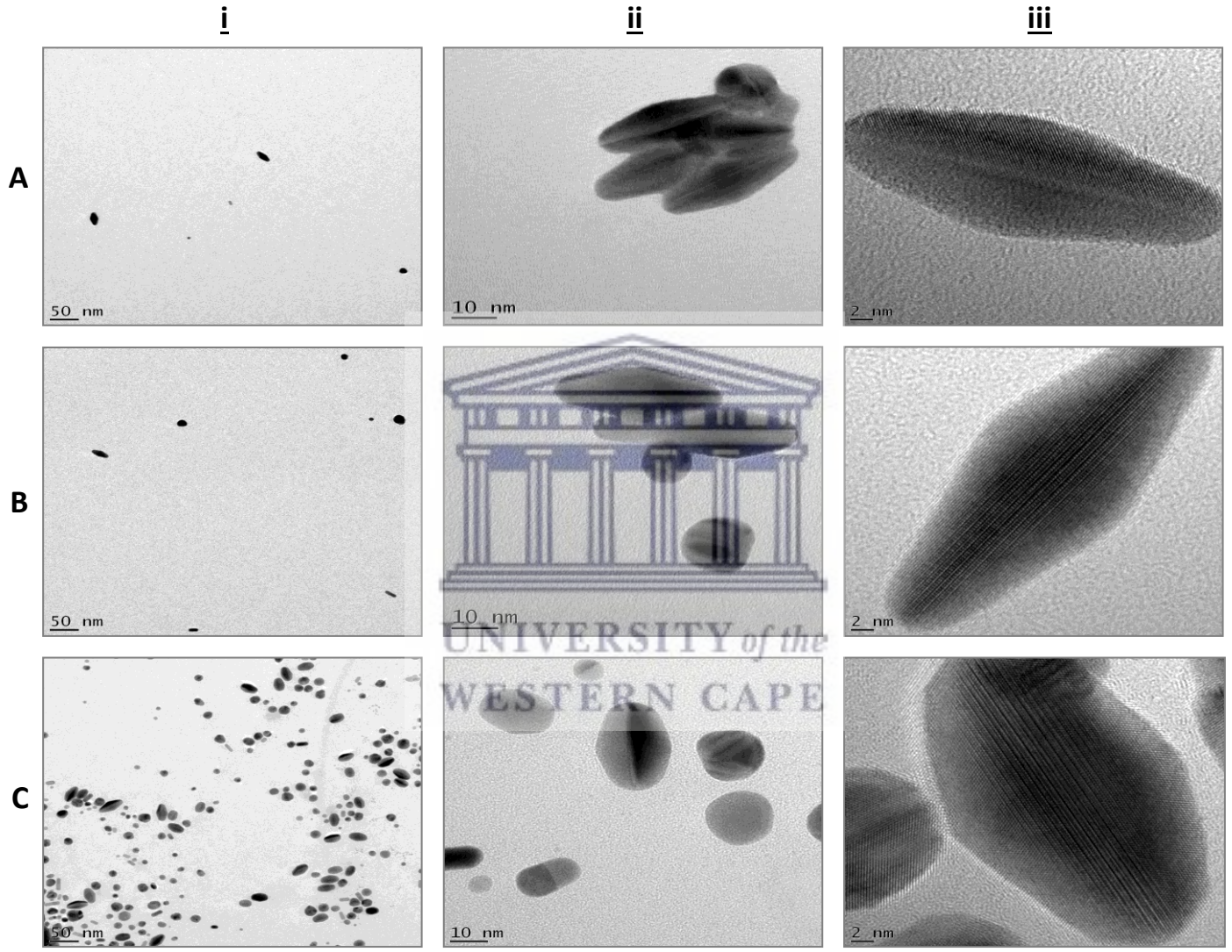

Figure 3.5: HR-TEM images of the AuNR samples. A, B and C represents G6S4, G8S2 and G9S1 NPs respectively, while i, ii and iii shows images of the samples taken at magnifications 50, 10 and 2nm resolution, respectively.

3.2.3. Purification of AuNR from G9S1 sample

3.2.3.1. Optical properties of the separated AuNPs

During AuNR synthesis, it is common for other shapes of AuNPs such as nanospheres, nanocubes, nanoprisms and nanocrystals to form (Xiong *et al*., 2011), which is clearly visible in Figure 3.5. Thus there was a need to separate the AuNPs based on their shapes. Previous studies employed centrifugation for separation of AuNR from AuNPs with other shapes (Ahmad *et al*., 2014; Scaletti *et al.* 2014; Robertson *et al*., 2016 & Boksebeld *et al*., 2017). This separation technique is based on the differential sedimentation rates of NP with different shapes and sizes (Xiong *et al*., 2011).

Following a method described by Scaletti *et al.* (2014), a differential centrifugation technique was used to successfully separate AuNRs from AuNPs with other shapes. The G9S1 sample was centrifuged as described in Chapter 2 (Section 2.2.1.2.) to produce a pellet and a supernatant. Figure 3.6.A shows UV-Vis spectra of AuNPs in the supernatant fraction, while Figure 3.6.B shows the UV-Vis spectra of AuNPs in the pellet fraction. The UV-Vis spectrum of the supernatant showed two defined peaks, one in the visible region (200-500nm) and one in the NIR region (700-1100nm), which is similar to the spectrum obtained for the G9S1 sample (before differential centrifugation). This is a clear indication of the presence of AuNRs. The UV-Vis spectrum generated for the pellet was less defined with a high absorbance in the NIR region of the spectrum. However, this spectrum is not indicative of AuNRs, suggesting that the AuNR were absent from the pellet.

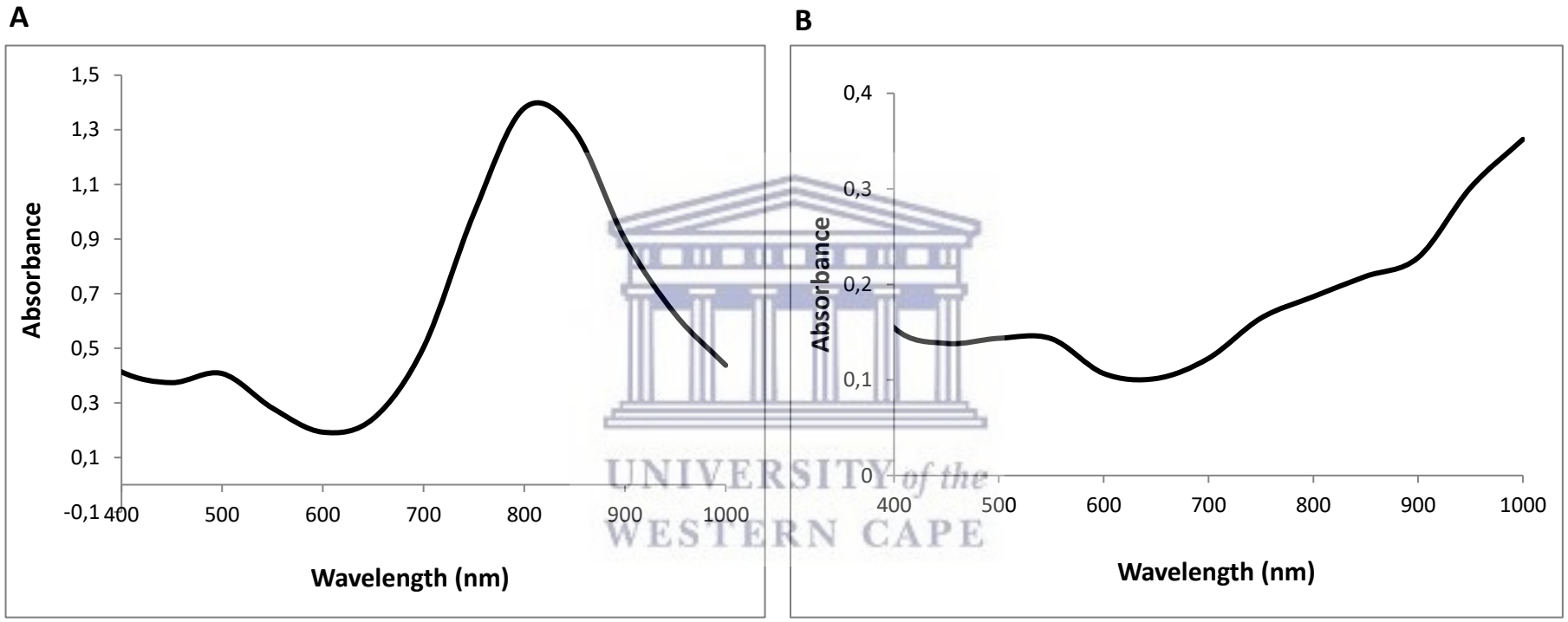

Figure 3.6: UV-Vis spectra of the fractions of AuNP produced after differential centrifugation of G9S1 sample. A shows the UV-VIS spectrum of the supernatant, while B shows the spectrum of the pellet.

3.2.3.2. EDX and HR-TEM analysis of the two NP fractions generated by centrifugation

To confirm that the AuNRs was successfully separated from AuNPs with other shapes, the two fractions (the pellet and supernatant) were subjected to HR-TEM and EDX analysis. The EDX spectra (Figures 3.7) suggest that Au is present in both the supernatant and the pellet suspensions. However the spectra for the two samples were very different, suggesting that the composition of the two suspensions may also differ. The TEM micrographs (Figures 3.8) show that the supernatant contains mostly the AuNRs (with minimal sphere production), while the pellet contains a mixture of AuNRs and AuNPs with various morphologies. The TEM images substantiate the UV-Vis analysis (Figure 3.6) and confirm that the supernatant contains the AuNRs. Based on the TEM images, the length of the majority of the AuNRs present in the supernatant fraction was 21-25nm and the diameter was 6-8nm, suggesting an aspect ratio of 3 to 3.5. Although the diameter of 80% of the AuNR was 6-8nm, a significant variation in the length of the AuNR was observed for AuNRs in the supernatant. Approximately 85% of the AuNRs in the supernatant can be divided into four groups based on their lengths (10-15, 16-20, 21-25 and 26-30nm) (Figure 3.9). Approximately 28%, which is the majority of the AuNRs, had a length of 21-25nm, 24% had a length of 16-20nm, 17% had a length of 26-30nm and another 17% had a length of 10-15nm. The properties are summarised in Table 3.1. The study by Jia *et al*. (2015) used a seed-to-Au (III) ions ratio similar to the ratio used to synthesise G9S1 AuNRs. Jia *et al.* (2015) produced AuNRs with a length of approximately 45nm, a diameter of 9nm and an aspect ratio of 5. In the current study, temperature was not efficiently controlled which may explain why the characteristics of the AuNR produced in this study was different from the AuNRs produced by Jia *et al*. (2015). Only the supernatant fraction of the G9S1 was used in subsequent experiments.

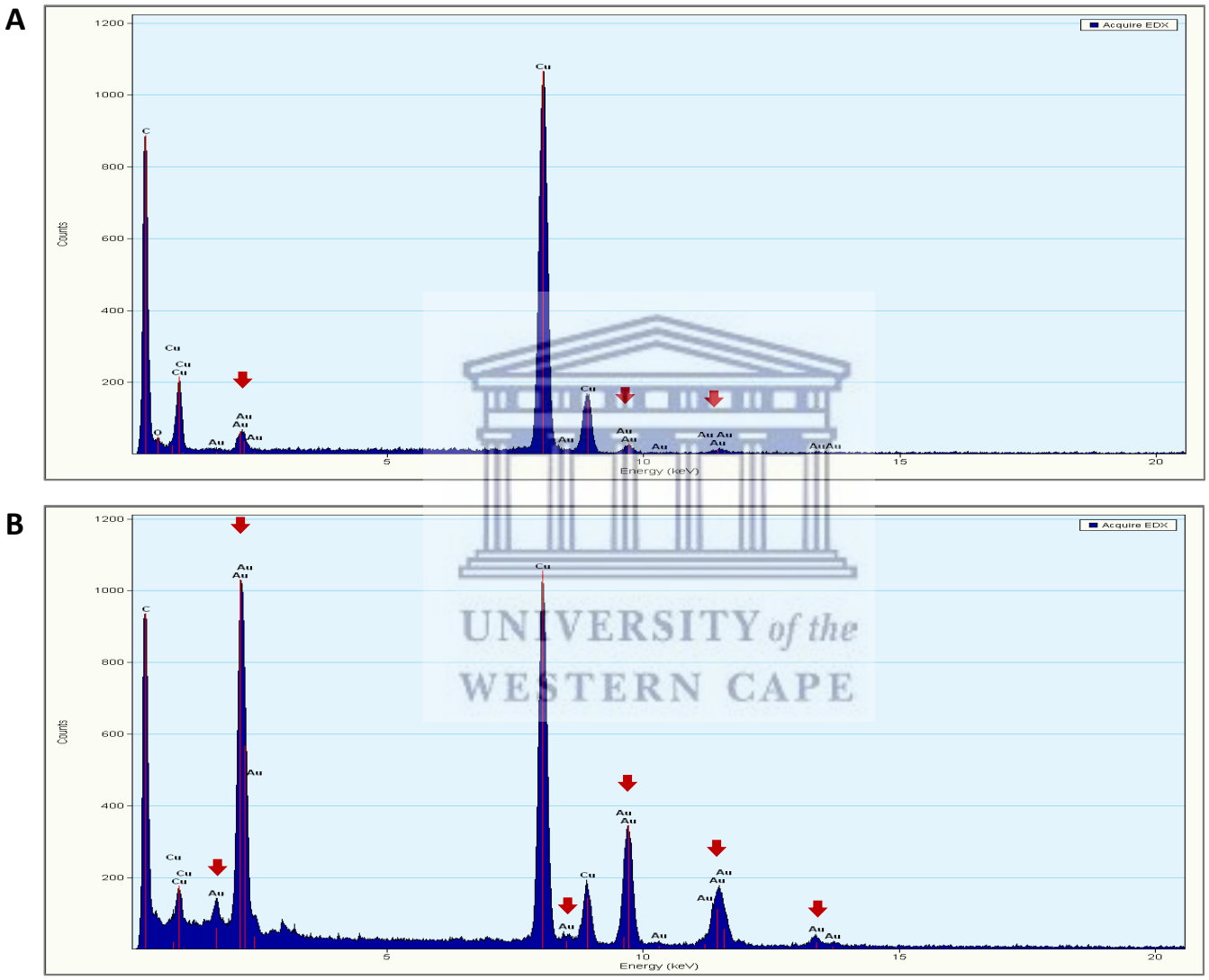

Figure 3.7: EDX spectra of the two fractions generated by centrifugation. A and B shows the spectrum of the supernatant and pellet, respectively. The individual peaks are labelled with the symbols for the different elements that was detected in the samples. The red arrows point to the peaks representing Au.

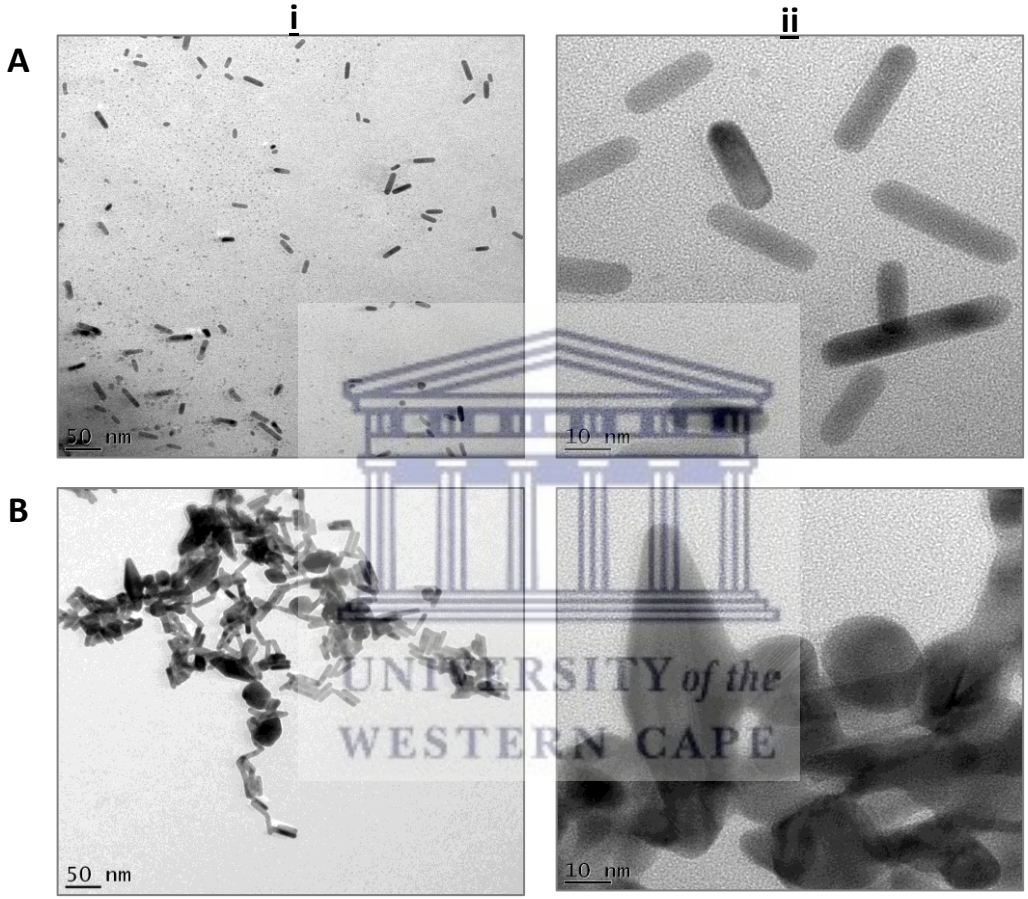

Figure 3.8: HR-TEM images of the two AuNP fractions generated from the G9S1 sample. A and B represents the supernatant and pellet respectively, while i and ii shows images of the supernatant and pellet at magnifications 50 and 10nm resolution, respectively.

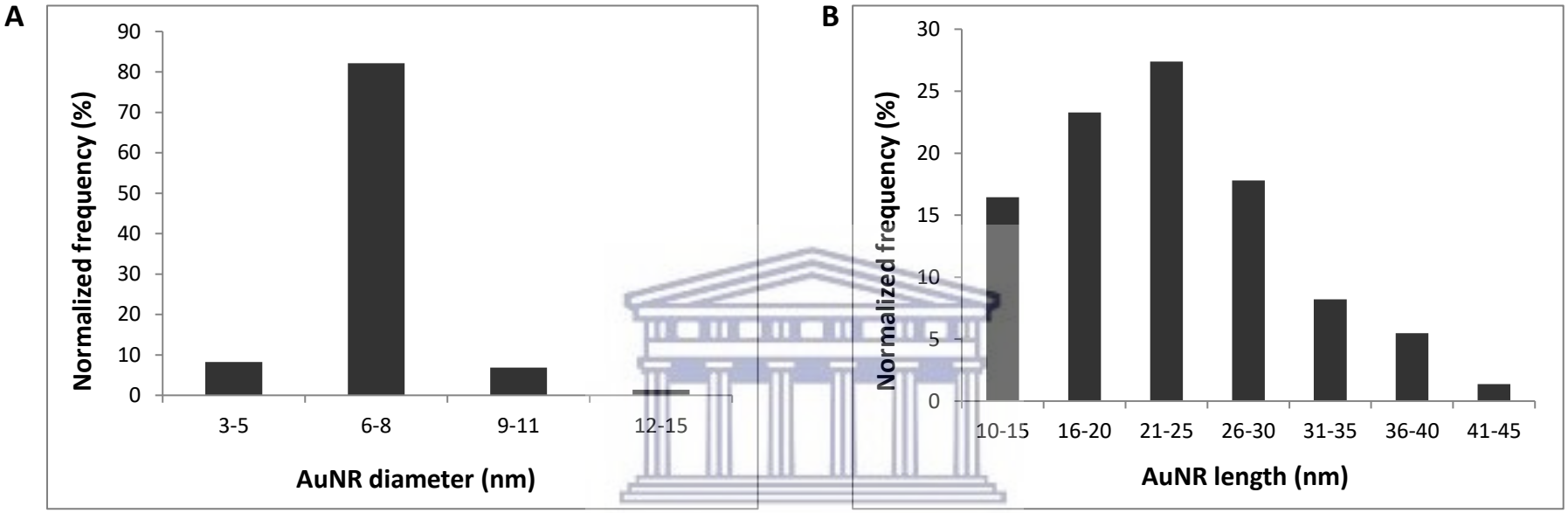

Figure 3.9: AuNR size distribution of the supernatant fraction of G9S1 AuNR. The A) length and B) diameter of each AuNR was determined using ImageJ software. The number of NPs analysed (N) = 75.

Table 3.1: Plasmonic properties, sizes, and number yields of the AuNR samples.

	AuNR preparations		
AuNR parameters	**G6S4**	**G8S2**	**G9S1**
λ_L (nm)	705	730	800
λ_T (nm)	505	505	505
Peak intensity (units)	0.3	0.7	1.12
Diameter (nm)	_	_	6 - 8
Length (nm)	_	_	21 - 25
Aspect ratio	_	_	3 - 3.5
Number yield (%)	_	_	85

λ_L = Longitudinal plasmon wavelength (Figure 3.3); λ_T = Transverse plasmon wavelength (Figure 3.3); Peak intensity = The peak intensity of the longitudinal plasmon wavelength (Figure 3.3); Diameter = Diameter of the majority of the AuNRs (Figure 3.9); Length = Length of the majority of the AuNRs (Figure 3.9); Aspect ratio refers to the ratio of the length to the diameter; Number yield refers to the percentage of the number of AuNRs in the total number of NPs in the supernatant as determined by ImageJ; - = Data was not analysed.

3.2.4. Pegylation of the AuNRs

CTAB is a cationic surfactant that plays a key role in the growth of the AuNRs. It simultaneously serves as a template for growth, while after synthesis it prevents aggregation of the NRs. CTAB inhibits aggregation by forming a bilayer micelle around AuNRs (Nikoobakht and El-Sayed, 2001). The positive charge of the bilayer results in reclusive forces between the AuNRs, preventing the AuNR from aggregating, which cause the AuNRs to stay in solution. However, there are two main problems regarding CTAB stabilization of AuNRs. The first is that CTAB physisorbs on Au, i.e. there is no strong chemical interaction between CTAB and the Au surface (Abtahi, 2013). Therefore, physisorbed CTAB on the surface is always in equilibrium with excess CTAB in the solution. If the CTAB in solution decreases, then CTAB will desorb from the AuNRs, which can result in the aggregation of AuNRs. The second problem is that the excess CTAB in solution is cytotoxic. Thus, using CTAB coated AuNRs in equilibrium with CTAB solution for medical applications could be problematic. Therefore, many researchers have attempted to replace CTAB with more biocompatible coatings (Liu *et al*., 2015 & Tebbe *et al*., 2015). In this study, CTAB was replaced with dH_2O before the AuNRs were functionalised with PEG and peptides as

described in Chapter 2 (Section 2.2.1.2). Once CTAB was replaced the AuNRs were denoted as the G sample (Figure 3.1), which was used in subsequent experiments.

Sosibo *et al.* (2015) demonstrated pegylation of AuNSs using thiolated PEG (SH-PEG-OH and SH-PEG-Biotin). The authors report that the use of SH-PEG-OH only to stabilize AuNSs was not successful as the NPs agglomerated within a short period of time (Sosibo *et al*., 2015). To solve this problem, the stabilization was achieved by using the two PEG molecules, SH-PEG-OH and SH-PEG-Biotin. SH-PEG-OH was chosen because of its versatility with regards to solubility and biological compatibility and SH-PEG-Biotin was employed to facilitate biotin-streptavidin conjugation of streptavidin tagged peptides. The same strategy was employed in this study to convert AuNRs (G) to pegylated AuNRs to produce GP. A mixture of SH-PEG-Biotin and SH-PEG-OH (mixed at a 1:10 ratio) was used to pegylate the AuNRs (G) as described in Chapter 2 (Section 2.2.2.) to produce pegylated AuNRs (GP). Following pegulation with a mixture of SH-PEG-Biotin and SH-PEG-OH, the AuNRs (G) were again analysed by UV-Vis spectroscopy. Figure 3.10A shows the UV-vis analysis of AuNRs before and after pegylation. Figure 3.10A shows that in the presence of PEG the UV-vis of AuNRs (GP) is red-shifted from 785nm to 800nm. This shift is the result of an increase in the local refractive index at the AuNR surface, which suggests that PEG were successfully conjugated to the AuNP surface. For NPs with uneven shapes such as AuNRs this local refractive index change is more profound due to a further enhancement of the electromagnetic field at points of "unevenness" at the particle surface (Yang *et al*., 2005). HR-TEM analysis of the pegylated AuNRs (GP) shows rod-shaped NPs that are well dispersed and not aggregating (Figure 3.10B).

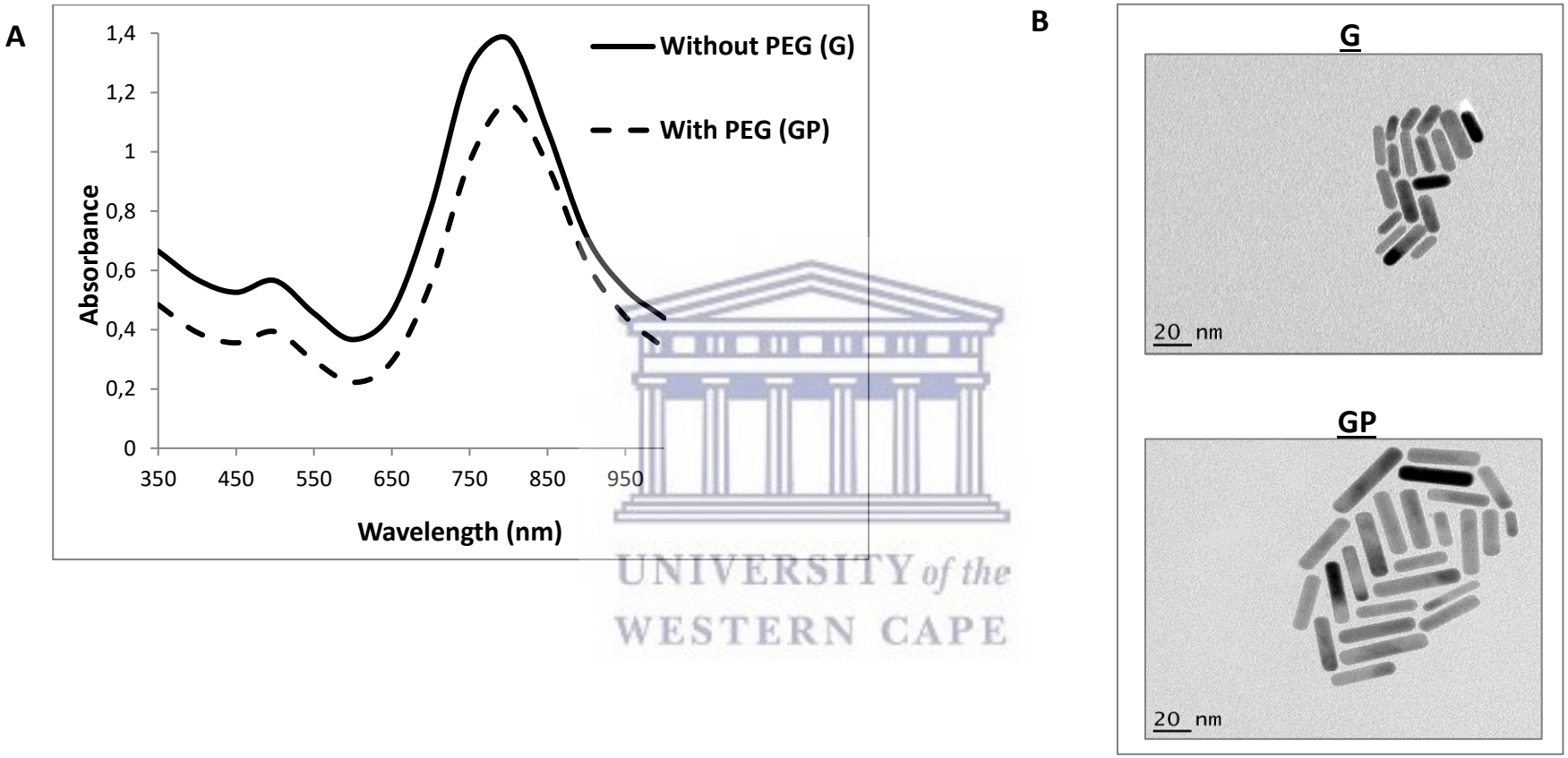

Figure 3.10: UV-Vis Spectra and HR-TEM images of pegylated AuNRs (GP). A respresents the UV-Vis and B respresents the HR-TEM images of the NPs, at a magnification of 20nm resolution.

3.2.5. Evaluating the stability of the pegylated AuNRs (GP)

It is important that AuNPs, used in biological applications, retain their stability in biological environments. One way to test if AuNPs will be stable in biological environments is to place NPs for extended periods in buffers that simulate various biological conditions (Chanda *et al*., 2011). In this study, the pegylated AuNRs were incubated in six different buffer solutions (dH_2O, 0.5% Bovine Serum Albumin (BSA), 1X PBS, 10% FBS, non-complete DMEM media and complete DMEM media) as described in Chapter 2 (Section 2.2.3.2). The stability of AuNRs in these buffers was monitored by recording changes in the UV-Vis spectra over time (Figure 3.11). The AuNRs demonstrated excellent stability in dH_2O, BSA and FBS, by retaining their SPR (Figure 3.11).

On the other hand the AuNRs did not show a similar stability upon incubation with PBS and media (both non-complete and complete) as indicated by significant changes in their respective UV-Vis spectra as shown in Figure 3.11. There is a blue shift in the SPR, which could be due to NP aggregation caused by the interaction of the AuNR with constituents of the media and PBS. Stability of NP suspensions is usually affected by the molar concentration and ionic strength of NaCl and destabilizing counterions such as Ca^{2+} and Mg^{2+} present in DMEM and PBS which bind to the surface of the NPs and prevent their cellular up take (Maiorano *et al.,* 2010). Studies show that un-functionalised NP suspensions are very unstable in biological systems and further (steric) stabilization with molecules such as peptides are usually necessary to prevent binding of ions and thereby increase bioavailability (Maiorano *et al.,* 2010 & Pavlin and Bregar, 2012). Furthermore, a negative absorbance can be observed when NPs were incubated in DMEM (complete and incomplete) resulting in a downward peak at ~550nm. DMEM contains phenol red which absorbs at a wavelength of ~560nm (Xu *et al*., 2006). Thus a possible explanation for the negative absorbance could be attributable to the competition between the AuNPs and phenol red for the absorbance of light at 550nm. The interference of phenol red could significantly affect the cell viability readings of the NP cytotoxicity assays, as all the bioassays were

performed in phenol-containing media. Replacing the phenol-containing DMEM with phenol-free DMEM would eliminate the ambiguity of the stability test of the NPs. Thus, a comparative study between the stability of peptide-functionalised NPs in phenol-containing DMEM and in phenol-free DMEM should be done. Furthermore, there is a decrease in the intensities of the maximum absorbance of the NPs over time in all buffers. The reduction could be attributed to NP precipitation over time, due to the removal of NPs at each time point.

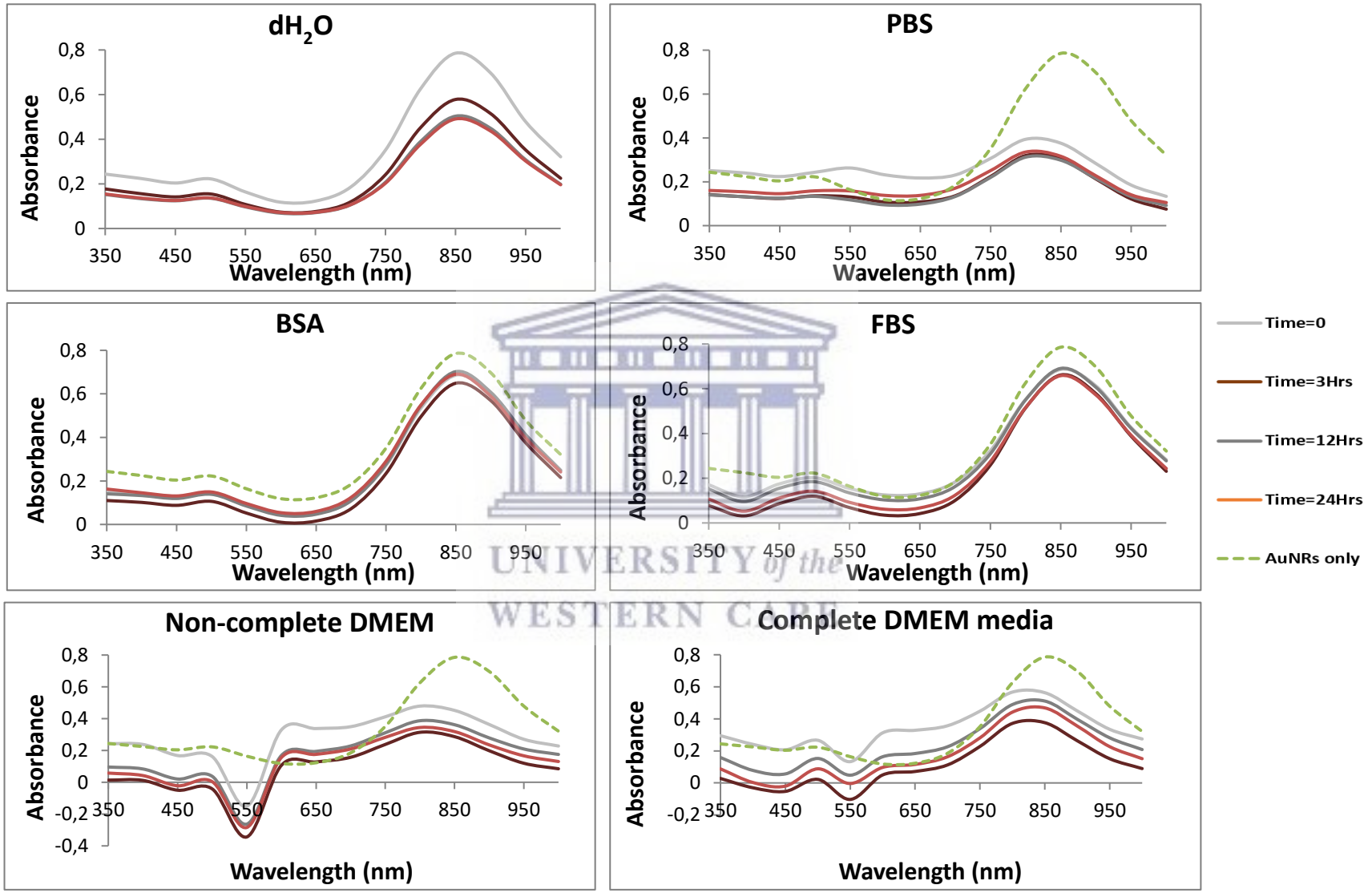

Figure 3.11: Changes in UV-Vis spectra of Pegylated AuNRs (GP) over a 24hr period in different buffers. GP was incubated in dH_2O; 1X PBS; 0.5% BSA; 10% FBS; non-complete DMEM media and Complete DMEM media

3.2.6. Functionalization of AuNRs (GP) with peptides to synthesise AGK, GK and AG.

3.2.6.1. Characterisation of AuNRs that was functionalised with peptides by UV-Vis

The pegylated AuNRs (GP) were bi-functionalised by conjugating the targeting (AHP) peptide and therapeutic $_D(KLAKLAK)_2$ peptide to the NP through ligand exchange as described in Chapter 2 (Section 2.2.2). Briefly, PEG-OH, PEG-Biotin and the $_D(KLAKLAK)_2$ peptide all contain a thiol (SH) group to facilitate conjugation to the AuNR surface. The three molecules were added simultaneously to the AuNR suspension to form GK (pegylated AuNR + $_D(KLAKLAK)_2$). The biotinylated AHP which contained a streptavidin tag to facilitate binding of the peptide to PEG-Biotin was added to GP to form AG (pegylated AuNR + AHP). Similarly the biotinylated AHP was added to GK to form AGK (pegylated AuNR + AHP + $_D(KLAKLAK)_2$). AG and GK served as control NPs as AG are expected to target cells but have no therapeutic effect and GK are expected to not exert its therapeutic effects on cells as it is unable to bind to the target of interest.

Figure 3.12 shows the UV-Vis analysis of G, GP, GK, AG and AGK. All five samples show a λ_T peak at 495nm. The λ_L peaks for G, GP, GK, AG and AGK was 794nm, 804nm, 806nm, 808nm and 812nm respectively. This suggests that the λ_L peaks for AuNRs that were functionalised (GP, GK, AG and AGK) were slightly redshifted. As explained previously, this is an indication of changes on the surface of AuNPs and may also indicate successful functionalisation. When comparing the NPs functionalised with peptides (GK, AG and AGK) to the pegylated NP (GP), the redshift was more pronounced for AGK. This may be due to the fact that the surface changes on AGK were more substantial, since it is the only AuNR that was conjugated with two different peptides. It can also be observed that there was a decrease in the peak intensities of the λ_L peaks of AG and AGK compared to G, GP and GK. This may be

attributed to the additional centrifugation steps during synthesis of AG and AGK resulting in the loss of NPs and therefore intensity.

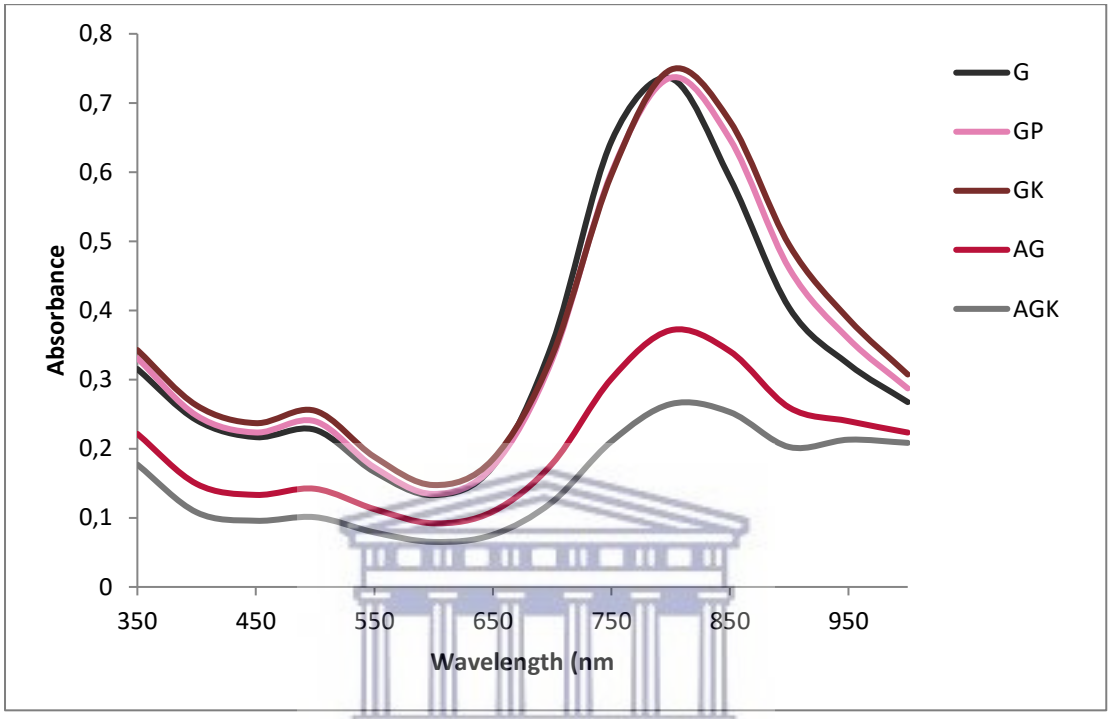

Figure 3.12: UV-vis spectra of AuNRs functionalised with peptides. The UV-Vis spectra of G, GP, GK, AG and AGK is shown. G = AuNRs before functionalisation, GP = pegylated AuNRs, GK = AuNRs functionalised with the $_{D}$(KLAKLAK)$_2$ peptide only; AG = AuNRs functionalised with the AHP peptide only and AGK = AuNRs functionalised with both AHP and $_{D}$(KLAKLAK)$_2$ peptides.

3.2.6.2. Characterisation of surface charge of AuNRs

The zeta(ζ)-potential of a NP solution is a measure of the surface charge of the NP. ζ-potential determines the behaviour of NPs in solution. It provides information about NP stability in solution (Leroy *et al.*, 2011). NPs with higher ζ-potential exhibit increased stability due to a larger electrostatic repulsion between NPs. NPs with a ζ-potential between −10 and +10mV are considered to be neutral (Clogston and Patri, 2011). NPs with a ζ-potential greater than +30mV are strongly cationic, while NPs with a ζ-potential less than −30mV are strongly anionic. These values can be used to predict how readily the NPs will aggregate in solution. NPs with ζ-potential values greater than +30 mV, but less than -30mV, are highly stable and are less prone to

aggregation, while NPs with lower ζ-potential values closer to zero can easily flocculate when dispersed in a solution (Clogston and Patri, 2011).

The ζ-potential of G, GP, GK, AG and AGK was determined using a Malvern Zetasizer Nano ZS as described in Chapter 2 (Section 2.2.3.3.) and is shown in Table 3.2. The ζ-potential of G, GP, GK, AG and AGK was determined to be -0.224, + 19.52, +16.13, +7.73 and +4.51mV, respectively. This implies that pegylation and the conjugation of peptides to G resulted in a significant increase of the surface charge of the AuNRs. The molecules attached on the AuNRs increased their ζ-potential from neutral in G to a more cationic charge when GK, AG and AGK was produced. The changes in the charge are attributable to molecules attached to the AuNP surface and indicate modification of the AuNP surfaces. AuNPs with a large negative or positive ζ-potential values will repel each other in suspension and there will be no aggregation of the NPs. AuNPs with a more neutral ζ-potential will easily flocculate since the force between them is not strong enough to cause repulsion. Based on the values and charges obtained, G is highly unstable and that in comparison, GK, AG and AGK may be more stable.

Table 3.2: Zeta potential measurements of AuNRs.

AuNR Conjugates	Zeta Potential (mV)
G	-0.224
GP	+19.52
GK	+16.13
AG	+7.73
AGK	+4.51

G = AuNRs before functionalisation, GP = pegylated AuNRs, GK = AuNRs functionalised with the $_D$(KLAKLAK)$_2$ peptide only; AG = AuNRs functionalised with the AHP peptide only and AGK = AuNRs functionalised with both AHP and $_D$(KLAKLAK)$_2$ peptides.

3.2.6.3. HR-TEM analysis of functionalised AuNRs

The size distribution, quality and morphology (shape) of the peptide-conjugated AuNRs were characterized by HR-TEM analysis. Representative TEM micrographs of the different AuNRs are shown in Figure 3.13. The yield of rod-shaped NPs were high, with a few spheres and squares formed during the synthesis of GK which is unavoidable (Figure 3.13). The variation in brightness of the NRs are attributed to diffraction contrast within the specimen. Diffraction contrast is the variation in intensity of diffraction (bending of waves around obstacles) across the sample (Fultz and Howe, 2012). When comparing the functionalised AuNRs (GP, GK, AG and AGK) to unfunctionalised AuNRs (G), the functionalised NRs are more dispersed in solution, while G appears to be clumping together due to aggregation. Furthermore, AG and AGK had a high yield even though the peak intensities were lower than the other NPs (Figure 3.12). A possible reason for this is that the AG and AGK suspensions were more concentrated when subjecting the samples to TEM analysis compared to UV-Vis analysis. Importantly, the functionalised AuNR dispersions showed no signs of aggregation following functionalisation.

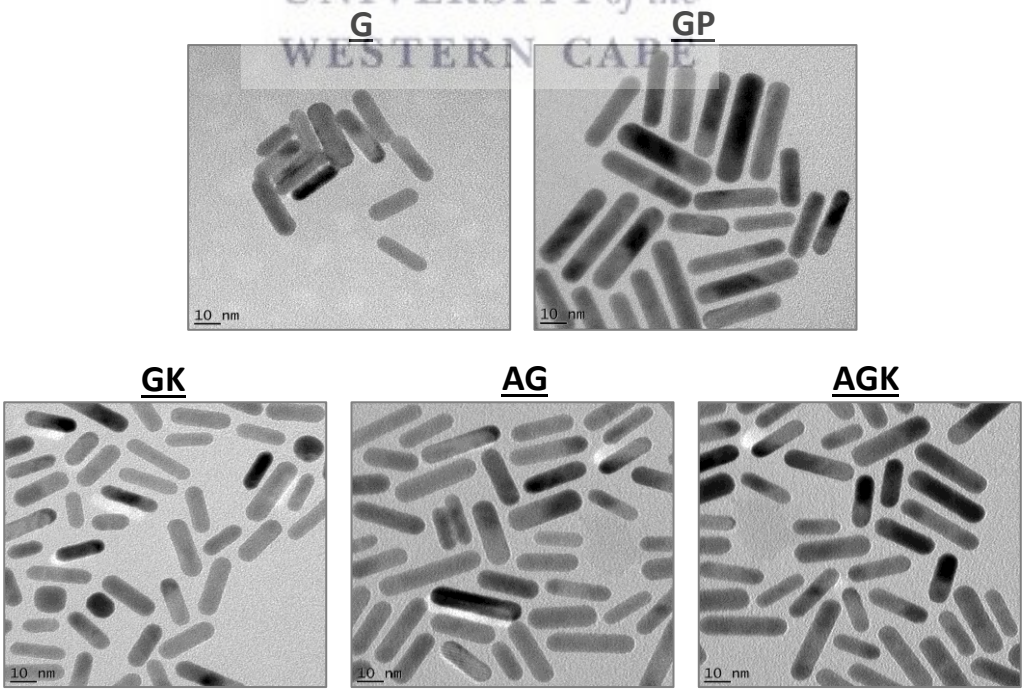

Figure 3.13: HR-TEM images of AuNRs functionalised with KLAK and AHP peptides. The HR-TEM images represents G, GP, GK, AG and AGK taken at a magnification of 10nm resolution. G = AuNRs before functionalisation, GP = pegylated AuNRs, GK = AuNRs functionalised with the $_D(KLAKLAK)_2$ peptide only; AG = AuNRs functionalised with the AHP peptide only and AGK = AuNRs functionalised with both AHP and $_D(KLAKLAK)_2$ peptides.

3.3. Conclusion

The aim of this chapter was to synthesise AuNR conjugates for application in PTT. AuNRs were synthesised at three different seed-to-Au (III) ion ratios to produce three different AuNR preparations (G6S4, G8S2 and G9S1) in order to identify the ideal ratio for the synthesis of <10nm AuNRs. UV-Vis analysis showed that the G9S1 preparation had the longest λ_L peak compared to the other preparations, suggesting it would absorb NIR more efficiently. It also delivered a higher yield of AuNRs as determined by HR-TEM. Thus the G9S1 preparation was used in subsequent experiments. A differential centrifugation technique was used to successfully separate the AuNRs from AuNPs with other shapes. The length of the majority of the AuNRs was 21-25nm and the diameter was 6-8nm. Based on these physical characteristics these AuNRs could be used for PTT.

The AuNRs were coated with CTAB, which is known to be highly toxic. Using ligand exchange, CTAB was exchanged for PEG molecules, which are more biocompatible. The pegylated AuNRs were denoted as GP. To test the stability of GP, the NPs were placed in buffers that simulate various biological buffer conditions, and were found to be stable in dH_2O, BSA and FBS. GP was successfully bi-functionalised with the targeting (AHP) peptide and therapeutic peptide ($_D$(KLAKLAK)$_2$), denoted as AGK. AuNPs lacking AHP (GK) and $_D$(KLAKLAK)$_2$ (AG) were also synthesised to serve as controls. UV-Vis analysis showed shifts in the λ_L peaks upon conjugation of the peptides, suggesting successful modification of the AuNR surface. This was further confirmed by ζ-potential measurements obtained for the AuNRs. HR-TEM analysis showed that the functionalised AuNR conjugates were well dispersed in solution and showed no signs of aggregation following functionalisation. In Chapter 4, the toxicity of the functionalised AuNRs will be evaluated.

Chapter Four: Investigation of the therapeutic and photothermal effects of AHP functionalised gold nanorods

4.1. Introduction

The development of nanotechnology-based therapy has potential for the treatment of chronic diseases such as obesity and cancer. The nanotherapeutics can be directly targeted to disease-associated markers and confine its therapeutic activities to the target cells only. The use of bi-functionalised nanoparticles with both targeting and therapeutic drugs could greatly enhance the specificity and sensitivity of the therapy. Nanotechnology-enabled targeted therapy could facilitate the development of precision medicine and diagnostics systems that can specifically identify and/or eradicate diseased cells with minimal effects to healthy tissues (Byrne *et al*., 2008).

A vast number of experimental bi-functionalised nanotherapies has been described in the literature (Palanca-Wessels *et al*., 2016 & Ding *et al*., 2017) and several nanodrugs are currently undergoing clinical trials for targeted treatment of cancer (Tabernero *et al*., 2013; Zhou *et al*., 2016 & Rudin *et al*., 2017). Of interest to this study, is therapeutics using AuNP formulations as drug delivery vehicles in photothermal therapy (PTT). As discussed previously (Chapter 1, Section 1.8.3.3), NPs that can effectively convert absorbed Near Infrared (NIR) light into heat are able to eliminate cancer cells (Pattani *et al*., 2015). Several studies have shown the great promise PTT holds for cancer treatment through the use of AuNRs (Tsai *et al*., 2013; Mooney *et al*., 2014 & Abadeer and Murphy, 2016). Changing the shape and composition of the NP to rod-shaped can shift the surface plasmon absorption of the NPs into the NIR transmission window and trigger its PTT activities (Chen *et al*., 2007 & Wiley *et al*., 2007). The goal in this chapter was to examine the effects of the AuNR conjugates on PHB-expressing cell lines in an attempt to improve the therapeutic effect of $_{D}(KLAKLAK)_2$ by PTT. The study by Sibuyi *et al.* (2017) demonstrated that PHB-targeted AuNSs could induce apoptosis in PHB-expressing cells, the colon cancer cell line, Caco-2 cells. The targeting peptide, AHP, facilitated the uptake of the AuNSs

by cells that express the PHB receptor on their cell surface. Once bound, the AuNSs were internalized and the therapeutic peptide, $_D(KLAKLAK)_2$ triggered apoptosis in Caco-2 cells. These AuNSs were unable to trigger apoptosis in cells that did not express the receptor on their surface. In this Chapter, the cellular toxicity of the AuNRs (described in Chapter 3) was evaluated.

4.2. Results and Discussion

4.2.1. Evaluating PHB expression in human cell cultures

The application of the targeted AuNRs produced in this study was to selectively bind to the PHB receptor, which is not only expressed by vascular endothelial cells of the WAT of obese subjects (Zheng *et al.*, 2013) but also on the surface of some cancer cells as well (Jemal *et al.*, 2011; Siegel *et al.*, 2013; Torre *et al.*, 2015 & Sibuyi *et al.*, 2017). The objective of the work in this section of Chapter 4 was to assess expression and localization of PHB protein in selected human cancerous and non-cancerous cell lines.

A panel of cancer cell lines (listed in Table 2.5) were cultured to at least 70% confluency. PHB expression in these cells was investigated by immunocytochemistry (ICC) using a PHB polyclonal antibody as described in Chapter 2 (Section 2.2.5). Antibody binding was visualised by chromogenic staining using DAB (3,3'-diaminobenzidine) [Figure 4.1] and fluorescence staining using an anti-PHB Alexa Fluor-488 secondary antibody (Figure 4.2). Chromogenic staining was visualised using light microscopy and fluorescence staining was detected using fluorescence confocal microscopy.

The principle of chromogenic staining using DAB involves the oxidation of DAB by hydrogen peroxide in a reaction that is catalysed by horseradish peroxidase (HRP), which is why a HRP-conjugated secondary antibody was used to detect the PHB primary antibody as described in Chapter 2 (Section 2.2.5.1). The oxidation of DAB

produces a brown, alcohol-insoluble precipitate at the site of enzymatic activity (Gustashaw *et al*., 2010). Counterstaining with haematoxylin maintains morphological detail of the surrounding tissue intact and allows visualization of the protein of interest (O'hurley *et al*., 2014).

Figure 4.1 shows the results of ICC using DAB. Three cancer cell lines (Caco-2, PC-3 and U-87) show the presence of brown staining in the cells, suggesting high expression levels of PHB in these cell lines, while A549, CaOv-3, Caski, H157, Hek-293, Hep-G2, LnCap, MCF-7 and SKOV-3 do not express PHB. Previous studies have reported that Caco-2 cells express PHB on the cell surface (Nijtmans *et al*., 2000; Sharma and Qadri, 2004; Thovhogi *et al*., 2015 & Sibuyi *et al*., 2017). However, the expression of PHB in PC-3 and U87 has not been as extensively reported.

The intensity of the brown stain appears to differ between the three cell lines, with the intensity in Caco-2 cells being more intense than in PC-3 and U-87 cells. This may suggest that the expression levels of PHB are higher in Caco-2 cells. In general, it appears that PHB is not expressed in the nuclei of these cells. However since ICC was done using light microscopy and since there appear to be some traces of brown staining in the nuclei of PC-3 cells (Figure 4.1), it is still possible that PHB is expressed at low levels in the nucleus. Moreover, a study by Gamble *et al.* (2007) reported that the cells express PHB in the mitochondria and nucleus. The same study also reported PHB expression in the mitochondria and nucleus of LnCaP and MCF-7 cell lines (Gamble *et al*., 2007). However, the current study contradicts this finding since brown staining was not present in LnCaP and MCF-7 cells, suggesting that these cells do not express PHB (Figure 4.1). The study by Sibuyi *et al.* (2017) has also demonstrated PHB expression in MCF-7 and Caco-2 cells by means of Western blot analysis. The study by Sibuyi *et al.* (2017) also shows that PHB is not expressed on the surface of the MCF-7 cells, but rather in the cytoplasm. It is therefore possible that ICC performed in the current study is only detecting PHB expression located on the surface of the cells and not at the intracellular location.

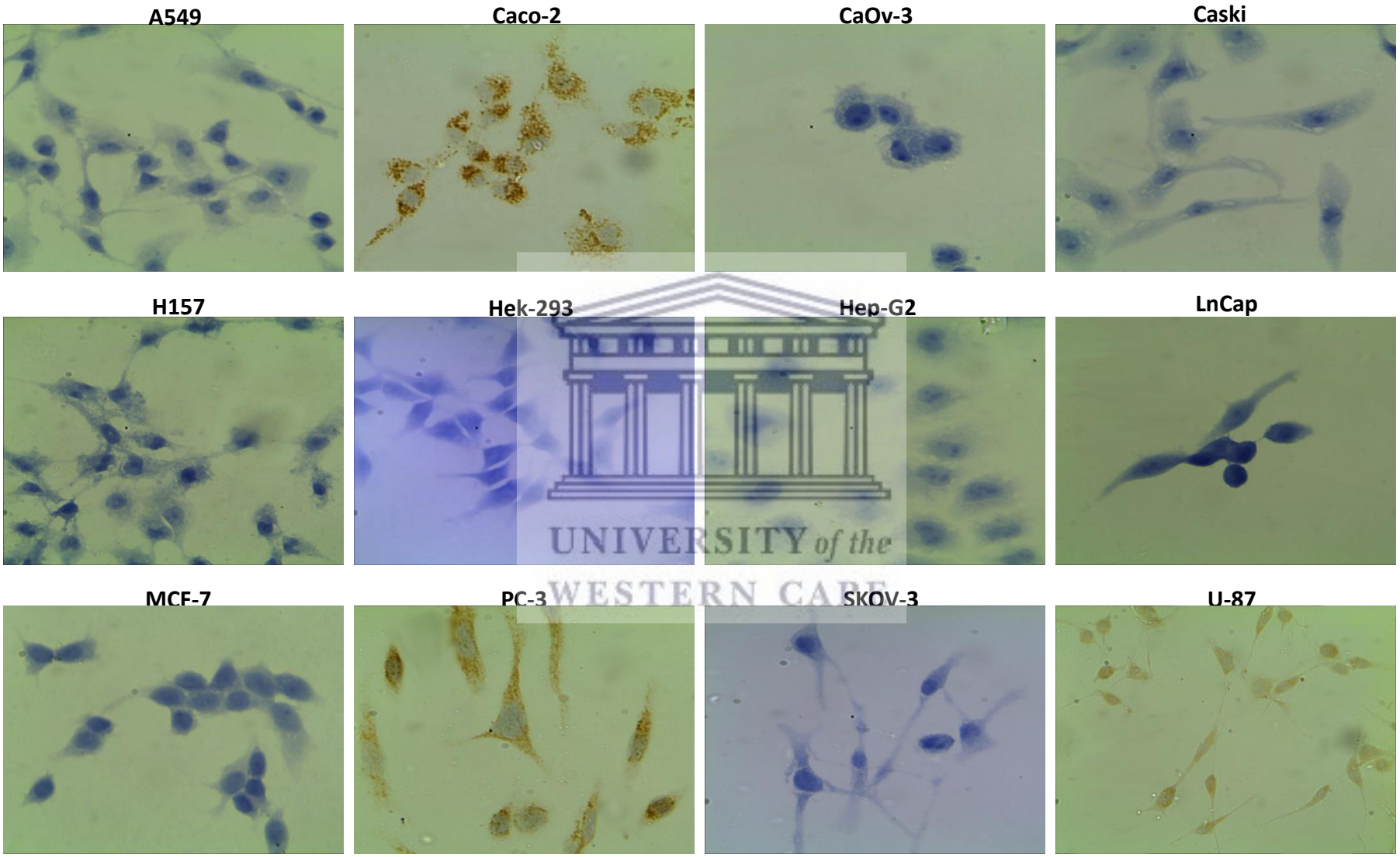

Figure 4.1: Immunostaining of PHB expression in a panel of human cell lines. The cells were stained with the PHB antibody and hematoxylin. The dark purple stain shows the location of the nucleus, while the brown stain shows PHB expression. Images were taken at 40X magnification.

Cell fixation, which is used in ICC can modify the three-dimensional structure of antigens, which can render them undetectable by antibodies resulting in false negative results (Ramos-Vara *et al*., 2015). In addition to conformational changes, fixation can cause changes in the electrostatic charge of proteins, which is critical for the initial attraction between antigen and antibody (Ramos-Vara *et al*., 2015). Moreover, polyclonal antibodies, which can be raised in rabbits, have higher affinity but lower specificity than monoclonal antibodies (Ramos-Vara *et al*., 2015). Consequently, polyclonal antibodies can also produce false results due to non-specific binding. A false positive or additional signal can be produced if the antibody binds to molecules that are structurally related to the target antigen (Hewitt *et al*., 2014).

In an attempt to confirm the immunostaining results, a second ICC technique was performed using confocal microscopy. It is based on immunofluorescence / darkfield imaging of cells against a dark background using an antibody that is chemically attached to a fluorochrome in order to visualize protein expression (Jordan *et al*., 2002). Confocal microscopy coupled with Z-stacking is a powerful tool for tracking intracellular localization of proteins. Z-stacking or focus stacking is a process where images are taken of a sample at different focal distances, which are then combined into one image and as a result the final image has a much higher resolution (Edgett *et al*., 2009). This technique is ideal for co-localisation studies and was used here to resolve some of the ambiguous results produced in Figure 4.1; more specifically, it addressed the question of PHB expression in the nuclei of Caco-2, PC-3 and U-87 cells.

Caco-2, PC-3 and U-87 cells were probed with a PHB primary antibody, which was detected using an anti-rabbit Alexa Fluor-488 secondary antibody as described in Chapter 2 (Section 2.2.5.2). Figure 4.2 shows that Caco-2, PC-3 and U-87 cells displayed green fluorescence due to the presence of Alexa Fluor-488, which is an indication of the presence of PHB. This data corroborates ICC done by chromogenic staining in Figure 4.1. However, no fluorescence was detected in the nuclei of the cells, suggesting that PHB is expressed either in the cytoplasm or on the surface of these cells and not the nucleus. Since no concurrent staining with markers of cell

structure (e.g. an antibody to a transmembrane protein or an antibody to a protein that is only expressed in the cytosol) were used to verify the localisation of PHB, this study could not confirm whether PHB is expressed on the cell surface or membrane.

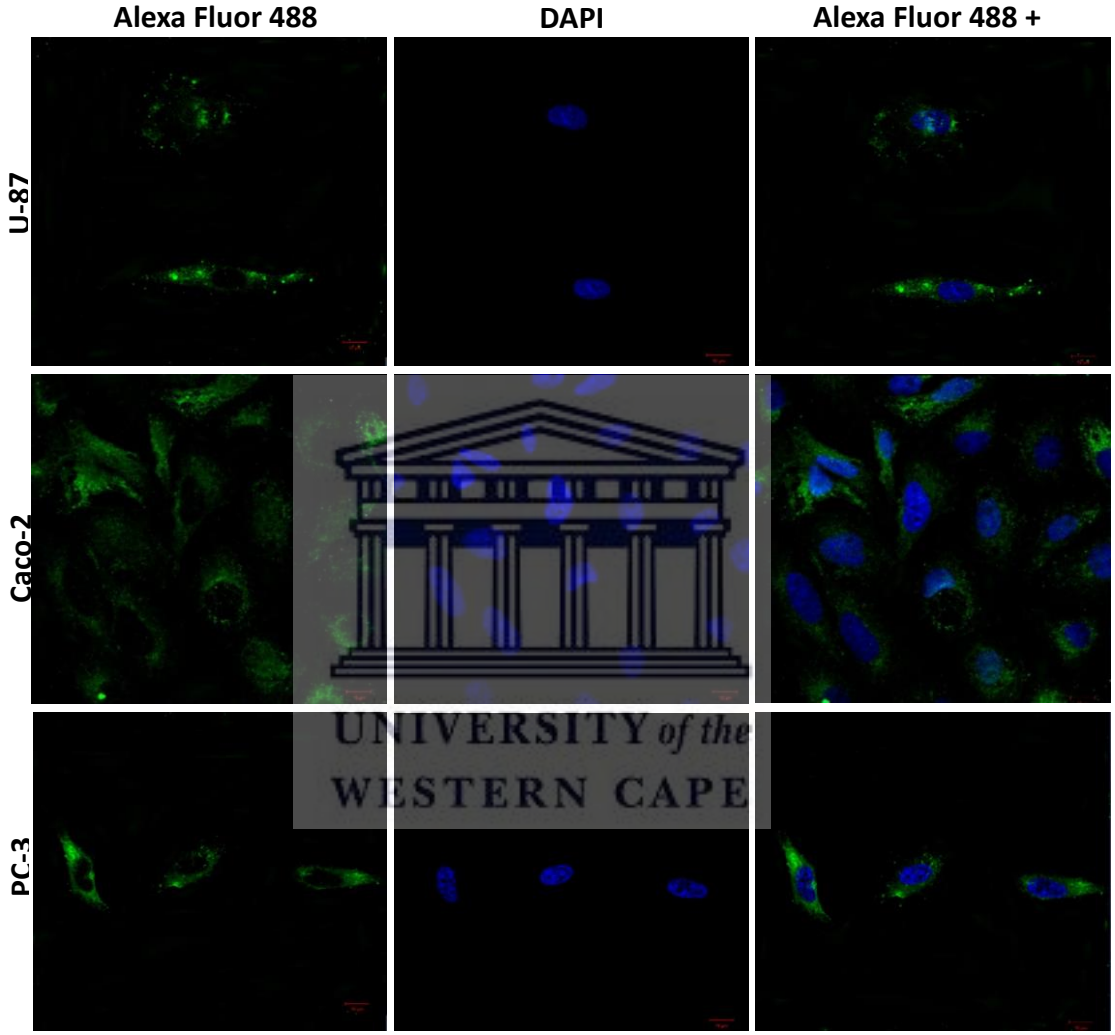

Figure 4.2: Immunoflourescence analysis of PHB expression in cancerous cell lines. The cells were fixed and treated with a PHB antibody, followed by Alexa Flour 488 anti-rabbit secondary antibody. The cells were then mounted in DAPI flouroshield and images were taken with a confocal microscope at 60X magnification.

4.2.2. Therapeutic potential of the PHB-targeted nanotherapy

Targeted nanotherapies offer hope for the treatment of chronic diseases such as cancer due to improved specificity and efficacy. Preclinical and human trials conducted using such therapies provide concrete evidence of the therapeutic potential of regimens that may be capable of treating debilitating diseases such as cancer (Kumar *et al*., 2014).

A previous study by Sibuyi *et al.* (2017) demonstrated that a PHB-targeted nanotherapy (AuNS functionalised with the AHP and $_D$(KLAKLAK)$_2$ peptides) were able to specifically eliminate Caco-2 cells, which are PHB expressing cells, through the activation of apoptosis (Sibuyi *et al*., 2017). The aim of the current study was to show that AuNR that are similarly functionalised with AHP and $_D$(KLAKLAK)$_2$ can induce death in PHB expressing cells through apoptosis and PTT. The expectation was that these NPs would therefore be more cytotoxic to the target cells (PHB expressing cells) than the AuNSs produced by Sibuyi *et al.* (2017).

In this section of Chapter 4, the aim was to investigate the toxicity of the peptide functionalised AuNRs, AGK (which was described in Chapter 3) on Caco-2, U-87 and PC-3, which were shown to express PHB in Section 4.2.1. The toxicity and therapeutic potential of the AGK was investigated on both the cancerous (Caco-2, U-87, PC-3) and non-cancerous (MCF-12A) cell lines. Cell viability was monitored using the WST-1 assay after treatment with GP, GK, AG and AGK AuNRs. Sibuyi *et al.* (2017) demonstrated that cell death induced by AHP and $_D$(KLAKLAK)$_2$ functionalised AuNSs induce apoptosis in the target cells. In this study, the APOPercentage^{TM} assay was used to investigate if growth inhibition induced by GP, GK, AG and AGK AuNRs was due to apoptosis.

4.2.2.1. Effects of AuNR on cell viability: WST-1 assay

Caco-2, PC-3, U-87 and MCF-12A cells were exposed for 24hrs to increasing concentrations of the AuNRs (GP, GK, AG and AGK). MCF-12A cells were included as a non-cancerous control cell line. Cell viability was measured using the WST-1 cell proliferation assay as described in Chapter 2 (Section 2.2.6.1). The assay principle involves the conversion of tetrazolium salt (WST-1) through the action of mitochondrial dehydrogenase into a yellow coloured product that is measurable by spectrophotometry at 440nm. The colour change is directly proportional to the amount of mitochondrial dehydrogenase in a sample, which is a reflection of the number of live cells. The interference test was performed to determine whether the AuNRs (at the concentrations used in this study) interferes with the WST-1 assay. This was done by incubating the AuNRs with the WST-1 dye reagent and measuring the absorbance of the sample. No interference was observed for all the AuNRs used in this study (data no shown).

DMSO is known to be toxic to cells at high doses (Vergara *et al*., 2014 & Siddiqui *et al*., 2016) and was used as a positive control in the viability assays. DMSO treatment resulted in a significant reduction in the viability of the four cell lines (Figure 4.3). The viability of PC-3 cells treated with AGK AuNRs at concentrations of 200µg/ml and higher was significantly reduced. Although the viability of PC-3 cells was affected by AG AuNRs, at the highest dose of 300µg/ml, the reduction in viability appears not to be significant. The reduction in viability in AGK treated PC-3 cells appears to be dose dependent. GP, GK and AG AuNRs did not affect the viability of PC-3 cells. There was no significant reduction in the viability of Caco-2, U-87 and MCF-12A after exposure to the AuNRs (Figure 4.3). The results for Caco-2 and U-87 cells was unexpected, since Caco-2 and U-87 was shown to express PHB and was therefore expected to be susceptible to the toxic effects of AGK. Moreover, the results in Figure 4.1 suggest that Caco-2 cells express high levels of PHB and these cells were expected to be even more susceptible to the effects of AGK AuNRs than PC-3 cells. Of note, the cells were treated with a NR concentration range of 3-1000µg/ml, however, NR concentrations of >300µg/ml were severely cytotoxic to PC-3 cells. The NRs showed no toxicity

towards Caco-2, U-87 and MCF-12A at the same concentration range. Thus, the NP concentration range of 0-300µg/ml was used as it clearly depicts a dose-dependent loss of PC-3 cell viability.

Based on the design (Figure 3.1) of the AuNRs; Caco-2, PC-3 and U-87 cells should be able to take up AGK and AG AuNRs, since these cells express the PHB receptor. Even though the expression of PHB in MCF-12A cells was not investigated in this study, it was expected that these cells may not express high levels of PHB, since they are non-cancerous cells. It was also expected that AGK, but not AG AuNRs would be toxic to the cells, since AG AuNRs are not functionalised with the pro-apoptotic peptide, $_{D}(KLAKLAK)_{2}$. The response of PC-3 cells, but not Caco-2 and U-87 cells were in line with these expectations. Even though Sibuyi *et al*. (2017) showed that 50% of Caco-2 cells are eliminated using a concentration of 0.3nM spherical AGK AuNPs, it is not clear why the viability of Caco-2 and U-87 cells treated with AGK AuNRs were not affected in the current study. It is possible that higher concentrations of the AuNRs are needed or that PC-3 cells do express higher levels of the PHB receptor. It is also possible that the different size and shape of the AuNRs may have affected the conjugation of the peptides onto the AuNR surface, when compared to the AuNSs used in the Sibuyi study. Caco-2, PC-3 and U-87 cells are cancer cells and cancer cells are known to have numerous genetic mutations, especially in genes involved in the control of cell growth and apoptosis. It is also possible that the differences in the responses observed in Caco-2, PC-3 and U-87 cells treated with AGK AuNRs can be due to different genetic mutations in these cells. I.e. it is possible that Caco-2 and U-87 cells are more resistant to apoptosis induced by AGK AuNRs.

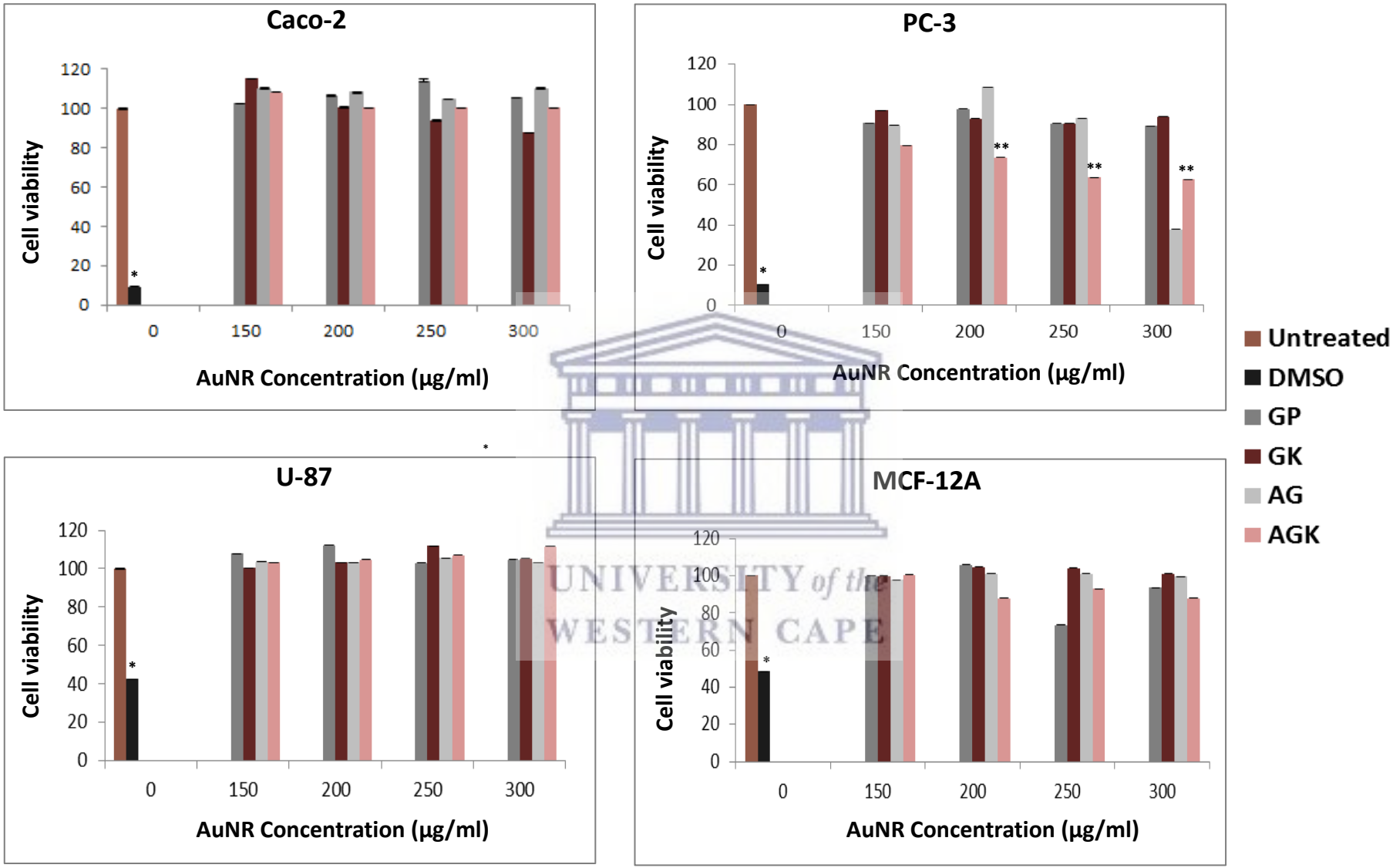

Figure 4.3: Effects of AuNR conjugates on viability of human cell cultures. The cell viability of Caco-2, PC-3, U-87 and MCF-12A cells was analysed using the WST-1 assay. Cells were treated with increasing concentrations of AuNR conjugates for 24 hours. Results represent the average of two independent experiments performed in triplicate. A two-tailed, unpaired t-test was used to analyse statistical significance. * = $p < 0.05$ and ** = $p < 0.01$ significant difference compared to the untreated sample.

4.2.2.2. Cellular uptake analysis of AuNRs by ICP-OES

To quantify the cellular uptake of AuNRs, elemental analysis of cell lysates (prepared from cells that was exposed to the AuNRs) was carried out by ICP-OES. Caco-2, PC-3 and U-87 cells were treated for 24hrs with 200 µg/ml of GP and AGK AuNRs. After 24hrs the cells were lysed in aqua regia and analysed for the presence of Au by ICP-OES as described in Chapter 2 (Section 2.2.6.2). The amount of Au taken up by the cells were calculated and expressed as a percentage of the total amount of Au the cells were treated with. Figure 4.4 shows the percentage of AuNRs taken up by the cells, as a function of the initial amount applied.

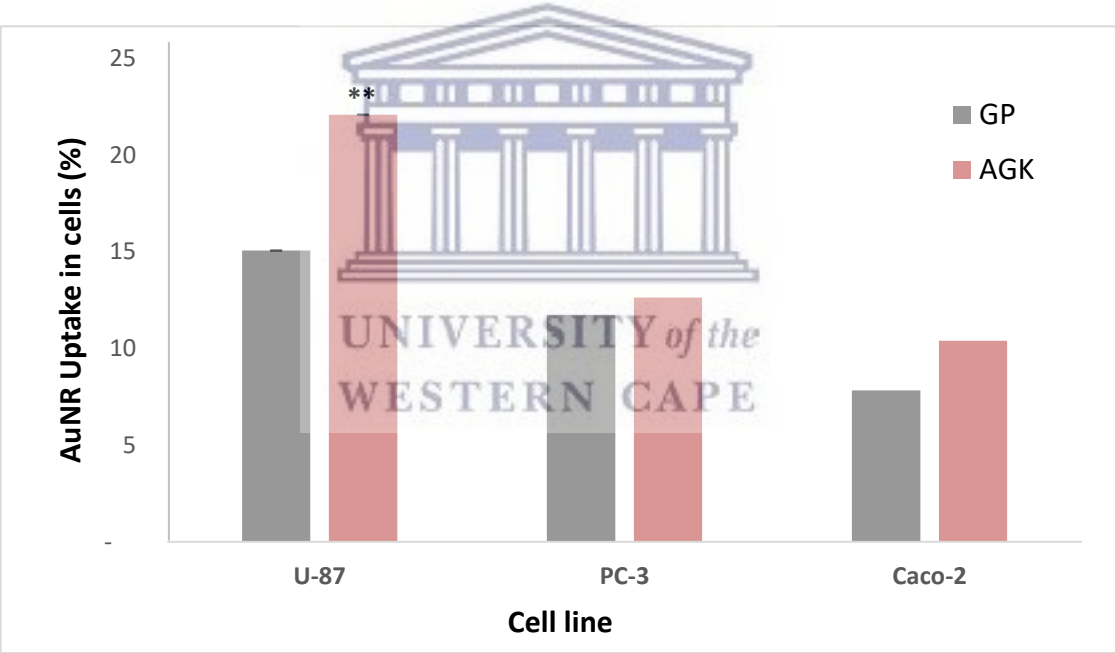

Figure 4.4: Quantification of internalized AuNRs in cells by ICP-OES. The cells were incubated with 200µg/ml of nanomaterials at 37°C for 24hrs. Cells were washed, lysed in aqua regia (3:1 hydrochloric acid: nitric acid) and analysed for gold concentration by ICP-OES. The percentage of AuNRs taken up by the cells was determined as a function of the total amount of AuNRs applied. GP = Pegylated NPs, AGK = has both targeting and therapeutic peptides. A two-tailed, unpaired t-test was used to analyse significance. ** = p< 0.01 significant difference compared to untreated sample.

The three cell lines (Caco-2, PC-3 and U-87 cells) show the presence of Au, suggesting these cells have taken up the AuNRs. The uptake of both AuNRs (GP and AGK) in all cell lines was below 25%. However, U-87 was the only cell line that showed significant uptake of AGK AuNPs. This suggested target specific uptake of AGK AuNRs by U-87 cells. However Caco-2 and PC-3 cells did not take up AGK AuNRs at significant levels. This was unexpected since all three of these cell lines was shown to express PHB. Moreover, Sibuyi *et al*., (2017) demonstrated the targeted delivery of AGK AuNSs to Caco-2 cells. It is not clear why Caco-2 and PC-3 cells did not demonstrate targeted up take of AGK AuNRs. It is possible that the expression levels of PHB are higher in U-87 cells. Even though the ICC results indicate that U-87 cells have a lower expression level of PHB compared to PC-3 and Caco-2 cells (Figure 4.1), it is possible that U-87 cells express higher levels of the PHB receptor on the cell surface. Thus, the PHB expression should be confirmed with western blot analysis and cell surface expression could be confirmed with plasma membrane staining. In addition, a time-based uptake study should be optimised as AGK could have exited the Caco-2 and PC-3 cells before the up take study was performed. It is also possible that conjugation of the targeting peptide, AHP is more efficient for AuNSs compared to AuNRs, as a result AGK AuNSs can be delivered to Caco-2 cells more effectively. A comparative study between the cytotoxicity of AGK AuNSs and AuNRs on PC-3 cells should be done to confirm this.

Interestingly, even though the uptake of AGK AuNRs appears to be very low, these NPs were still able to induce cell death in PC-3 cells (Figure 4.3). U-87 and Caco-2 cells were unaffected by AGK treatment, suggesting that the NPs were taken up by the cells but not at levels high enough to cause cell death. Higher concentrations of the AGK AuNRs are therefore required.

4.2.3. Investigating possible apoptotic cell death induced by AuNRs

Section 4.2.2.1 demonstrated that AGK and possibly also AG AuNRs induce cell death in PC-3 cells. Based on the results obtained with the WST-1 assay, the AuNRs did not

significantly affect the viability of Caco-2 and U-87 cells. Since AGK AuNRs are functionalised with the pro-apoptotic peptide, $_D$(KLAKLAK)$_2$ it is expected that cell death induced by these NPs is due to the activation of apoptosis. The $_D$(KLAKLAK)$_2$ peptide has pro-apoptotic activity and has been shown to induce cell death through apoptosis when internalized by cells (Ellerby *et al*., 1999).

To assess the mode of growth inhibition following exposure of cells to AuNRs, the APOPercentage™ assay was used to determine if AGK AuNRs induced apoptosis in PC-3, Caco-2 and U-87 cells. It was also important to confirm using another assay that AGK AuNRs did not induce cell death in Caco-2 and U-87 cells. The APOPercentage™ assay employs the disodium salt of 3,4,5,6,-tetrachloro-2' ,4' ,5' ,7'–tetraiodofluorescein which stains apoptotic cells purple-red. Only apoptotic cells that undergo the translocation of the phosphatidyl serine (PS) from the inner cell membrane to the outer leaflet will take up the APOPercentage™ dye (Verhoven *et al*., 1995). Apoptosis was quantified by measuring the dye incorporated by apoptotic cells using the BD Accuri flow cytometer as described in Chapter 2 (Section 2.2.6.3). Caco-2, PC-3 and U-87 cells were exposed to GP and AGK AuNRs at a concentration of 200µg/ml for 24hrs and were thereafter stained with APOPercentage™ dye.

The number of apoptotic cells after GP treatment were not significantly different when compared to untreated cells except in the case of Caco-2, which produced even less apoptotic cells than the untreated control Figure 4.5. AGK AuNRs were able to induce significant levels of apoptosis in PC-3 cells (70%) when compared to the untreated control as shown in Figure 4.5. This correlates with the results obtained for the WST-1 assay in which these cells were susceptible to AGK AuNRs at the same concentration (200µg/ml) resulting in a reduction in the viability of the cells (Figure 4.3). The level of apoptosis in Caco-2 and U-87 cells treated with AGK AuNRs was not significantly higher than the untreated control. Results from this *in vitro* study showed that the targeted nanotherapy (AGK) had a more pronounced cytotoxic effect on PC-3 than the other AuNR-conjugates, which had negligible impact on cellular function at the dosage used here (Figure 4.3 and Figure 4.5). This data confirmed that the pro-apoptotic peptide, $_D$(KLAKLAK)$_2$ was responsible for the death

of PC-3 cells in response to AGK. Figure 4.5 also shows that the level of apoptosis in cells treated with DMSO, although it is higher than the untreated controls, is not significantly higher than the level of apoptosis in untreated controls. This may suggest that a higher concentration of DMSO must be used.

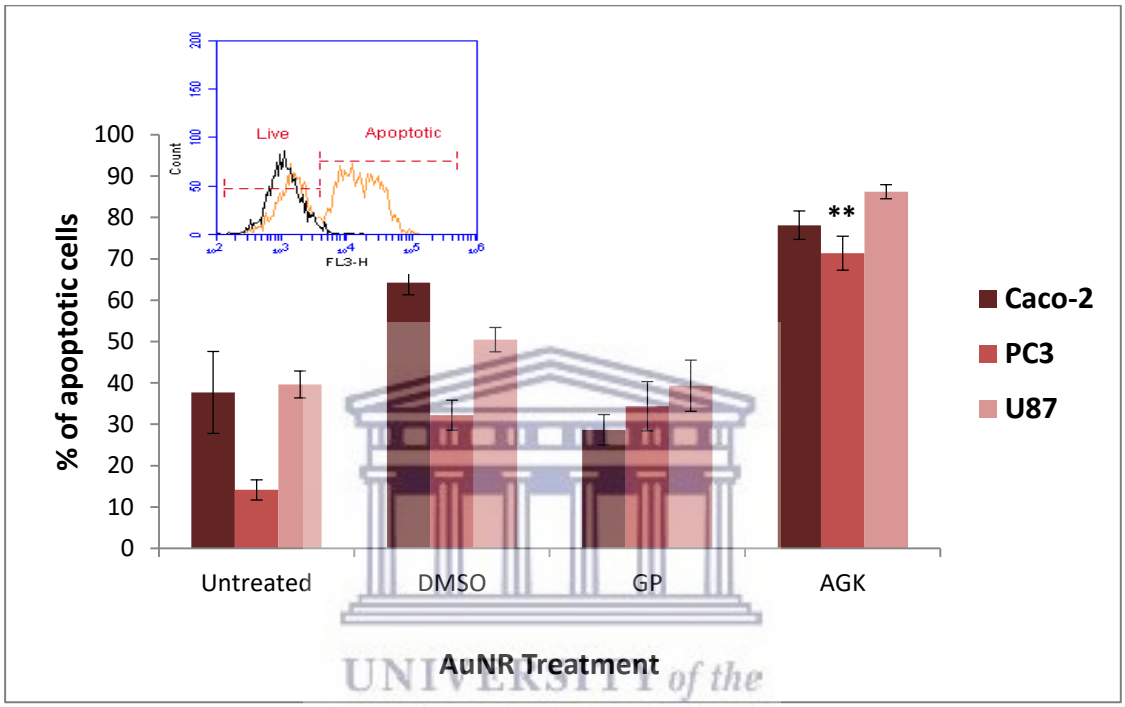

Figure 4.5: Analysis of the apoptotic effects induced by the AuNRs. Caco-2, PC-3 and U-87 cells were treated for 24 hrs with 200µg/ml of GP and AGK AuNRs, afterwich apoptosis was assessed by flow cytometry using the APOPercentage™ assay. The insert shows an example of the histogram data generated for AGK treated PC-3 cells. All treatments were done in triplicate and the bar graphs show the median percentage apoptosis cells, which was determined from the histograms. DMSO was used as a positive control. Untreated = negative control; DMSO = DMSO treated (XX) positive control; GP=Pegylated AuNRs; AGK = AuNRs with both targeting and therapeutic peptides. A two-tailed, unpaired t-test was used to analyse significance. * = $p < 0.05$ and ** = $p < 0.01$ significant difference compared to the untreated sample.

This study shows that the modification of the AuNR surface by chemical conjugation of peptides significantly influenced the interaction of the AuNRs with PC-3 cells, and their effects by increasing the cellular uptake and bioactivity. Similar effects have been reported for AuNPs in other studies where these AuNPs has been used as target specific delivery vehicles for anticancer therapies through the use of antibodies (Palanca-Wessels *et al.*, 2016 & Rudin *et al.*, 2017), aptamers (Hoellenriegel *et al.*,

2014 & Liu *et al*., 2013) and targeting ligands (Chen *et al*., 2014; McGuire *et al*., 2014; Wang *et al*., 2016 & Ding *et al*., 2017). The ability of targeting agents to target disease-specific markers provides a viable approach to reduce the off-target effects and increase the drug efficacy, which means that lower dosages of the drugs can be used (Ruoslahti *et al*., 2010). NP-based delivery systems have been extensively studied in cancer and several preclinical studies and have since progressed successfully to human trials, with a variety of drug candidates still in the pipeline. The recently evaluated human clinical trials for targeted nanotherapies provide evidence that these systems can provide improved and better treatment strategies (ClinicalTrials.gov numbers; NCT00356980, NCT00436410 and, NCT00848042).

4.2.4. Photothermal potential of AuNRs

Sibuyi *et al*. (2017) proved, using Caco-2 cells as a model, that PHB targeted AuNSs can trigger apoptosis in PHB expressing cells. It was demonstrated in Section 4.2.3 that AuNRs (i.e. AGK) that are similarly functionalised are able to induce apoptosis in PC-3 cells through the activation of apoptosis via the $_D$(KLAKLAK)$_2$ peptide. These AuNRs were not able to activate apoptosis in Caco-2 cells. The aim of this section of the study was to investigate if AuNRs that are similarly functionalised with peptides can also activate cell death through PTT. Since AuNRs (AGK and AG AuNRs) that have been functionalised with the targeting peptide (AHP) was not toxic to Caco-2 cells, these cells were selected as the model cell line to study photothermal activated cell death.

Caco-2 cells were exposed for 30min to 500µg/ml of AG AuNRs as described in Chapter 2 (Section 2.2.6.4). These AuNRs were pegylated and functionalised with the PHB targeting peptide, AHP. Thereafter, untreated control cells and cells treated with AG were exposed to a NIR (780nm) laser for a time period of 30sec to 5min. The distance of the laser from the cells was set at 15cm. Morphological changes were assessed via light microscopy and the cell viability was measured using the WST-1 cell proliferation assay as described in Chapter 2 (Section 2.2.6.1).

4.2.4.1. Effect of Photothermal therapy on cell morphology

The first and most readily noticeable effect following exposure of cells to toxic substances or stress is the alteration of cellular features such as shape and size (Häcker, 2000).

Caco-2 cells grow and differentiate into monolayers characterized by elongated shape that resemble the small intestinal epithelium under microscopy (Herold *et al*., 1994). Typical cellular features of Caco-2 cells are shown in untreated cells in Figure 4.6. Cells treated with the laser only showed no morphological changes, at all exposure times tested. The shape of the cells treated with DMSO is distinctly different from the untreated control cells. DMSO treated cells are more spherical and may be in the process of detaching from the plate. Cells treated with a combination of laser exposure and AG (AG + Laser treatment), also do not show distinctive morphological changes at all exposure times, as the cell density and shape was similar to that of the untreated control cells (Figures 4.6). Of note, as this was a gateway experiment, this protocol had not yet been optimized, thus it is possible that the cells might not have been exposed to laser treatment for long enough, as a result the PTT was not successful. The distance of laser from the cells may also have been too far.

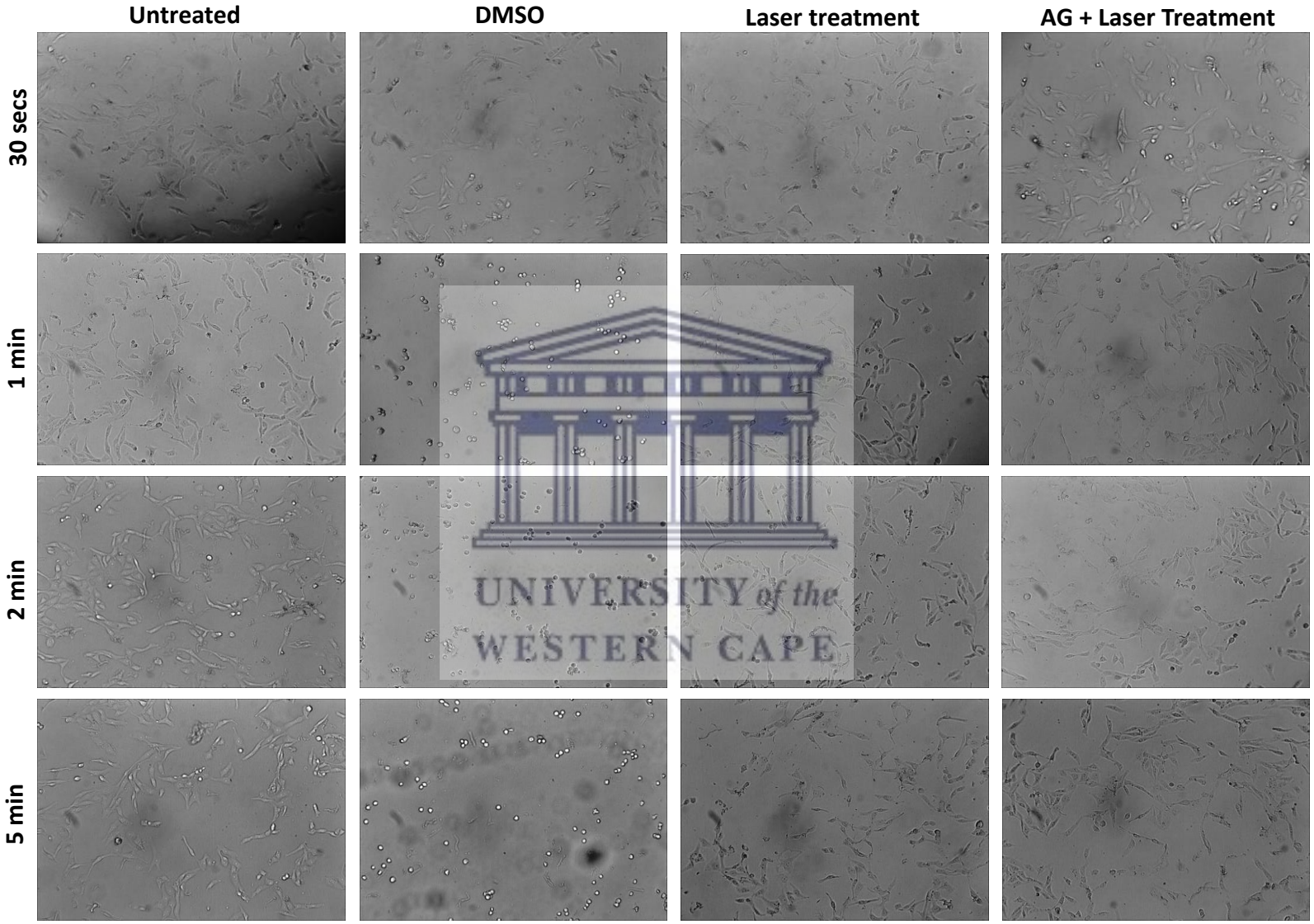

Figure 4.6: Effect of AG Photothermal therapy on Caco-2 cells. The cells were seeded in 96 well plates and treated for 30 minutes with gold nanorods functionalised with the targeting peptide AHP (AG). Following uptake, cells were exposed to a laser with a peak wavelength of 780nm for a time ranging between 30 seconds and 2 minutes. The cells were incubated for 24hrs post laser treatment and images taken with a light microscope at 10X magnification.

4.2.4.2. Effect of photothermal therapy on cell viability: WST-1 assay

In order to thoroughly investigate whether the AuNRs produced in this study could be used for PTT, the viability of Caco-2 cells was assessed using the WST-1 assay. The experimental set-up was exactly the same as described in Section 4.2.4.1.

The viability of cells treated with the laser only or with AG AuNRs only was not significantly different from that of untreated control cells (Figure 4.7), while the viability of cells treated with DMSO and cells exposed to laser treatment and co-treated with AG AuNRs was significantly reduced. The viability of DMSO treated cells was reduced to ±70%. Cells exposed to laser treatment for 2 and 5min and co-treated with AG AuNRs were significantly reduced to 72 and 49%, respectively. Laser treatment of 30sec and 1min did not have an effect on cell viability. The steep decline in viability after 5min of treatment could be an indication that AG AuNRs are effectively internalized and that an exposure time of 5min or more to the NIR laser results in photothermal effect, resulting in the death of the cells. The WST-1 assay thus show that even though no morphological changes were observed in Caco-2 cells subjected to laser treatment for 5min and co-treated with AG AuNRs, these cells were indeed affected by the co-treatment which resulted in the death of the cells.

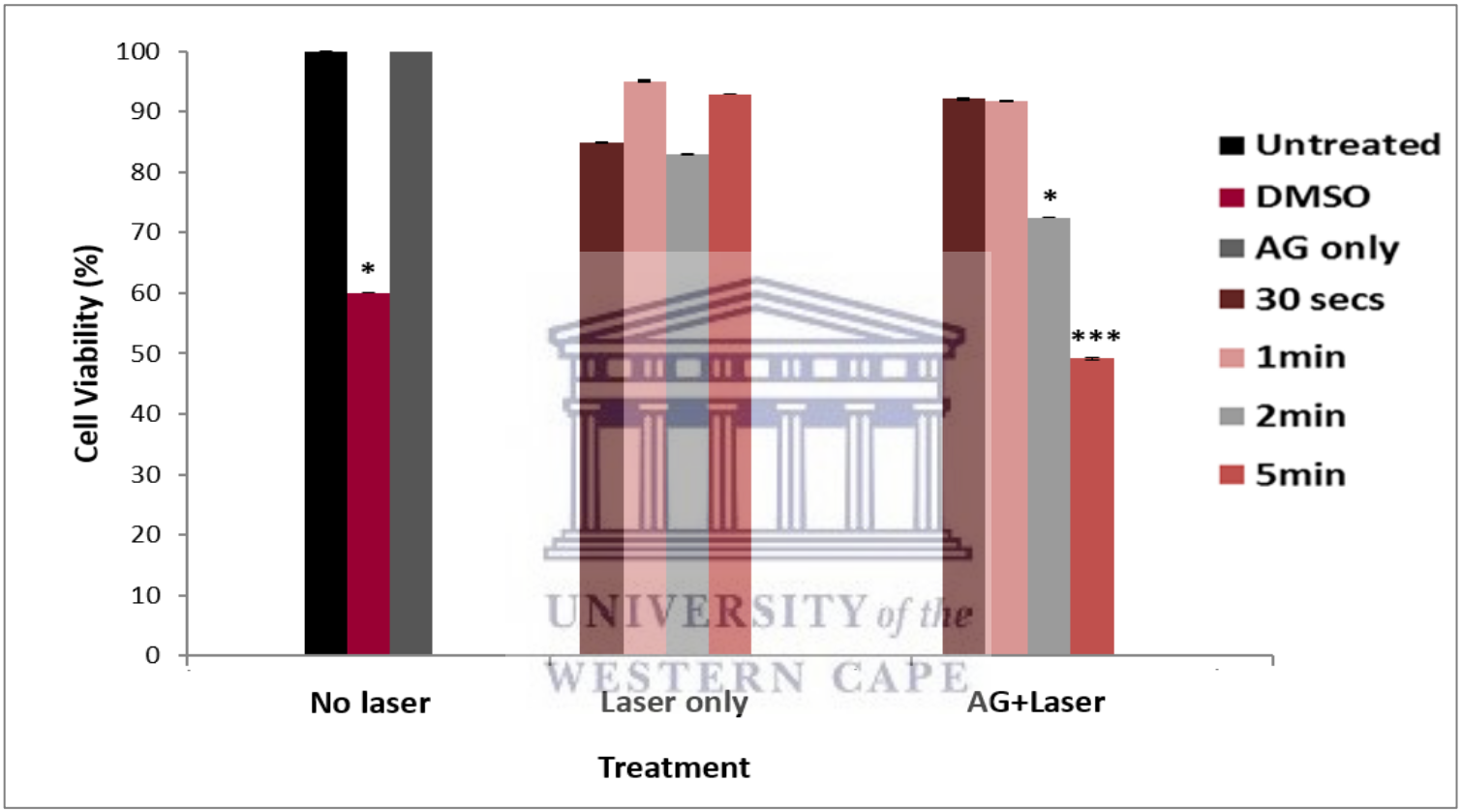

Figure 4.7: Effect of AG-induced photothermal therapy on Caco-2 cells. The cells were seeded in 96 well plates and treated for 30 minutes with gold nanorods functionalised with the targeting peptide AHP (AG). Following uptake, cells were exposed to a NIR laser with a peak emission wavelength of 780nm for time periods ranging between 30 secs and 5 min. The WST-1 assay was performed to assess cell viability. A two-tailed, unpaired t-test was used to analyse significance. * = $p < 0.05$ and *** = $p < 0.001$ significant difference compared to the untreated sample.

4.3. Conclusion

The aim of this chapter was to examine the cytotoxic effects of the AuNR conjugates on PHB-expressing cell lines. As the application of the targeted AuNRs is to selectively bind to the PHB receptor, the expression and localization of the PHB protein in selected human cell lines was assessed. Immunocytochemical staining confirmed the expression of PHB in Caco-2, PC-3 and U-87 cells. In general, it appears that PHB is expressed either in the cytoplasm or on the surface of these cells.

The toxicity of the AuNRs bi-functionalised with the targeting (AHP) peptide and therapeutic peptide ($_D$(KLAKLAK)$_2$) i.e. AGK was investigated on the PHB expressing cells. Although the three cell lines demonstrated the uptake of AGK AuNPs, U-87 was the only cell line that demonstrated target specific uptake of AGK AuNPs. However, the WST-1 assay showed that AGK was not toxic to Caco-2 and U-87 cells. PC-3 was the only cell line that was affected by AGK AuNRs. The results for Caco-2 and U-87 cells were unexpected, since Caco-2 and U-87 was shown to express PHB and was therefore expected to be susceptible to the toxic effects of AGK AuNRs. Even though AGK AuNRs were taken up by PC-3 cells the uptake cannot be attributed to the expression levels of the PHB receptor on these cells. Therefore the toxicity in PC-3 was likely due to PC- 3 cells being more susceptible to the toxicity of AGK at lower concentrations compared to Caco-2 and U-87. The APOPercentage™ assay correlates to the WST-1 assay as AGK had a more pronounced cytotoxic effect on PC-3 than the other AuNR-conjugates, confirming that the pro-apoptotic peptide, $_D$(KLAKLAK)$_2$ was responsible for the death of PC-3 cells in response to AGK. As AGK was not toxic to Caco-2 cells, these cells were selected as the model cell line to study PTT. Even though no morphological changes were observed in Caco-2 cells subjected to laser treatment, these cell were indeed affected by the co-treatment which resulted in the death of the cells.

The overall aim of this study was to examine the effects of AGK on PHB-expressing cell lines in an attempt to improve the therapeutic effect of $_D$(KLAKLAK)$_2$ by PTT. Therefore, a shortcoming of this chapter is that PHB-expressing cells have not been

co-treated with AGK and laser exposure in order to determine if PTT could in fact enhance the therapeutic effect of $_D$(KLAKLAK)$_2$ on these cells. This study has however shown that AGK selectively targets and induces apoptosis in PC-3 cells through $_D$(KLAKLAK)$_2$ induced apoptosis. Furthermore, it has shown that AG can eliminate PHB-expressing cells via PTT. Therefore, even though the overall objective of this study has not been investigated, the findings suggest great promise that the co-treatment of AGK and laser exposure could enhance the therapeutic effects of $_D$(KLAKLAK)$_2$.

Chapter five: Summary of this study

5.1. General discussion

Cancer is one of the leading causes of death, worldwide. It is a progressive disease, in that accumulative changes occur at the genetic level. Subsequently, presenting a disease that is complex and life-threatening (Pal and Nayak, 2010). Mortality tolls are estimated to reach approximately 13.1 million in 2030. These statistics suggest that current therapeutic strategies are not effective, highlighting the need for alternative therapeutic approaches (Sumer and Gao, 2008).

The non-specific distribution of conventional chemotherapeutic drugs through the body can result in severe toxicities (Agnihotri *et al*., 2011). As a result the drug dosages must be reduced which can severely affect the efficiency of chemotherapeutic drugs. Overall, the objective in the treatment of cancer is to deliver drugs through the blood circulation directly to the diseased tissues/cells, with little to no damage inflicted on healthy cells (Byrne *et al*., 2008). In view of this, the therapeutic goal of chemotherapy has shifted towards targeted drug delivery systems, which have been successfully demonstrated using nanotechnology. Nanomaterials have a large surface area to size ratio, which increases their capacity to carry drugs or biomolecules. These features can be exploited for bio-medical applications by attaching drugs, bio-active molecules or targeting moieties for either therapeutic and/or diagnostic purposes. Several NPs have been successfully used in cancer treatment, of which AuNPs have been applied as drug delivery vehicles (Niikura *et al*., 2013 & Paul *et al*., 2014). The unique properties exhibited by AuNPs are attributed to their optical properties, namely, their ability to strongly scatter light and enhance the local electric field (Jain *et al*., 2007, 2008). AuNRs in particular possess several advantages including large absorption cross sections, tunable longitudinal plasmon wavelengths, high chemical stability, and efficient photothermal conversion ability, enabling their applications as optically active agents for various biomedical applications, such as photothermal therapy (PTT) [Alkilany *et al*., 2012; Mooney *et al*., 2014 & Park *et al*., 2014].

A study by Sibuyi *et al.* (2017) demonstrated that AuNSs bi-conjugated with a PHB-targeting peptide (AHP) and a therapeutic peptide, the pro-apoptotic peptide $_D$(KLAKLAK)$_2$ are specifically taken up by cells that express the PHB (the colon cancer cell line Caco-2) on their surface. It was also demonstrated that the uptake of these AuNP resulted in the activation of apoptosis in these cells. This finding suggested that these AuNPs could potentially be used as a target specific therapeutic for the treatment of cancers where PHB was over expressed. However, if this nanotherapeutic was redesigned and the AuNSs were replaced with AuNRs, these nanoparticles could also be used as PTT. Hence the aim of the current study was to explore the synthesis and characterisation of AuNRs that was bi-conjugated with AHP and $_D$(KLAKLAK)$_2$. The therapeutic effect of these AuNRs was expected to be even higher when compared to the AuNSs reported in the Sibuyi study due to the synergistic effect brought about by the delivery of the pro-apoptotic peptide $_D$(KLAKLAK)$_2$ and PTT.

The first objective involved the synthesis and characterization of AuNRs, the functionalisation of the AuNRs with the targeting peptide (AHP) and the therapeutic peptide ($_D$(KLAKLAK)$_2$). Previous studies have shown that AuNRs become absorption-dominant if their diameters are less than 10nm (Ni *et al.*, 2008 & Chen *et al.*, 2010). Thus, it was crucial to control the size of the AuNRs in order to efficiently absorb NIR light. As the seed-to-Au (III) ions ratio in the growth solution has the most significant effect on the size of the AuNRs (Sau and Murphy, 2004 & Jia *et al.*, 2015), three different seed-to-Au (III) ion ratios were used for AuNR preparations (G6S4, G8S2 and G9S1) in order to identify the ideal ratio for the synthesis of AuNRs with a diameter <10nm. UV-Vis analysis showed that the G9S1 preparation had the longest λ_L peak compared to the other preparations, suggesting it would absorb NIR more efficiently. EDX and HR-TEM micrographs confirmed that Au was present in the samples and that the G9S1 sample had the highest AuNP yield, respectively.

During AuNR synthesis, it is common for other shapes of AuNPs such as nanospheres, nanocubes, nanoprisms and nanocrystals to form (Xiong *et al.*, 2011), which was evident in the HR-TEM images (Figure 3.4). Thus there was a need to separate the

AuNPs based on their shapes. Previous studies employed centrifugation for separation of AuNR from AuNPs of different morphologies (Ahmad *et al*., 2014; Scaletti *et al.* 2014; Robertson *et al*., 2016 & Boksebeld *et al*., 2017). This separation technique is based on the differential sedimentation rates of NP with different shapes and sizes (Xiong *et al*., 2011). The UV-Vis spectrum of the supernatant showed two defined peaks, one in the visible region (200-500nm) and one in the NIR region (700-1100nm), which is similar to the spectrum obtained for the G9S1 sample (before differential centrifugation). This is a clear indication of the presence of AuNRs. The UV-Vis spectrum generated for the pellet was much less defined, suggesting that the majority of AuNRs were absent from the pellet. To confirm that the AuNRs was successfully separated from AuNPs with other shapes, the two fractions (the pellet and supernatant) were subjected to HR-TEM and EDX analysis. The EDX spectra suggest that Au was present in both the supernatant and the pellet suspensions. The TEM images confirmed that the supernatant contained the majority of the AuNRs, while the pellet contained a mixture of other AuNP shapes. Based on the HR-TEM images, ImageJ determined that the length of the majority of the AuNRs present in the supernatant fraction was 21-25nm and the diameter was 6-8nm, suggesting an aspect ratio of 3 to 3.5. Although the diameter of 80% of the AuNR (which was denoted as G) was 6-8nm, a significant variation in the length of the AuNR was observed for AuNRs in the supernatant as a result of not strictly controlling the temperature during synthesis. Nevertheless the diameter produced was in the optimum range (i.e. <10nm) for PTT, according to Jia *et al.* (2015).

While CTAB simultaneously serves as a template for growth and prevents aggregation of AuNRs, it is extremely cytotoxic. Thus, the CTAB needed to be removed in order for the NRs to be used for biological application. CTAB molecules were removed from the AuNR surface and replaced with PEG molecules to prevent aggregation as described by Sosibo *et al.* (2015) to produce pegylated AuNRs (GP). Following pegylation, UV-Vis spectroscopy showed a red shift in GP compared to G. This shift is the result of an increase in the local refractive index at the AuNR surface, which suggests that PEG were successfully conjugated to the AuNR surface. It is important that the AuNRs retain their stability in biological environments. To test the stability of the GP, the

AuNRs were placed in buffers that simulate various biological buffer conditions. UV-Vis analysis indicated that the AuNRs were stable in dH_2O; BSA and FBS. However, the AuNRs were not stable in PBS and culture media.

The abovementioned data proved satisfactory to proceed with peptide functionalisation of the AuNRs for biological application. The strategy used to functionalise the AuNRs (GP) with peptides was exactly the same strategy used by Sibuyi *et al.* (2017) to functionalise AuNSs. GP was bi-functionalised by conjugating the targeting peptide (AHP) and therapeutic peptide ($_D$(KLAKLAK)$_2$) to the AuNRs through ligand exchange. Briefly, PEG-OH, PEG-Biotin and the $_D$(KLAKLAK)$_2$ peptide all contain a thiol (SH) group to facilitate conjugation to the AuNR surface. The three molecules were added simultaneously to the AuNR suspension to form GK (GP + $_D$(KLAKLAK)$_2$). The biotinylated AHP which contained a streptavidin tag to facilitate binding of the peptide to PEG-Biotin was added to GP to form AG (GP + AHP). Similarly, the biotinylated AHP was added to GK to form AGK (GP + AHP + $_D$(KLAKLAK)$_2$). AG and GK served as controls. When the targeting peptide (AHP) and therapeutic peptide ($_D$(KLAKLAK)$_2$) were incorporated onto the AuNRs, there was a red shift in the UV-Vis peak with every peptide added, indicating successful functionalization of the peptides onto the AuNR surface. This was further validated by ζ-potential measurements, which showed drastic changes in each AuNR conjugate, which is attributable to the modification of the AuNR surfaces. HR-TEM analysis showed that the functionalised AuNR conjugates were well dispersed in solution and showed no signs of aggregation following functionalisation.

As AuNRs were successfully synthesised, functionalised and characterised, the next objective was to test the ability of the AuNRs to target cancer cells and induce their destruction. This required appropriate cell culture models, i.e. cells that express PHB. The expression of PHB protein was investigated in 12 human cancer cell lines of which three cell lines (Caco-2, PC-3 and U-87) were found to express the protein.

Caco-2, U-87 and PC-3 were treated with the AuNR conjugates and the cell viability was measured using the WST-1 cell proliferation assay. The WST-1 assay showed that

AGK was not cytotoxic to Caco-2 and U-87 cells, however, AGK reduced the viability of PC-3 cells in a dose dependent manner. The results for Caco-2 and U-87 cells was unexpected, since Caco-2 and U-87 were shown to express PHB and were therefore expected to be susceptible to the toxic effects of AGK. Even though AGK was taken up by PC-3 cells, the uptake cannot be attributed to the expression levels of the PHB receptor on these cells. Therefore the toxicity in PC-3 was likely due to PC-3 cells being more susceptible to the toxicity of AGK at lower concentrations compared to Caco-2 and U-87.

Based on the results obtained with the WST-1 assay, it was demonstrated that AGK induce cell death in PC-3 cells and AGK did not significantly affect the viability of Caco-2 and U-87 cells. The next objective was to assess the mode of cell death following exposure of cells to the AuNRs. The APOPercentage™ assay was used to determine if AGK induced apoptosis in PC-3, Caco-2 and U-87 cells. The APOPercentage™ assay correlates with the WST-1 assay as AGK had a more pronounced cytotoxic effect on PC-3 than the other AuNR-conjugates, confirming that the pro-apoptotic peptide, $_D(KLAKLAK)_2$ was responsible for the death of PC-3 cells in response to AGK treatment.

The next objective of this study was to investigate if the AuNRs could activate cell death through PTT. Since AuNRs that have been functionalised with the targeting AHP peptide (AGK and AG AuNRs) was not toxic to Caco-2 cells, these cells were selected as the model cell line to study photothermal activated cell death. The cytotoxicity and change in morphology induced by AG in the presence and absence of laser treatment were investigated. No distinctive morphological changes were observed in cells treated with the laser only or with the co-treatment of the laser in combination with AG AuNRs at all exposure times as the cell density and shape was similar to untreated cells. The WST-1 assay indicated that the amount of viable cells following laser only treatment is similar to the untreated control, which correlates to the no change in morphology observed. Interestingly, cells subjected to AG + laser treatment showed a decrease in viability after 2min of laser exposure with a significant decrease after 5min. The steep decline in viability after 5min of laser

treatment could be an indication that AG AuNRs were effectively internalized and that an exposure time of 5min or more to the NIR laser results in the photothermal effect, resulting in the death of the cells. The WST-1 assay thus show that even though no morphological changes were observed in Caco-2 cells subjected to laser treatment for 5min and co-treated with AG AuNRs, these cells were indeed affected by the co-treatment which resulted in the death of the cells.

The overall aim of this study was to examine the effects of AGK on PHB-expressing cell lines in an attempt to improve the therapeutic effect of $_D(KLAKLAK)_2$ by PTT. Therefore, a shortcoming of this study is that the cells have not been subjected to AG + laser treatment in order to determine if PTT could enhance the therapeutic effect of $_D(KLAKLAK)_2$ on these cells. This study has however shown that AGK selectively eliminates PC-3 cells through $_D(KLAKLAK)_2$ induced apoptosis. Furthermore, it has shown that AG eliminates Caco-2 cells via PTT. Therefore, even though the overall objective of this study has not been achieved, the findings suggest great promise that the co-treatment of AG + laser treatment could enhance the therapeutic effects of $_D(KLAKLAK)_2$.

5.2. Conclusion

The main aim of this study was to develop a nanoparticle-based targeted drug delivery system using peptide directed AuNRs as a delivery vehicle and to evaluate whether photothermal therapy could enhance the therapeutic effect. AuNRs were successfully synthesised and functionalized for its application in a biological environment. This study identified three cancer cell lines (Caco-2, PC-3 and U-87 cells) that could be used for selective targeting of the nanotherapy. In an up take study, target specific up take of AGK AuNRs by U-87 cells were shown. However, this could not be demonstrated by Caco-2 and PC-3 cells. Higher concentrations of the AGK AuNRs are likely required to show selective uptake. Even through no up take was demonstrated, AGK AuNRs selectively eliminated PC-3 cells through $_D(KLAKLAK)_2$ induced apoptosis, which could possibly be exploited for the treatment of prostate

cancer. Furthermore, AG AuNRs eliminated Caco-2 cells through PTT, which could possibly be exploited for the treatment of colon cancer.

5.3. Future work

Future directions would aim to address limitations identified in this study. The literature extensively demonstrates the targeting and apoptotic ability of AHP and $_{D}(KLAKLAK)_2$, respectively. Thus the cell viability results for Caco-2 and U-87 cells was unexpected, since Caco-2 and U-87 were shown to express PHB and was therefore expected to be susceptible to the toxic effects of AGK. As PC-3 cells were susceptible to the toxic effect of AGK, it is possible that higher concentrations of the AuNRs are needed to exert toxic effects on Caco-2 and U-87. It is also possible that the different size and shape of the AuNRs may have affected the conjugation of the peptides onto the AuNR surface, when compared to the AuNSs used in the Sibuyi study. Thus additional techniques to confirm functionalisation should be employed such as Fourier-transform infrared spectroscopy (FTIR) which could identify the functional groups of the peptides if present (Kötting *et al.*, 2012). Another limitation encountered in this study was that Imuunocytochemistry could not confirm whether PHB is expressed on the cell surface or membrane. Western blot analysis would therefore be required and the collective data would validate PHB expression.

A crucial shortcoming of this study is that PHB-expressing cells have not been co-treated with AGK + laser exposure in order to determine if PTT could enhance the therapeutic effect of $_{D}(KLAKLAK)_2$ on these cells. Thus future investigations would focus on subjecting Caco-2, PC-3 and U-87 cells to the AGK + laser co-treatment. In addition, PC-3 and U-87 cells would be subjected to AG + Laser co-treatment to investigate whether the same toxicity is observed as Caco-2 cells. To corroborate the *in vitro* toxicity of the co-treatment of AG/AGK and PTT, *in vivo* investigations are necessary to clarify the mechanisms governing the toxicity. The PHB-targeted nanotherapy have previously shown pronounced effects on Caco-2 cells and this study has shown effects on PC-3 cells. Thus, the strategy requires further investigation to determine the effect of the PHB-targeted therapy in animal models

of colon cancer and prostate cancer. Since Caco-2 cells originate from a colon cancer patient and PC-3 cells from a prostate cancer patient (Chen *et al*., 2010 & O'Dwyer *et al*., 2011), PHB targeting might also be able to help in the treatment of colon cancer and prostate cancer. Thus, the expression of PHB in colon and prostate cancer patients need to be investigated as the protein has been shown to be upregulated in tissue samples of colon and prostate cancer patients.

References

1. Abadeer, N. S. and Murphy, C. J. (2016). Recent progress in cancer thermal therapy using gold nanoparticles. *The Journal of Physical Chemistry C*, *120*(9), 4691-4716.
2. Abtahi, S. M. H. (2013). *Synthesis and characterization of metallic nanoparticles with photoactivated surface chemistries* (Doctoral dissertation, Virginia Tech).
3. Agemy, L., Kotamraju, V. R., Friedmann-Morvinski, D., Sharma, S., Sugahara, K. N. and Ruoslahti, E. (2013). Proapoptotic peptide-mediated cancer therapy targeted to cell surface p32. *Molecular Therapy*, *21*(12), 2195-2204.
4. Agnihotri, J., Saraf, S. and Khale, A. (2011). Targeting: new potential carriers for targeted drug delivery system. *International Journal of pharmaceutical sciences Review and Research*, *8*(2), 117-123.
5. Ahmad, I., Zandvliet, H. J. and Kooij, E. S. (2014). Shape-induced separation of nanospheres and aligned nanorods. *Langmuir*, *30*(27), 7953-7961.
6. Ahmad, S., Zamry, A. A., Tan, H. T. T., Wong, K. K., Lim, J. and Mohamud, R. (2017). Targeting dendritic cells through gold nanoparticles: A review on the cellular uptake and subsequent immunological properties. *Molecular immunology*, *91*, 123-133.
7. Aina, O. H., Marik, J., Liu, R., Lau, D. H. and Lam, K. S. (2005). Identification of novel targeting peptides for human ovarian cancer cells using "one-bead one-compound" combinatorial libraries. *Molecular cancer therapeutics*, *4*(5), 806-813.
8. Ali, M. R., Panikkanvalappil, S. R. and El-Sayed, M. A. (2014). Enhancing the efficiency of gold nanoparticles treatment of cancer by increasing their rate of endocytosis and cell accumulation using rifampicin. *Journal of the American Chemical Society*, *136*(12), 4464-4467.
9. Ali, M. R., Ali, H. R., Rankin, C. R., and El-Sayed, M. A. (2016). Targeting heat shock protein 70 using gold nanorods enhances cancer cell apoptosis in low dose plasmonic photothermal therapy. *Biomaterials*, *102*, 1-8.
10. Ali, M.R., Rahman, M.A., Wu, Y., Han, T., Peng, X., Mackey, M.A., Wang, D., Shin, H.J., Chen, Z.G., Xiao, H. and Wu, R. (2017). Efficacy, long-term toxicity, and mechanistic studies of gold nanorods photothermal therapy of cancer in xenograft mice. *Proceedings of the National Academy of Sciences*, *114*(15), E3110-E3118.
11. Alkilany, A. M., Nagaria, P. K., Hexel, C. R., Shaw, T. J., Murphy, C. J. and Wyatt, M. D. (2009). Cellular uptake and cytotoxicity of gold nanorods: molecular origin of cytotoxicity and surface effects. *Small*, *5*(6), 701-708.
12. Alkilany, A. M. and Murphy, C. J. (2010). Toxicity and cellular uptake of gold nanoparticles: what we have learned so far?. *Journal of nanoparticle research*, *12*(7), 2313-2333.
13. Alkilany, A. M., Lohse, S. E. and Murphy, C. J. (2012). The gold standard: gold nanoparticle libraries to understand the nano–bio interface. *Accounts of chemical research*, *46*(3), 650-661.
14. Allen, J. E., Krigsfeld, G., Patel, L., Mayes, P. A., Dicker, D. T., Wu, G. S. and El-Deiry, W. S. (2015). Identification of TRAIL-inducing compounds highlights small molecule ONC201/TIC10 as a unique anti-cancer agent that activates the TRAIL pathway. *Molecular cancer*, *14*(1), 99.
15. American Cancer Society. (2016). Cancer Facts and Figures 2016. Atlanta, GA: American Cancer Society.
16. Anderson, M. A., Huang, D. and Roberts, A. (2014, July). Targeting BCL2 for the treatment of lymphoid malignancies. In *Seminars in hematology* (Vol. 51, No. 3, 219-227). WB Saunders.

17. Annunziato, L., Amoroso, S., Pannaccione, A., Cataldi, M., Pignataro, G., D'Alessio, A., Sirabella, R., Secondo, A., Sibaud, L. and Di Renzo, G.F. (2003). Apoptosis induced in neuronal cells by oxidative stress: role played by caspases and intracellular calcium ions. *Toxicology letters*, *139*(2), 125-133.
18. Apfel, S. C. (1996). Docetaxel neuropathy. *Neurology*, *46*(1), 2-3.
19. Arap, W., Pasqualini, R. and Ruoslahti, E. (1998). Cancer treatment by targeted drug delivery to tumor vasculature in a mouse model. *Science*, *279*(5349), 377-380.
20. Arranja, A.G., Pathak, V., Lammers, T. and Shi, Y. (2017). Tumor-targeted nanomedicines for cancer theranostics. *Pharmacological Research*, *115*, 87-95.
21. Ashkenazi, A. and Dixit, V. M. (1998). Death receptors: signaling and modulation. *Science*, *281*(5381), 1305-1308.
22. Ashley, C.E., Carnes, E.C., Phillips, G.K., Padilla, D., Durfee, P.N., Brown, P.A., Hanna, T.N., Liu, J., Phillips, B., Carter, M.B. and Carroll, N.J. (2011). The targeted delivery of multicomponent cargos to cancer cells via nanoporous particle-supported lipid bilayers. *Nature materials*, *10*(5), 389.
23. Bakhtiary, Z., Saei, A. A., Hajipour, M. J., Raoufi, M., Vermesh, O. and Mahmoudi, M. (2016). Targeted superparamagnetic iron oxide nanoparticles for early detection of cancer: Possibilities and challenges. *Nanomedicine: Nanotechnology, Biology and Medicine*, *12*(2), 287-307.
24. Bang, Y.J., Van Cutsem, E., Feyereislova, A., Chung, H.C., Shen, L., Sawaki, A., Lordick, F., Ohtsu, A., Omuro, Y., Satoh, T. and Aprile, G. (2010). Trastuzumab in combination with chemotherapy versus chemotherapy alone for treatment of HER2-positive advanced gastric or gastro-oesophageal junction cancer (ToGA): a phase 3, open-label, randomised controlled trial. *The Lancet*, *376*(9742), 687-697.
25. Barenholz, Y. C. (2012). Doxil®—the first FDA-approved nano-drug: lessons learned. *Journal of controlled release*, *160*(2), 117-134.
26. Bazak, R., Houri, M., El Achy, S., Kamel, S. and Refaat, T. (2015). Cancer active targeting by nanoparticles: a comprehensive review of literature. *Journal of cancer research and clinical oncology*, *141*(5), 769-784.
27. Béduneau, A., Saulnier, P., Hindré, F., Clavreul, A., Leroux, J. C. and Benoit, J. P. (2007). Design of targeted lipid nanocapsules by conjugation of whole antibodies and antibody Fab'fragments. *Biomaterials*, *28*(33), 4978-4990.
28. Beirnaert, E., Desmyter, A., Spinelli, S., Lauwereys, M., Aarden, L., Dreier, T., Loris, R., Silence, K., Pollet, C., Cambillau, C. and de Haard, H. (2017). Bivalent Llama single-domain antibody fragments against tumor necrosis factor have picomolar potencies due to intramolecular interactions. *Frontiers in immunology*, *8*, 867.
29. Benetatos, C.A., Mitsuuchi, Y., Burns, J.M., Neiman, E.M., Condon, S.M., Yu, G., Seipel, M.E., Kapoor, G.S., LaPorte, M.G., Rippin, S.R. and Deng, Y. (2014). Birinapant (TL32711), a bivalent SMAC mimetic, targets TRAF2-associated cIAPs, abrogates TNF-induced NF-κB activation, and is active in patient-derived xenograft models. *Molecular cancer therapeutics*, *13*(4), 867-879.
30. Beroukhim, R., Mermel, C.H., Porter, D., Wei, G., Raychaudhuri, S., Donovan, J., Barretina, J., Boehm, J.S., Dobson, J., Urashima, M. and Mc Henry, K.T. (2010). The landscape of somatic copy-number alteration across human cancers. *Nature*, *463*(7283), 899-905.
31. Bertrand, N., Wu, J., Xu, X., Kamaly, N. and Farokhzad, O. C. (2014). Cancer nanotechnology: the impact of passive and active targeting in the era of modern cancer biology. *Advanced drug delivery reviews*, *66*, 2-25.
32. Betof, A.S., Lascola, C.D., Weitzel, D., Landon, C., Scarbrough, P.M., Devi, G.R., Palmer, G., Jones, L.W. and Dewhirst, M.W. (2015). Modulation of murine breast tumor

vascularity, hypoxia, and chemotherapeutic response by exercise. *JNCI: Journal of the National Cancer Institute*, *107*(5).
33. Boksebeld, M., Blanchard, N. P., Jaffal, A., Chevolot, Y. and Monnier, V. (2017). Shape-selective purification of gold nanorods with low aspect ratio using a simple centrifugation method. *Gold Bulletin*, *50*(1), 69-76.
34. Brown, C. L., Whitehouse, M. W., Tiekink, E. R. T. and Bushell, G. R. (2008). Colloidal metallic gold is not bio-inert. *Inflammopharmacology*, *16*(3), 133-137.
35. Byrne, J. D., Betancourt, T. and Brannon-Peppas, L. (2008). Active targeting schemes for nanoparticle systems in cancer therapeutics. *Advanced drug delivery reviews*, *60*(15), 1615-1626.
36. Cai, Y., Wang, J., Zhang, L., Wu, D., Yu, D., Tian, X., Liu, J., Jiang, X., Shen, Y., Zhang, L. and Ren, M. (2015). Expressions of fatty acid synthase and HER2 are correlated with poor prognosis of ovarian cancer. *Medical oncology*, *32*(1), 391.
37. Caltabiano, R., Leonardi, R., Musumeci, G., Bartoloni, G., Rusu, M. C., Almeida, L. E. and Loreto, C. (2013). Apoptosis in temporomandibular joint disc with internal derangement involves mitochondrial-dependent pathways. An in vivo study. *Acta Odontologica Scandinavica*, *71*(3-4), 577-583.
38. Cao, Y., Liang, H., Zhang, F., Luan, Z., Zhao, S., Wang, X.A., Liu, S., Bao, R., Shu, Y., Ma, Q. and Zhu, J. (2016). Prohibitin overexpression predicts poor prognosis and promotes cell proliferation and invasion through ERK pathway activation in gallbladder cancer. *Journal of Experimental and Clinical Cancer Research*, *35*(1), 68.
39. Castedo, M., Perfettini, J.L., Roumier, T., Valent, A., Raslova, H., Yakushijin, K., Horne, D., Feunteun, J., Lenoir, G., Medema, R. and Vainchenker, W. (2004). Mitotic catastrophe constitutes a special case of apoptosis whose suppression entails aneuploidy. *Oncogene*, *23*(25), 4362.
40. Chanda, N., Shukla, R., Zambre, A., Mekapothula, S., Kulkarni, R.R., Katti, K., Bhattacharyya, K., Fent, G.M., Casteel, S.W., Boote, E.J. and Viator, J.A. (2011). An effective strategy for the synthesis of biocompatible gold nanoparticles using cinnamon phytochemicals for phantom CT imaging and photoacoustic detection of cancerous cells. *Pharmaceutical research*, *28*(2), 279-291.
41. Chang, D., Ma, K., Gong, M., Cui, Y., Liu, Z.H., Zhou, X.G., Zhou, C.N. and Wang, T.Y., (2010). SLP-2 overexpression is associated with tumour distant metastasis and poor prognosis in pulmonary squamous cell carcinoma. *Biomarkers*, *15*(2), 104-110.
42. Chapman, G., Sparrow, D. B., Kremmer, E., and Dunwoodie, S. L. (2010). Notch inhibition by the ligand DELTA-LIKE 3 defines the mechanism of abnormal vertebral segmentation in spondylocostal dysostosis. *Human molecular genetics*, *20*(5), 905-916.
43. Che, Y. J., Wu, H. W., Hung, L. Y., Liu, C. A., Chang, H. Y., Wang, K. and Lee, G. B. (2015). An integrated microfluidic system for screening of phage-displayed peptides specific to colon cancer cells and colon cancer stem cells. *Biomicrofluidics*, *9*(5), 054121.
44. Chen, J., Wang, D., Xi, J., Au, L., Siekkinen, A., Warsen, A., Li, Z.Y., Zhang, H., Xia, Y. and Li, X. (2007). Immuno gold nanocages with tailored optical properties for targeted photothermal destruction of cancer cells. *Nano letters*, *7*(5), 1318-1322.
45. Chen, H., Shao, L., Ming, T., Sun, Z., Zhao, C., Yang, B. and Wang, J. (2010). Understanding the photothermal conversion efficiency of gold nanocrystals. *Small*, *6*(20), 2272-2280.
46. Chen, W. H., Luo, G. F., Xu, X. D., Jia, H. Z., Lei, Q., Han, K. and Zhang, X. Z. (2014). Cancer-targeted functional gold nanoparticles for apoptosis induction and real-time imaging based on FRET. *Nanoscale*, *6*(16), 9531-9535.
47. Cheng, W. W. and Allen, T. M. (2010). The use of single chain Fv as targeting agents for immunoliposomes: an update on immunoliposomal drugs for cancer treatment. *Expert opinion on drug delivery*, *7*(4), 461-478.

48. Chi, Y. H., Hsiao, J. K., Lin, M. H., Chang, C., Lan, C. H. and Wu, H. C. (2017). Lung Cancer-Targeting Peptides with Multi-subtype Indication for Combinational Drug Delivery and Molecular Imaging. *Theranostics*, *7*(6), 1612.
49. Chiu, C. F., Ho, M. Y., Peng, J. M., Hung, S. W., Lee, W. H., Liang, C. M. and Liang, S. M. (2013). Raf activation by Ras and promotion of cellular metastasis require phosphorylation of prohibitin in the raft domain of the plasma membrane. *Oncogene*, *32*(6), 777.
50. Cho, K., Wang, X. U., Nie, S. and Shin, D. M. (2008). Therapeutic nanoparticles for drug delivery in cancer. *Clinical cancer research*, *14*(5), 1310-1316.
51. Choi, Y.J., Saez, B., Anders, L., Hydbring, P., Stefano, J., Bacon, N.A., Cook, C., Kalaszczynska, I., Signoretti, S., Young, R.A. and Scadden, D.T. (2014). D-cyclins repress apoptosis in hematopoietic cells by controlling death receptor Fas and its ligand FasL. *Developmental cell*, *30*(3), 255-267.
52. Chung, E.J., Cheng, Y., Morshed, R., Nord, K., Han, Y., Wegscheid, M.L., Auffinger, B., Wainwright, D.A., Lesniak, M.S. and Tirrell, M.V. (2014). Fibrin-binding, peptide amphiphile micelles for targeting glioblastoma. *Biomaterials*, *35*(4), 1249-1256.
53. Clogston, J. D. and Patri, A. K. (2011). Zeta potential measurement. *Characterization of nanoparticles intended for drug delivery*, 697, 63-70.
54. Cowell, J. K., Teng, Y., Bendzunas, N. G., Ara, R., Arbab, A. S. and Kennedy, E. J. (2017). Suppression of Breast Cancer Metastasis Using Stapled Peptides Targeting the WASF Regulatory Complex. *Cancer growth and metastasis*, *10*, 1179064417713197.
55. Danhier, F., Feron, O. and Préat, V. (2010). To exploit the tumor microenvironment: passive and active tumor targeting of nanocarriers for anti-cancer drug delivery. *Journal of controlled release*, *148*(2), 135-146.
56. Danhier, F. (2016). To exploit the tumor microenvironment: Since the EPR effect fails in the clinic, what is the future of nanomedicine?. *Journal of Controlled Release*, *244*, 108-121.
57. Davis, M.E., Zuckerman, J.E., Choi, C.H.J., Seligson, D., Tolcher, A., Alabi, C.A., Yen, Y., Heidel, J.D. and Ribas, A. (2010). Evidence of RNAi in humans from systemically administered siRNA via targeted nanoparticles. *nature*, *464*(7291), 1067-1070.
58. de Barros, A. B., Tsourkas, A., Saboury, B., Cardoso, V. N. and Alavi, A. (2012). Emerging role of radiolabeled nanoparticles as an effective diagnostic technique. *EJNMMI research*, *2*(1), 1.
59. Desmarais, J. A., Unger, C., Damjanov, I., Meuth, M. and Andrews, P. (2016). Apoptosis and failure of checkpoint kinase 1 activation in human induced pluripotent stem cells under replication stress. *Stem cell research and therapy*, *7*(1), 17.
60. Di Martino, A., Kucharczyk, P., Capakova, Z., Humpolicek, P. and Sedlarik, V. (2017). Enhancement of temozolomide stability by loading in chitosan-carboxylated polylactide-based nanoparticles. *Journal of Nanoparticle Research*, *19*(2), 71.
61. Ding, H., Gangalum, P.R., Galstyan, A., Fox, I., Patil, R., Hubbard, P., Murali, R., Ljubimova, J.Y. and Holler, E. (2017). HER2-positive breast cancer targeting and treatment by a peptide-conjugated mini nanodrug. *Nanomedicine: Nanotechnology, Biology and Medicine*, *13*(2), 631-639.
62. Dong, W.Q., Chao, M., Lu, Q.H., Chai, W.L., Zhang, W., Chen, X.Y., Liang, E.S., Wang, L.B., Tian, H.L., Chen, Y.G. and Zhang, M.X. (2016). Prohibitin overexpression improves myocardial function in diabetic cardiomyopathy. *Oncotarget*, *7*(1), 66.
63. Durante, M. and Loeffler, J. S. (2010). Charged particles in radiation oncology. *Nature reviews Clinical oncology*, *7*(1), 37.
64. Dykman, L. A. and Khlebtsov, N. G. (2011). Gold nanoparticles in biology and medicine: recent advances and prospects. *Acta Naturae (англоязычная версия)*, *3*(2 (9)).

65. Edgett, K.S., Ravine, M.A., Caplinger, M.A., Ghaemi, F.T., Schaffner, J.A., Malin, M.C., Baker, J.M., DiBiase, D.R., Laramee, J., Maki, J.N. and Willson, R.G. (2009, March). The mars science laboratory (MSL) mars hand lens imager (MAHLI) flight instrument. In *Lunar and Planetary Science Conference* (Vol. 40).
66. Elbagory, A. M., Cupido, C. N., Meyer, M. and Hussein, A. A. (2016). Large scale screening of Southern African plant extracts for the green synthesis of gold nanoparticles using microtitre-plate method. *Molecules*, *21*(11), 1498.
67. Elder, A., Yang, H., Gwiazda, R., Teng, X., Thurston, S., He, H. and Oberdörster, G. (2007). Testing nanomaterials of unknown toxicity: an example based on platinum nanoparticles of different shapes. *Advanced materials*, *19*(20), 3124-3129.
68. Ellerby, H.M., Arap, W., Ellerby, L.M., Kain, R., Andrusiak, R., Del Rio, G., Krajewski, S., Lombardo, C.R., Rao, R., Ruoslahti, E. and Bredesen, D.E. (1999). Anti-cancer activity of targeted pro-apoptotic peptides. *Nature medicine*, *5*(9), 1032-1038.
69. Elmore, S. (2007). Apoptosis: a review of programmed cell death. *Toxicologic pathology*, *35*(4), 495-516.
70. Farokhzad, O. C., Jon, S., Khademhosseini, A., Tran, T. N. T., LaVan, D. A. and Langer, R. (2004). Nanoparticle-aptamer bioconjugates: a new approach for targeting prostate cancer cells. *Cancer research*, *64*(21), 7668-7672.
71. Farokhzad, O.C., Cheng, J., Teply, B.A., Sherifi, I., Jon, S., Kantoff, P.W., Richie, J.P. and Langer, R. (2006). Targeted nanoparticle-aptamer bioconjugates for cancer chemotherapy in vivo. *Proceedings of the National Academy of Sciences*, *103*(16), 6315-6320.
72. Favi, P. M., Gao, M., Johana Sepúlveda Arango, L., Ospina, S. P., Morales, M., Pavon, J. J. and Webster, T. J. (2015). Shape and surface effects on the cytotoxicity of nanoparticles: gold nanospheres versus gold nanostars. *Journal of Biomedical Materials Research Part A*, *103*(11), 3449-3462.
73. Fernández, T. D., Pearson, J. R., Leal, M. P., Torres, M. J., Blanca, M., Mayorga, C. and Le Guével, X. (2015). Intracellular accumulation and immunological properties of fluorescent gold nanoclusters in human dendritic cells. *Biomaterials*, *43*, 1-12.
74. Fesik, S. W. (2000). Insights into programmed cell death through structural biology. *Cell*, *103*(2), 273-282.
75. Finlay, D., Teriete, P., Vamos, M., Cosford, N. D. and Vuori, K. (2017). Inducing death in tumor cells: roles of the inhibitor of apoptosis proteins. *F1000Research*, *6*.
76. Food and Drug Administration. (2017). Hematology/oncology (cancer) approvals and safety notifications.
77. Fox, J. L. and MacFarlane, M. (2016). Targeting cell death signalling in cancer: Minimising 'Collateral damage'. *British journal of cancer*, *115*(1), 5-11.
78. Fratoddi, I., Venditti, I., Cametti, C. and Russo, M. V. (2015). How toxic are gold nanoparticles? The state-of-the-art. *Nano Research*, *8*(6), 1771-1799.
79. Fulda, S. and Vucic, D. (2012). Targeting IAP proteins for therapeutic intervention in cancer. *Nature reviews Drug discovery*, *11*(2), 109-124.
80. Fultz, B. and Howe, J. M. (2012). *Transmission electron microscopy and diffractometry of materials*. Springer Science & Business Media.
81. Fytianos, K., Rodriguez-Lorenzo, L., Clift, M.J., Blank, F., Vanhecke, D., Von Garnier, C., Petri-Fink, A. and Rothen-Rutishauser, B. (2015). Uptake efficiency of surface modified gold nanoparticles does not correlate with functional changes and cytokine secretion in human dendritic cells in vitro. *Nanomedicine: Nanotechnology, Biology and Medicine*, *11*(3), 633-644.
82. Gagliardi, M., Bertero, A. and Bifone, A. (2017). Molecularly Imprinted Biodegradable Nanoparticles. *Scientific Reports*, *7*, 40046.

83. Gamble, S.C., Chotai, D., Odontiadis, M., Dart, D.A., Brooke, G.N., Powell, S.M., Reebye, V., Varela-Carver, A., Kawano, Y., Waxman, J. and Bevan, C.L. (2007). Prohibitin, a protein downregulated by androgens, represses androgen receptor activity. *Oncogene*, *26*(12), 1757-1768.
84. Garrido, C., Galluzzi, L., Brunet, M., Puig, P. E., Didelot, C. and Kroemer, G. (2006). Mechanisms of cytochrome c release from mitochondria. *Cell Death and Differentiation*, *13*(9), 1423-1433.
85. Ghaffari, S., Jagani, Z., Kitidis, C., Lodish, H. F. and Khosravi-Far, R. (2003). Cytokines and BCR-ABL mediate suppression of TRAIL-induced apoptosis through inhibition of forkhead FOXO3a transcription factor. *Proceedings of the National Academy of Sciences*, *100*(11), 6523-6528.
86. Ghazy, A. A., El-Etreby, N. M. and Rashad, R. (2017). Prohibitin: targeting peptide coupled to ovarian cancer, luteinization and TGF-β pathways. *Journal of ovarian research*, *10*(1), 28.
87. Godonoga, M., Lin, T.Y., Oshima, A., Sumitomo, K., Tang, M.S., Cheung, Y.W., Kinghorn, A.B., Dirkzwager, R.M., Zhou, C., Kuzuya, A. and Tanner, J.A. (2016). A DNA aptamer recognising a malaria protein biomarker can function as part of a DNA origami assembly. *Scientific reports*, *6*, 21266.
88. Gorgoulis, V. G., Vassiliou, L. V. F., Karakaidos, P. and Zacharatos, P. (2005). Activation ov the DNA damage checkpoint and genomic instability in human precancerous lesions. *Nature*, *434*(7035), 907.
89. Goy, A., Younes, A., McLaughlin, P., Pro, B., Romaguera, J.E., Hagemeister, F., Fayad, L., Dang, N.H., Samaniego, F., Wang, M. and Broglio, K. (2005). Phase II study of proteasome inhibitor bortezomib in relapsed or refractory B-cell non-Hodgkin's lymphoma. *Journal of Clinical Oncology*, *23*(4), 667-675.
90. Guerlavais, V. and Sawyer, T. K. (2014). Advancements in stapled peptide drug discovery & development. In *Annual Reports in Medicinal Chemistry* (Vol. 49, 331-345). Academic Press.
91. Gupta, K. and Zhang, J. (2005). Angiogenesis: a curse or cure?. *Postgraduate Medical Journal*, *81*(954), 236-242.
92. Gupta, S. C., Francis, S. K., Nair, M. S., Mo, Y. Y. and Aggarwal, B. B. (2013). Azadirone, a Limonoid Tetranortriterpene, Induces Death Receptors and Sensitizes Human Cancer Cells to Tumor Necrosis Factor-related Apoptosis-inducing Ligand (TRAIL) through a p53 Protein-independent Mechanism EVIDENCE FOR THE ROLE OF THE ROS-ERK-CHOP-DEATH RECEPTOR PATHWAY. *Journal of Biological Chemistry*, *288*(45), 32343-32356.
93. Gupta, S., Kesarla, R., Chotai, N., Misra, A. and Omri, A. (2017). Systematic Approach for the Formulation and Optimization of Solid Lipid Nanoparticles of Efavirenz by High Pressure Homogenization Using Design of Experiments for Brain Targeting and Enhanced Bioavailability. *BioMed Research International*, *2017*.
94. Gustashaw, K. M., Najmabadi, P. and Potts, S. J. (2010). Measuring Protein Expression in Tissue: The Complementary Roles of Brightfield and Fluorescence in Whole Slide Scanning. *Laboratory Medicine*, *41*(3), 135-142.
95. Häcker, G. (2000). The morphology of apoptosis. *Cell and tissue research*, *301*(1), 5-17.

96. Haiss, W., Thanh, N. T., Aveyard, J. and Fernig, D. G. (2007). Determination of size and concentration of gold nanoparticles from UV− Vis spectra. *Analytical chemistry*, *79*(11), 4215-4221.
97. Haley, B. and Frenkel, E. (2008, January). Nanoparticles for drug delivery in cancer treatment. In *Urologic Oncology: Seminars and original investigations* (Vol. 26, No. 1, pp. 57-64). Elsevier.
98. Hanahan, D. and Weinberg, R. A. (2000). The hallmarks of cancer. *cell*, *100*(1), 57-70.
99. Hanahan, D. and Weinberg, R.A. (2011). Hallmarks of cancer: the next generation. *cell*, *144*(5), 646-674.
100. Hansen, A.E., Petersen, A.L., Henriksen, J.R., Boerresen, B., Rasmussen, P., Elema, D.R., Rosenschöld, P.M.A., Kristensen, A.T., Kjær, A. and Andresen, T.L. (2015). Positron emission tomography based elucidation of the enhanced permeability and retention effect in dogs with cancer using copper-64 liposomes. *ACS nano*, *9*(7), 6985-6995.
101. Hartland, G. V. (2011). Optical studies of dynamics in noble metal nanostructures. *Chemical reviews*, *111*(6), 3858-3887.
102. Heinrich, A. K., Lucas, H., Schindler, L., Chytil, P., Etrych, T., Mäder, K. and Mueller, T. (2016). Improved tumor-specific drug accumulation by polymer therapeutics with pH-sensitive drug release overcomes chemotherapy resistance. *Molecular cancer therapeutics*.
103. Hejmadi, M. (2010). Introduction to Cancer Biology. Bookboon.
104. Hengartner, M. O. (2000). The biochemistry of apoptosis. *Nature*, *407*(6805), 770.
105. Herold, G., Rogler, G., Rogler, D. and Stange, E. F. (1994). Morphology of CaCo-2 cells varies in different cell batches. *In Vitro Cellular and Developmental Biology-Animal*, *30*(5), 289-291.
106. Hewitt, S. M., Baskin, D. G., Frevert, C. W., Stahl, W. L. and Rosa-Molinar, E. (2014). Controls for immunohistochemistry: the Histochemical Society's standards of practice for validation of immunohistochemical assays. *Journal of Histochemistry and Cytochemistry*, *62*(10), 693-697.
107. Hill, M. M., Adrain, C., Duriez, P. J., Creagh, E. M. and Martin, S. J. (2004). Analysis of the composition, assembly kinetics and activity of native Apaf-1 apoptosomes. *The EMBO journal*, *23*(10), 2134-2145.
108. Hills, S. A. and Diffley, J. F. (2014). DNA replication and oncogene-induced replicative stress. *Current biology*, *24*(10), R435-R444.
109. Hleb, E. Y., Hafner, J. H., Myers, J. N., Hanna, E. Y., Rostro, B. C., Zhdanok, S. A. and Lapotko, D. O. (2008). LANTCET: elimination of solid tumor cells with photothermal bubbles generated around clusters of gold nanoparticles. *Nanomedicine*, *3*(5), 647-667.
110. Hoellenriegel, J., Zboralski, D., Maasch, C., Rosin, N.Y., Wierda, W.G., Keating, M.J., Kruschinski, A. and Burger, J.A. (2014). The Spiegelmer NOX-A12, a novel CXCL12 inhibitor, interferes with chronic lymphocytic leukemia cell motility and causes chemosensitization. *Blood*, *123*(7), 1032-1039.
111. Hoffman, J.A., Giraudo, E., Singh, M., Zhang, L., Inoue, M., Porkka, K., Hanahan, D. and Ruoslahti, E. (2003). Progressive vascular changes in a transgenic mouse model of squamous cell carcinoma. *Cancer cell*, *4*(5), 383-391.
112. Hrkach, J., Von Hoff, D., Ali, M.M., Andrianova, E., Auer, J., Campbell, T., De Witt, D., Figa, M., Figueiredo, M., Horhota, A. and Low, S. (2012). Preclinical development and clinical translation of a PSMA-targeted docetaxel nanoparticle with a differentiated pharmacological profile. *Science translational medicine*, *4*(128), 128ra39-128ra39.
113. Hu, M., Chen, J., Li, Z.Y., Au, L., Hartland, G.V., Li, X., Marquez, M. and Xia, Y. (2006). Gold nanostructures: engineering their plasmonic properties for biomedical applications. *Chemical Society Reviews*, *35*(11), 1084-1094.

114. Hu, Q., Gao, X., Kang, T., Feng, X., Jiang, D., Tu, Y., Song, Q., Yao, L., Jiang, X., Chen, H. and Chen, J. (2013). CGKRK-modified nanoparticles for dual-targeting drug delivery to tumor cells and angiogenic blood vessels. *Biomaterials*, *34*(37), 9496-9508.
115. Huang, X., El-Sayed, I. H., Qian, W. and El-Sayed, M. A. (2006). Cancer cell imaging and photothermal therapy in the near-infrared region by using gold nanorods. *Journal of the American Chemical Society*, *128*(6), 2115-2120.
116. Huang, X. and El-Sayed, M. A. (2010). Gold nanoparticles: optical properties and implementations in cancer diagnosis and photothermal therapy. *Journal of advanced research*, *1*(1), 13-28.
117. Huang, H. C., Rege, K. and Heys, J. J. (2010). Spatiotemporal temperature distribution and cancer cell death in response to extracellular hyperthermia induced by gold nanorods. *ACS nano*, *4*(5), 2892-2900.
118. Hudis, C. A. (2007). Trastuzumab—mechanism of action and use in clinical practice. *New England Journal of Medicine*, *357*(1), 39-51.
119. Ichim, G. and Tait, S. W. (2016). A fate worse than death: apoptosis as an oncogenic process. *Nature Reviews Cancer*, *16*, 539-548.
120. İlem-Özdemir, D., Gündoğdu, E., Ekinci, M. and Aşikoğlu, M. (2015). Nanoparticles: From Diagnosis to Therapy. *Int J Med Nano Res*, *2*, 15.
121. Inoue-Yamauchi, A., Jeng, P.S., Kim, K., Chen, H.C., Han, S., Ganesan, Y.T., Ishizawa, K., Jebiwott, S., Dong, Y., Pietanza, M.C. and Hellmann, M.D. (2017). Targeting the differential addiction to anti-apoptotic BCL-2 family for cancer therapy. *Nature communications*, *8*, ncomms16078.
122. Jain, P. K., Huang, X., El-Sayed, I. H. and El-Sayed, M. A. (2007). Review of some interesting surface plasmon resonance-enhanced properties of noble metal nanoparticles and their applications to biosystems. *Plasmonics*, *2*(3), 107-118.
123. Jain, P. K., Huang, X., El-Sayed, I. H. and El-Sayed, M. A. (2008). Noble metals on the nanoscale: optical and photothermal properties and some applications in imaging, sensing, biology, and medicine. *Accounts of chemical research*, *41*(12), 1578-1586.
124. Janzen, D. M., Tiourin, E., Salehi, J. A., Paik, D. Y., Lu, J., Pellegrini, M. and Memarzadeh, S. (2015). An apoptosis-enhancing drug overcomes platinum resistance in a tumour-initiating subpopulation of ovarian cancer. *Nature communications*, *6*.
125. Javadpour, M.M., Juban, M.M., Lo, W.C.J., Bishop, S.M., Alberty, J.B., Cowell, S.M., Becker, C.L. and McLaughlin, M.L. (1996). De novo antimicrobial peptides with low mammalian cell toxicity. *Journal of medicinal chemistry*, *39*(16), 3107-3113.
126. Jemal, A., Center, M. M., DeSantis, C. and Ward, E. M. (2010). Global patterns of cancer incidence and mortality rates and trends. *Cancer Epidemiology and Prevention Biomarkers*, *19*(8), 1893-1907.
127. Jemal, A., Siegel, R., Xu, J. and Ward, E. (2010). Cancer statistics, 2010. *CA: a cancer journal for clinicians*, *60*(5), 277-300.
128. Jemal, A., Bray, F., Center, M. M., Ferlay, J., Ward, E. and Forman, D. (2011). Global cancer statistics. *CA: a cancer journal for clinicians*, *61*(2), 69-90.
129. Jia, H., Fang, C., Zhu, X. M., Ruan, Q., Wang, Y. X. J. and Wang, J. (2015). Synthesis of absorption-dominant small gold nanorods and their plasmonic properties. *Langmuir*, *31*(26), 7418-7426.
130. Jordan, R. C., Daniels, T. E., Greenspan, J. S. and Regezi, J. A. (2002). Advanced diagnostic methods in oral and maxillofacial pathology. Part II: Immunohistochemical and immunofluorescent methods. *Oral Surgery, Oral Medicine, Oral Pathology, Oral Radiology, and Endodontology*, *93*(1), 56-74.
131. Kanamala, M., Wilson, W. R., Yang, M., Palmer, B. D. and Wu, Z. (2016). Mechanisms and biomaterials in pH-responsive tumour targeted drug delivery: a review. *Biomaterials*, *85*, 152-167.

132. Kataoka, T., Schröter, M., Hahne, M., Schneider, P., Irmler, M., Thome, M., Froelich, C.J. and Tschopp, J. (1998). FLIP prevents apoptosis induced by death receptors but not by perforin/granzyme B, chemotherapeutic drugs, and gamma irradiation. *The Journal of Immunology*, *161*(8), 3936-3942.
133. Khan, A. K., Rashid, R., Murtaza, G. and Zahra, A. (2014). Gold nanoparticles: synthesis and applications in drug delivery. *Tropical journal of pharmaceutical research*, *13*(7), 1169-1177.
134. Kim, D., Jeong, Y. Y. and Jon, S. (2010). A drug-loaded aptamer− gold nanoparticle bioconjugate for combined CT imaging and therapy of prostate cancer. *ACS nano*, *4*(7), 3689-3696.
135. Kim, K., Kim, J. H., Park, H., Kim, Y. S., Park, K., Nam, H., Lee, S., Park, J.H., Park, R.W., Kim, I.S. and Choi, K. (2010). Tumor-homing multifunctional nanoparticles for cancer theragnosis: Simultaneous diagnosis, drug delivery, and therapeutic monitoring. *Journal of controlled release*, *146*(2), 219-227.
136. Kim, M. S., Kim, S. S., Yoo, N. J. and Lee, S. H. (2012). Rare somatic mutation of pro-apoptotic BAX and BAK genes in common human cancers. *Tumori*, *98*(6), 149e-51e.
137. Köhler, G. and Milstein, C. (1975). Continuous cultures of fused cells secreting antibody of predefined specificity. *Nature*, *256*(5517), 495.
138. Kolonin, M. G., Saha, P. K., Chan, L., Pasqualini, R. and Arap, W. (2004). Reversal of obesity by targeted ablation of adipose tissue. *Nature medicine*, *10*(6).
139. Korrapati, P.S., Karthikeyan, K., Satish, A., Krishnaswamy, V.R., Venugopal, J.R. and Ramakrishna, S. (2016). Recent advancements in nanotechnological strategies in selection, design and delivery of biomolecules for skin regeneration. *Materials Science and Engineering: C*, *67*, 747-765.
140. Korsmeyer, S. J. (1992). Bcl-2 initiates a new category of oncogenes: regulators of cell death. *blood*, *80*(4), 879-886.
141. Kötting, C., Güldenhaupt, J. and Gerwert, K. (2012). Time-resolved FTIR spectroscopy for monitoring protein dynamics exemplified by functional studies of Ras protein bound to a lipid bilayer. *Chemical Physics*, *396*, 72-83.
142. Küçük, İ., Tanoğlu, A., Öncü, K., Yılmaz, İ., Kara, M., Beyazıt, Y., Akyol, T., Kaplan, M., Özarı, H.O. and Yazgan, Y. (2016). Immunohistochemical activity of Prohibitin-2 and Stomatin-Like Protein-2 in patients with ulcerative colitis. *The Turkish Journal of Gastroenterology*, *27*, 233-8.
143. Kumar, A., Ma, H., Zhang, X., Huang, K., Jin, S., Liu, J., Wei, T., Cao, W., Zou, G. and Liang, X.J. (2012). Gold nanoparticles functionalised with therapeutic and targeted peptides for cancer treatment. *Biomaterials*, *33*(4), 1180-1189.
144. Kumar, V., Abbas, A. K., Fausto, N. and Aster, J. C. (2014). *Robbins and Cotran pathologic basis of disease, professional edition e-book*. elsevier health sciences.
145. Kumari, P., Ghosh, B. and Biswas, S. (2016). Nanocarriers for cancer-targeted drug delivery. *Journal of drug targeting*, *24*(3), 179-191.
146. Lammers, T., Peschke, P., Kühnlein, R., Subr, V., Ulbrich, K., Debus, J., Huber, P., Hennink, W. and Storm, G. (2007). Effect of radiotherapy and hyperthermia on the tumor accumulation of HPMA copolymer-based drug delivery systems. *Journal of controlled release*, *117*(3), 333-341.
147. Lammers, T., Kiessling, F., Hennink, W.E. and Storm, G. (2012). Drug targeting to tumors: principles, pitfalls and (pre-) clinical progress. *Journal of controlled release*, *161*(2), 175-187.
148. Lao, Y. H., Phua, K. K. and Leong, K. W. (2015). Aptamer nanomedicine for cancer therapeutics: barriers and potential for translation. *ACS nano*, *9*(3), 2235-2254.
149. Le Garrec, D., Gori, S., Luo, L., Lessard, D., Smith, D.C., Yessine, M.A., Ranger, M. and Leroux, J.C. (2004). Poly (N-vinylpyrrolidone)-block-poly (D, L-lactide) as a new

polymeric solubilizer for hydrophobic anticancer drugs: in vitro and in vivo evaluation. *Journal of Controlled Release*, *99*(1), 83-101.
150. le Guével, X., Palomares, F., Torres, M. J., Blanca, M., Fernandez, T. D. and Mayorga, C. (2015). Nanoparticle size influences the proliferative responses of lymphocyte subpopulations. *RSC Advances*, *5*(104), 85305-85309.
151. Lee, S.H., Shin, M.S., Kim, H.S., Lee, H.K., Park, W.S., Kim, S.Y., Lee, J.H., Han, S.Y., Park, J.Y., Oh, R.R. and Kang, C.S. (2001). Somatic mutations of TRAIL-receptor 1 and TRAIL-receptor 2 genes in non-Hodgkin's lymphoma. *Oncogene*, *20*(3), 399-403.
152. Lee, J. H., Yigit, M. V., Mazumdar, D. and Lu, Y. (2010). Molecular diagnostic and drug delivery agents based on aptamer-nanomaterial conjugates. *Advanced drug delivery reviews*, *62*(6), 592-605.
153. Lee, K. J., Lee, J. H., Chung, H. K., Ju, E. J., Song, S. Y., Jeong, S. Y. and Choi, E. K. (2016). Application of peptide displaying phage as a novel diagnostic probe for human lung adenocarcinoma. *Amino acids*, *48*(4), 1079-1086.
154. Lemke, J. V., Von Karstedt, S., Zinngrebe, J. and Walczak, H. (2014). Getting TRAIL back on track for cancer therapy. *Cell Death and Differentiation*, *21*(9), 1350-1364.
155. Leroy, P., Tournassat, C. and Bizi, M. (2011). Influence of surface conductivity on the apparent zeta potential of TiO 2 nanoparticles. *Journal of Colloid and Interface Science*, *356*(2), 442-453.
156. Li, L. Y., Luo, X. and Wang, X. (2001). Endonuclease G is an apoptotic DNase when released from mitochondria. *Nature*, *412*(6842), 95-99.
157. Li, Y. Q., Chen, P., Haimovitz-Friedman, A., Reilly, R. M. and Wong, C. S. (2003). Endothelial apoptosis initiates acute blood–brain barrier disruption after ionizing radiation. *Cancer research*, *63*(18), 5950-5956.
158. Li, W., Sun, X., Wang, Y., Niu, G., Chen, X., Qian, Z. and Nie, L. (2014). In vivo quantitative photoacoustic microscopy of gold nanostar kinetics in mouse organs. *Biomedical optics express*, *5*(8), 2679-2685.
159. Li, Q., Sun, W., Yuan, D., Lv, T., Yin, J., Cao, E., Xiao, X. and Song, Y. (2016). Efficacy and safety of recombinant human tumor necrosis factor application for the treatment of malignant pleural effusion caused by lung cancer. *Thoracic cancer*, *7*(1), 136-139.
160. Liang, J. W., Zhang, J. J., Zhang, T. and Zheng, Z. C. (2014). Clinicopathological and prognostic significance of HER2 overexpression in gastric cancer: a meta-analysis of the literature. *Tumor Biology*, *35*(5), 4849-4858.
161. Liao, Q., Guo, X., Li, X., Xiong, W., Li, X., Yang, J., Chen, P., Zhang, W., Yu, H., Tang, H. and Deng, M. (2013). Prohibitin is an important biomarker for nasopharyngeal carcinoma progression and prognosis. *European Journal of Cancer Prevention*, *22*(1), 68-76.
162. Libutti, S.K., Paciotti, G.F., Byrnes, A.A., Alexander, H.R., Gannon, W.E., Walker, M., Seidel, G.D., Yuldasheva, N. and Tamarkin, L. (2010). Phase I and pharmacokinetic studies of CYT-6091, a novel PEGylated colloidal gold-rhTNF nanomedicine. *Clinical cancer research*, *16*(24), 6139-6149.
163. Liss, M., Petersen, B., Wolf, H. and Prohaska, E. (2002). An aptamer-based quartz crystal protein biosensor. *Analytical Chemistry*, *74*(17), 4488-4495.
164. Liu, S.C., Alomran, R., Chernikova, S.B., Lartey, F., Stafford, J., Jang, T., Merchant, M., Zboralski, D., Zöllner, S., Kruschinski, A. and Klussmann, S. (2013). Blockade of SDF-1 after irradiation inhibits tumor recurrences of autochthonous brain tumors in rats. *Neuro-oncology*, *16*(1), 21-28.
165. Liu, B., Che, W., Xue, J., Zheng, C., Tang, K., Zhang, J., Wen, J. and Xu, Y. (2013). SIRT4 prevents hypoxia-induced apoptosis in H9c2 cardiomyoblast cells. *Cellular physiology and biochemistry*, *32*(3), 655-662.

166. Liu, K., Zheng, Y., Lu, X., Thai, T., Lee, N. A., Bach, U. and Gooding, J. J. (2015). Biocompatible gold nanorods: One-step surface functionalization, highly colloidal stability, and low cytotoxicity. *Langmuir*, *31*(17), 4973-4980.
167. Locksley, R. M., Killeen, N. and Lenardo, M. J. (2001). The TNF and TNF receptor superfamilies: integrating mammalian biology. *Cell*, *104*(4), 487-501.
168. Loreto, C., Almeida, L. E., Trevilatto, P. and Leonardi, R. (2011). Apoptosis in displaced temporomandibular joint disc with and without reduction: an immunohistochemical study. *Journal of oral pathology and medicine*, *40*(1), 103-110.
169. Lu, R. M., Chang, Y. L., Chen, M. S. and Wu, H. C. (2011). Single chain anti-c-Met antibody conjugated nanoparticles for in vivo tumor-targeted imaging and drug delivery. *Biomaterials*, *32*(12), 3265-3274.
170. Lu, T.H., Tseng, T.J., Su, C.C., Tang, F.C., Yen, C.C., Liu, Y.Y., Yang, C.Y., Wu, C.C., Chen, K.L., Hung, D.Z. and Chen, Y.W. (2014). Arsenic induces reactive oxygen species-caused neuronal cell apoptosis through JNK/ERK-mediated mitochondria-dependent and GRP 78/CHOP-regulated pathways. *Toxicology letters*, *224*(1), 130-140.
171. Luan, Z., He, Y., Alattar, M., Chen, Z. and He, F. (2014). Targeting the prohibitin scaffold-CRAF kinase interaction in RAS-ERK-driven pancreatic ductal adenocarcinoma. *Molecular cancer*, *13*(1), 1.
172. Lynch, I. and Dawson, K. A. (2008). Protein-nanoparticle interactions. *Nano today*, *3*(1), 40-47.
173. Ma, C., Yin, G., Yan, D., He, X., Zhang, L., Wei, Y. and Huang, Z. (2013). A novel peptide specifically targeting ovarian cancer identified by in vivo phage display. *Journal of Peptide Science*, *19*(12), 730-736.
174. Maeda, H., Wu, J., Sawa, T., Matsumura, Y. and Hori, K. (2000). Tumor vascular permeability and the EPR effect in macromolecular therapeutics: a review. *Journal of controlled release*, *65*(1), 271-284.
175. Maiorano, G., Sabella, S., Sorce, B., Brunetti, V., Malvindi, M. A., Cingolani, R. and Pompa, P. P. (2010). Effects of cell culture media on the dynamic formation of protein–nanoparticle complexes and influence on the cellular response. *ACS nano*, *4*(12), 7481-7491.
176. Mandal, S. (2013). NANO-approaches for Cancer therapy or diagnostics. Unpublished Doctor of Philosophy thesis. Italy: International School for Advance Studies.
177. Marasca, R. and Maffei, R. (2014). NOX-A12: mobilizing CLL away from home. *Blood*, *123*(7), 952-953.
178. Martin, O.A., Anderson, R.L., Russell, P.A., Cox, R.A., Ivashkevich, A., Swierczak, A., Doherty, J.P., Jacobs, D.H., Smith, J., Siva, S. and Daly, P.E. (2014). Mobilization of viable tumor cells into the circulation during radiation therapy. *International Journal of Radiation Oncology* Biology* Physics*, *88*(2), 395-403.
179. Massey, R. L., Kim, H. K. and Abdi, S. (2014). Brief review: chemotherapy-induced painful peripheral neuropathy (CIPPN): current status and future directions. *Canadian Journal of Anesthesia/Journal canadien d'anesthésie*, *61*(8), 754-762.
180. Matsumura, Y. and Maeda, H. (1986). A new concept for macromolecular therapeutics in cancer chemotherapy: mechanism of tumoritropic accumulation of proteins and the antitumor agent smancs. *Cancer research*, *46*(12 Part 1), 6387-6392.
181. Matzinger, O., Viertl, D., Tsoutsou, P., Kadi, L., Rigotti, S., Zanna, C., Wiedemann, N., Vozenin, M.C., Vuagniaux, G. and Bourhis, J. (2015). The radiosensitizing activity of the SMAC-mimetic, Debio 1143, is TNFα-mediated in head and neck squamous cell carcinoma. *Radiotherapy and Oncology*, *116*(3), 495-503.
182. Mauer, K., O'Kelley, R., Podda, N., Flanagan, S. and Gadani, S. (2015). New treatment modalities for hepatocellular cancer. *Current gastroenterology reports*, *17*(5), 1-12.

183. Mazieres, J., Peters, S., Lepage, B., Cortot, A.B., Barlesi, F., Beau-Faller, M., Besse, B., Blons, H., Mansuet-Lupo, A., Urban, T. and Moro-Sibilot, D. (2013). Lung cancer that harbors an HER2 mutation: epidemiologic characteristics and therapeutic perspectives. *Journal of clinical oncology*, *31*(16), 1997-2003.
184. McClung, J.K., Danner, D.B., Stewart, D.A., Smith, J.R., Schneider, E.L., Lumpkin, C.K., Dell'Orco, R.T. and Nuell, M.J. (1989). Isolation of a cDNA that hybrid selects antiproliferative mRNA from rat liver. *Biochemical and biophysical research communications*, *164*(3), 1316-1322.
185. McGuire, M.J., Gray, B.P., Li, S., Cupka, D., Byers, L.A., Wu, L., Rezaie, S., Liu, Y.H., Pattisapu, N., Issac, J. and Oyama, T. (2014). Identification and characterization of a suite of tumor targeting peptides for non-small cell lung cancer. *Scientific reports*, *4*.
186. Mehta, A. (2012). Ultraviolet-Visible (UV-Vis) Spectroscopy-Derivation of Beer-Lambert Law. *Analytical Chemistry. Available at pharmaxchange. info*.
187. Meyer, M., Essack, M., Kanyanda, S. and Rees, J. (2008). A low-cost flow cytometric assay for the detection and quantification of apoptosis using an anionic halogenated fluorescein dye. *Biotechniques*, *45*(3), 317-320.
188. Ming, T., Feng, W., Tang, Q., Wang, F., Sun, L., Wang, J. and Yan, C. (2009). Growth of tetrahexahedral gold nanocrystals with high-index facets. *Journal of the American Chemical Society*, *131*(45), 16350-16351.
189. Mishra, S., Murphy, L. C., Nyomba, B. G. and Murphy, L. J. (2005). Prohibitin: a potential target for new therapeutics. *Trends in molecular medicine*, *11*(4), 192-197.
190. Miura, M., Zhu, H., Rotello, R., Hartwieg, E. A. and Yuan, J. (1993). Induction of apoptosis in fibroblasts by IL-1β-converting enzyme, a mammalian homolog of the C. elegans cell death gene ced-3. *Cell*, *75*(4), 653-660.
191. Mooney, R., Roma, L., Zhao, D., Van Haute, D., Garcia, E., Kim, S.U., Annala, A.J., Aboody, K.S. and Berlin, J.M. (2014). Neural stem cell-mediated intratumoral delivery of gold nanorods improves photothermal therapy. *ACS nano*, *8*(12), 12450-12460.
192. Mozhi, A., Ahmad, I., Okeke, C. I., Li, C. and Liang, X. J. (2017). pH-sensitive polymeric micelles for the Co-delivery of proapoptotic peptide and anticancer drug for synergistic cancer therapy. *RSC Advances*, *7*(21), 12886-12896.
193. Muñoz-Pinedo, C. (2012). Sinaling pathway that regulate life and cell death. *Self and Nonself*, 124.
194. Murphy, C.J., Sau, T.K., Gole, A.M., Orendorff, C.J., Gao, J., Gou, L., Hunyadi, S.E. and Li, T. (2005). Anisotropic metal nanoparticles: synthesis, assembly, and optical applications. *The Journal of Physical Chemistry, 109* (29), 13857–13870.
195. Nakamura, T., Tamura, A., Murotani, H., Oishi, M., Jinji, Y., Matsuishi, K. and Nagasaki, Y. (2010). Large payloads of gold nanoparticles into the polyamine network core of stimuli-responsive PEGylated nanogels for selective and noninvasive cancer photothermal therapy. *Nanoscale*, *2*(5), 739-746.
196. Ni, W., Kou, X., Yang, Z. and Wang, J. (2008). Tailoring longitudinal surface plasmon wavelengths, scattering and absorption cross sections of gold nanorods. *Acs Nano*, *2*(4), 677-686.
197. Ni, X., Castanares, M., Mukherjee, A. and Lupold, S. E. (2011). Nucleic acid aptamers: clinical applications and promising new horizons. *Current medicinal chemistry*, *18*(27), 4206-4214.
198. Nichols, J.W. and Bae, Y.H. (2014). EPR: evidence and fallacy. *Journal of Controlled Release*, *190*, 451-464.
199. Nie, L., Wang, S., Wang, X., Rong, P., Ma, Y., Liu, G., Huang, P., Lu, G. and Chen, X. (2014). In vivo volumetric photoacoustic molecular angiography and therapeutic monitoring with targeted plasmonic nanostars. *small*, *10*(8), 1585-1593.

200. Niikura, K., Matsunaga, T., Suzuki, T., Kobayashi, S., Yamaguchi, H., Orba, Y., Kawaguchi, A., Hasegawa, H., Kajino, K., Ninomiya, T. and Ijiro, K. (2013). Gold nanoparticles as a vaccine platform: influence of size and shape on immunological responses in vitro and in vivo. *ACS nano*, *7*(5), 3926-3938.
201. Nijtmans, L.G., de Jong, L., Sanz, M.A., Coates, P.J., Berden, J.A., Back, J.W., Muijsers, A.O., van der Spek, H. and Grivell, L.A. (2000). Prohibitins act as a membrane-bound chaperone for the stabilization of mitochondrial proteins. *The EMBO journal*, *19*(11), 2444-2451.
202. Nikoobakht, B. and El-Sayed, M. A. (2001). Evidence for bilayer assembly of cationic surfactants on the surface of gold nanorods. *Langmuir*, *17*(20), 6368-6374.
203. Noonan, A.M., Bunch, K.P., Chen, J.Q., Herrmann, M.A., Lee, J.M., Kohn, E.C., O'sullivan, C.C., Jordan, E., Houston, N., Takebe, N. and Kinders, R.J. (2016). Pharmacodynamic markers and clinical results from the phase 2 study of the SMAC mimetic birinapant in women with relapsed platinum-resistant or-refractory epithelial ovarian cancer. *Cancer*, *122*(4), 588-597.
204. O'Dwyer, D., Ralton, L. D., O'Shea, A. and Murray, G. I. (2011). The proteomics of colorectal cancer: identification of a protein signature associated with prognosis. *PloS one*, *6*(11), e27718.
205. O'hurley, G., Sjöstedt, E., Rahman, A., Li, B., Kampf, C., Pontén, F., Gallagher, W.M. and Lindskog, C. (2014). Garbage in, garbage out: a critical evaluation of strategies used for validation of immunohistochemical biomarkers. *Molecular oncology*, *8*(4), 783-798.
206. Paino, I. M. M., Marangoni, V. S., de Oliveira, R. D. C. S., Antunes, L. M. G. and Zucolotto, V. (2012). Cyto and genotoxicity of gold nanoparticles in human hepatocellular carcinoma and peripheral blood mononuclear cells. *Toxicology letters*, *215*(2), 119-125.
207. Pal, D. and Nayak, A. K. (2010). Nanotechnology for targeted delivery in cancer therapeutics. *International Journal of Current Pharmaceutical Review and Research*, *1*(1), 1-7.
208. Palanca-Wessels, M.C., Booth, G.C., Convertine, A.J., Lundy, B.B., Berguig, G.Y., Press, M.F., Stayton, P.S. and Press, O.W. (2016). Antibody targeting facilitates effective intratumoral siRNA nanoparticle delivery to HER2-overexpressing cancer cells. *Oncotarget*, *7*(8), 9561.
209. Pan, Y., Neuss, S., Leifert, A., Fischler, M., Wen, F., Simon, U., Schmid, G., Brandau, W. and Jahnen-Dechent, W. (2007). Size-dependent cytotoxicity of gold nanoparticles. *Small*, *3*(11), 1941-1949.
210. Park, K., Biswas, S., Kanel, S., Nepal, D. and Vaia, R. A. (2014). Engineering the optical properties of gold nanorods: independent tuning of surface plasmon energy, extinction coefficient, and scattering cross section. *The Journal of Physical Chemistry C*, *118*(11), 5918-5926.
211. Park, D.H., Cho, J., Kwon, O.J., Yun, C.O. and Choy, J.H. (2016). Biodegradable inorganic nanovector: passive versus active tumor targeting in siRNA transportation. *Angewandte Chemie International Edition*, *55*(14), 4582-4586.
212. Parton, M., Bardia, A., Kummel, S., Estevez, L.G., Huang, C.S., Castan, J.C., Ruiz Borrego, M., Telli, M.L., Lluch, A., Lopez, R. and Beck, J.T. (2015). A phase II, open-label, neoadjuvant, randomized study of LCL161 with paclitaxel in patients with triple-negative breast cancer (TNBC). *Journal of Clinical Oncology, 33*(15), 1014.
213. Pattani, V. P., Shah, J., Atalis, A., Sharma, A. and Tunnell, J. W. (2015). Role of apoptosis and necrosis in cell death induced by nanoparticle-mediated photothermal therapy. *Journal of Nanoparticle Research*, *17*(1), 20.
214. Paul, A.M., Shi, Y., Acharya, D., Douglas, J.R., Cooley, A., Anderson, J.F., Huang, F. and Bai, F. (2014). Delivery of antiviral small interfering RNA with gold nanoparticles inhibits dengue virus infection in vitro. *Journal of General Virology*, *95*(8), 1712-1722.

215. Pavlin, M. and Bregar, V. B. (2012). Stability of nanoparticle suspensions in different biologically relevant media. *Digest Journal of Nanomaterials & Biostructures (DJNB)*, *7*(4).
216. Pérez-Juste, J., Pastoriza-Santos, I., Liz-Marzán, L. M. and Mulvaney, P. (2005). Gold nanorods: synthesis, characterization and applications. *Coordination Chemistry Reviews*, *249*(17), 1870-1901.
217. Peter, M. E. and Krammer, P. H. (2003). The CD95 (APO-1/Fas) DISC and beyond. *Cell death and differentiation*, *10*(1), 26.
218. Pitsillides, C. M., Joe, E. K., Wei, X., Anderson, R. R. and Lin, C. P. (2003). Selective cell targeting with light-absorbing microparticles and nanoparticles. *Biophysical journal*, *84*(6), 4023-4032.
219. Qi, L., Cölfen, H. and Antonietti, M. (2001). Synthesis and characterization of CdS nanoparticles stabilized by double-hydrophilic block copolymers. *Nano Letters*, *1*(2), 61-65.
220. Rao, C. N. R. and Biswas, K. (2009). Characterization of nanomaterials by physical methods. *Annual Review of Analytical Chemistry*, *2*, 435-462.
221. Ramos-Vara, J. A., Avery, P. R. and Avery, A. C. (2015). Advanced diagnostic techniques. *Canine and Feline Cytology-E-Book: A Color Atlas and Interpretation Guide*, 453.
222. Rastogi, S., Joshi, B., Dasgupta, P., Morris, M., Wright, K. and Chellappan, S. (2006). Prohibitin facilitates cellular senescence by recruiting specific corepressors to inhibit E2F target genes. *Molecular and cellular biology*, *26*(11), 4161-4171.
223. Rieger, H., Fredrich, T. and Welter, M. (2016). Physics of the tumor vasculature: Theory and experiment. *The European Physical Journal Plus*, *131*(2), 31.
224. Robertson, J.D., Rizzello, L., Avila-Olias, M., Gaitzsch, J., Contini, C., Magoń, M.S., Renshaw, S.A. and Battaglia, G. (2016). Purification of nanoparticles by size and shape. *Scientific reports*, *6*, 27494.
225. Richards, D.A., Maruani, A. and Chudasama, V. (2017). Antibody fragments as nanoparticle targeting ligands: a step in the right direction. *Chemical Science*, *8*(1), 63-77.
226. Riley, R. S. and Day, E. S. (2017). Gold nanoparticle-mediated photothermal therapy: applications and opportunities for multimodal cancer treatment. *Wiley Interdisciplinary Reviews: Nanomedicine and Nanobiotechnology*. *9*(4), e1449.
227. Rivankar, S. (2014). An overview of doxorubicin formulations in cancer therapy. *Journal of cancer research and therapeutics*, *10*(4), 853.
228. Roberts, A.W., Davids, M.S., Pagel, J.M., Kahl, B.S., Puvvada, S.D., Gerecitano, J.F., Kipps, T.J., Anderson, M.A., Brown, J.R., Gressick, L. and Wong, S. (2016). Targeting BCL2 with venetoclax in relapsed chronic lymphocytic leukemia. *New England Journal of Medicine*, *374*(4), 311-322.
229. Rodríguez-León, E., Iñiguez-Palomares, R., Navarro, R. E., Herrera-Urbina, R., Tánori, J., Iñiguez-Palomares, C. and Maldonado, A. (2013). Synthesis of silver nanoparticles using reducing agents obtained from natural sources (Rumex hymenosepalus extracts). *Nanoscale research letters*, *8*(1), 318.
230. Rønning, S. B., Andersen, P. V., Pedersen, M. E. and Hollung, K. (2017). Primary bovine skeletal muscle cells enters apoptosis rapidly via the intrinsic pathway when available oxygen is removed. *PloS one*, *12*(8), e0182928.
231. Ruan, S., Yuan, M., Zhang, L., Hu, G., Chen, J., Cun, X., Zhang, Q., Yang, Y., He, Q. and Gao, H. (2015). Tumor microenvironment sensitive doxorubicin delivery and release to glioma using angiopep-2 decorated gold nanoparticles. *Biomaterials*, *37*, 425-435.
232. Rudin, C.M., Hann, C.L., Garon, E.B., De Oliveira, M.R., Bonomi, P.D., Camidge, D.R., Chu, Q., Giaccone, G., Khaira, D., Ramalingam, S.S. and Ranson, M.R. (2012). Phase II study of

single-agent navitoclax (ABT-263) and biomarker correlates in patients with relapsed small cell lung cancer. *Clinical Cancer Research*, *18*(11), 3163-3169.
233. Rudin, C.M., Pietanza, M.C., Bauer, T.M., Ready, N., Morgensztern, D., Glisson, B.S., Byers, L.A., Johnson, M.L., Burris III, H.A., Robert, F. and Han, T.H. (2017). Rovalpituzumab tesirine, a DLL3-targeted antibody-drug conjugate, in recurrent small-cell lung cancer: a first-in-human, first-in-class, open-label, phase 1 study. *The Lancet Oncology*, *18*(1), 42-51.
234. Ruoslahti, E., Bhatia, S. N. and Sailor, M. J. (2010). Targeting of drugs and nanoparticles to tumors. *The Journal of cell biology*, *188*(6), 759-768.
235. Saelens, X., Festjens, N., Walle, L. V., Van Gurp, M., van Loo, G. and Vandenabeele, P. (2004). Toxic proteins released from mitochondria in cell death. *Oncogene*, *23*(16), 2861-2874.
236. Sanna, V., Pala, N. and Sechi, M. (2014). Targeted therapy using nanotechnology: focus on cancer. *International journal of nanomedicine*, *9*, 467.
237. Sato, T., Sakamoto, T., Takita, K. I., Saito, H., Okui, K. and Nakamura, Y. (1993). The human prohibitin (PHB) gene family and its somatic mutations in human tumors. *Genomics*, *17*(3), 762-764.
238. Sau, T. K. and Murphy, C. J. (2004). Seeded high yield synthesis of short Au nanorods in aqueous solution. *Langmuir*, *20*(15), 6414-6420.
239. Saunders, L.R., Bankovich, A.J., Anderson, W.C., Aujay, M.A., Bheddah, S., Black, K., Desai, R., Escarpe, P.A., Hampl, J., Laysang, A. and Liu, D. (2015). A DLL3-targeted antibody-drug conjugate eradicates high-grade pulmonary neuroendocrine tumor-initiating cells in vivo. *Science translational medicine*, *7*(302), 302ra136-302ra136.
240. Scaletti, F., Kim, C. S., Messori, L. and Rotello, V. M. (2014). Rapid purification of gold nanorods for biomedical applications. *MethodsX*, *1*, 118-123.
241. Sergeev, I. N. and Song, Q. (2014). High vitamin D and calcium intakes reduce diet-induced obesity in mice by increasing adipose tissue apoptosis. *Molecular nutrition and food research*, *58*(6), 1342-1348.
242. Shadidi, M. and Sioud, M. (2003). Selective targeting of cancer cells using synthetic peptides. *Drug Resistance Updates*, *6*(6), 363-371.
243. Sharma, A. and Qadri, A. (2004). Vi polysaccharide of *Salmonella typhi* targets the prohibitin family of molecules in intestinal epithelial cells and suppresses early inflammatory responses. *Proceedings of the National Academy of Sciences of the United States of America*, *101*(50), 17492-17497.
244. Shimizu, S., Eguchi, Y., Kamiike, W., Itoh, Y., Hasegawa, J.I., Yamabe, K., Otsuki, Y., Matsuda, H. and Tsujimoto, Y. (1996). Induction of apoptosis as well as necrosis by hypoxia and predominant prevention of apoptosis by Bcl-2 and Bcl-XL. *Cancer research*, *56*(9), 2161-2166.
245. Sibuyi, N.R.S, Thovhogi, N., Gabuza, K.B., Meyer, M.D., Drah, M., Onani, M.O., Skepu, A., Madiehe, A.M. and Meyer, M. (2017). Peptide-functionalised nanoparticles for the selective induction of apoptosis in target cells. *Nanomedicine*, *12*(14), 1631-1645.
246. Siddiqui, M. S. I., Parvin, R., Giasuddin, M., Chowdhury, S. M. Z. H., Islam, M. R. and Chowdhury, E. H. (2016). The effect of different concentrations of Dimethyl sulfoxide (DMSO) and glycerol as cryoprotectant in preserving Vero cells. *Bangladesh Veterinarian*, *33*(1), 1-7.
247. Siegel, R., Naishadham, D. and Jemal, A. (2013). Cancer statistics, 2013. *CA: a cancer journal for clinicians*, *63*(1), 11-30.
248. Sims, L. B., Curtis, L. T., Frieboes, H. B. and Steinbach-Rankins, J. M. (2016). Enhanced uptake and transport of PLGA-modified nanoparticles in cervical cancer. *Journal of nanobiotechnology*, *14*(1), 1.

249. Singh, S., D'Britto, V., Prabhune, A. A., Ramana, C. V., Dhawan, A. and Prasad, B. L. V. (2010). Cytotoxic and genotoxic assessment of glycolipid-reduced and-capped gold and silver nanoparticles. *New Journal of Chemistry*, *34*(2), 294-301.
250. Sioud, M. and Mobergslien, A. (2012). Selective killing of cancer cells by peptide-targeted delivery of an anti-microbial peptide. *Biochemical pharmacology*, *84*(9), 1123-1132.
251. Smith, C. A., Farrah, T. and Goodwin, R. G. (1994). The TNF receptor superfamily of cellular and viral proteins: activation, costimulation, and death. *Cell*, *76*(6), 959-962.
252. Smolkova, B., El Yamani, N., Collins, A. R., Gutleb, A. C. and Dusinska, M. (2015). Nanoparticles in food. Epigenetic changes induced by nanomaterials and possible impact on health. *Food and Chemical Toxicology*, *77*, 64-73.
253. Söderstjerna, E., Bauer, P., Cedervall, T., Abdshill, H., Johansson, F. and Johansson, U. E. (2014). Silver and gold nanoparticles exposure to in vitro cultured retina–studies on nanoparticle internalization, apoptosis, oxidative stress, glial-and microglial activity. *PLoS One*, *9*(8), e105359.
254. Soepenberg, O.,Dumez, H., Verweij, J., Semiond, D., deJonge, M.J.A., Eskens, F.A.L.M., ter Steeg, J., Selleslach, J., Assadourian, S., Sanderink, G., Sparreboom, A. and van Oosterom, A.T. (2005). Phase I and Pharmacokinetic Study of Oral Irinotecan Given Once Daily for 5 Days Every 3 Weeks in Combination With Capecitabine in Patients With Solid Tumors. *Journal of Clinical Oncology*, 23(4), 889-898.
255. Sosibo, N. M., Keter, F. K., Skepu, A., Tshikhudo, R. T. and Revaprasadu, N. (2015). Facile Attachment of TAT Peptide on Gold Monolayer Protected Clusters: Synthesis and Characterization. *Nanomaterials*, *5*(3), 1211-1222.
256. Souers, A.J., Leverson, J.D., Boghaert, E.R., Ackler, S.L., Catron, N.D., Chen, J., Dayton, B.D., Ding, H., Enschede, S.H., Fairbrother, W.J. and Huang, D.C. (2013). ABT-199, a potent and selective BCL-2 inhibitor, achieves antitumor activity while sparing platelets. *Nature medicine*, *19*(2), 202.
257. Sridhar, R., Lakshminarayanan, R., Madhaiyan, K., Barathi, V.A., Lim, K.H.C. and Ramakrishna, S. (2015). Electrosprayed nanoparticles and electrospun nanofibers based on natural materials: applications in tissue regeneration, drug delivery and pharmaceuticals. *Chemical Society Reviews*, *44*(3), 790-814.
258. Srinivasan, M., Rajabi, M. and Mousa, S. A. (2015). Multifunctional Nanomaterials and Their Applications in Drug Delivery and Cancer Therapy. *Nanomaterials*, *5*(4), 1690-1703.
259. Steichen, S. D., Caldorera-Moore, M. and Peppas, N. A. (2013). A review of current nanoparticle and targeting moieties for the delivery of cancer therapeutics. *European journal of pharmaceutical sciences*, *48*(3), 416-427.
260. Su, M., Mei, Y. and Sinha, S. (2013). Role of the crosstalk between autophagy and apoptosis in cancer. *Journal of oncology*, *2013*.
261. Sultana, S., Khan, M. R., Kumar, M., Kumar, S. and Ali, M. (2013). Nanoparticles-mediated drug delivery approaches for cancer targeting: a review. *Journal of drug targeting*, *21*(2), 107-125.
262. Sumer, B. and Gao, J. (2008). Theranostic nanomedicine for cancer. *Nanomedicine*, *3*(2), 137-140.
263. Tabernero, J., Shapiro, G.I., LoRusso, P.M., Cervantes, A., Schwartz, G.K., Weiss, G.J., Paz-Ares, L., Cho, D.C., Infante, J.R., Alsina, M. and Gounder, M.M. (2013). First-in-humans trial of an RNA interference therapeutic targeting VEGF and KSP in cancer patients with liver involvement. *Cancer discovery*, *3*(4), 406-417.
264. Talekar, M., Kendall, J., Denny, W. and Garg, S. (2011). Targeting of nanoparticles in cancer: drug delivery and diagnostics. *Anti-Cancer Drugs*, *22*(10), 949-962.

265. Tartaglia, L. A., Ayres, T. M., Wong, G. H. and Goeddel, D. V. (1993). A novel domain within the 55 kd TNF receptor signals cell death. *Cell*, *74*(5), 845-853.
266. Tebbe, M., Kuttner, C., Männel, M., Fery, A. and Chanana, M. (2015). Colloidally stable and surfactant-free protein-coated gold nanorods in biological media. *ACS applied materials and interfaces*, *7*(10), 5984-5991.
267. Teng, Y., Ren, M., Cheney, R., Sharma, S. and Cowell, J. K. (2010). Inactivation of the WASF3 gene in prostate cancer cells leads to suppression of tumorigenicity and metastases. *British journal of cancer*, *103*(7), 1066-1075.
268. Teng, Y., Bahassan, A., Dong, D., Hanold, L. E., Ren, X., Kennedy, E. J. and Cowell, J. K. (2016). Targeting the WASF3–CYFIP1 complex using stapled peptides suppresses cancer cell invasion. *Cancer research*, *76*(4), 965-973.
269. Thistlethwaite Jr, J.R., Cosimi, A.B., Delmonico, F.L., Rubin, R.H., Talkoff-Rubin, N., Nelson, P.W., Fang, L. and Russell, P.S. (1984). Evolving use of OKT3 monoclonal antibody for treatment of renal allograft rejection. *Transplantation*, *38*(6), 695-700.
270. Thovhogi, N., Sibuyi, N., Meyer, M., Onani, M. and Madiehe, A. (2015). Targeted delivery using peptide-functionalised gold nanoparticles to white adipose tissues of obese rats. *Journal of Nanoparticle Research*, *17*(2), 112.
271. Tomić, S., Đokić, J., Vasilijić, S., Ogrinc, N., Rudolf, R., Pelicon, P., Vučević, D., Milosavljević, P., Janković, S., Anžel, I. and Rajković, J. (2014). Size-dependent effects of gold nanoparticles uptake on maturation and antitumor functions of human dendritic cells in vitro. *PloS one*, *9*(5), e96584.
272. Tomuleasa, C., Soritau, O., Orza, A., Dudea, M., Petrushev, B., Mosteanu, O., Susman, S., Florea, A., Pall, E., Aldea, M. and Kacso, G. (2012). Gold nanoparticles conjugated with cisplatin/doxorubicin/capecitabine lower the chemoresistance of hepatocellular carcinoma-derived cancer cells. *Journal of Gastrointestinal and Liver Diseases*, *21*(2).
273. Torre, L. A., Bray, F., Siegel, R. L., Ferlay, J., Lortet-Tieulent, J. and Jemal, A. (2015). Global cancer statistics, 2012. *CA: a cancer journal for clinicians*, *65*(2), 87-108.
274. Truong, J., Yan, A. T., Cramarossa, G. and Chan, K. K. (2014). Chemotherapy-induced cardiotoxicity: detection, prevention, and management. *Canadian Journal of Cardiology*, *30*(8), 869-878.
275. Tsai, M. F., Chang, S. H. G., Cheng, F. Y., Shanmugam, V., Cheng, Y. S., Su, C. H. and Yeh, C. S. (2013). Au nanorod design as light-absorber in the first and second biological near-infrared windows for in vivo photothermal therapy. *ACS nano*, *7*(6), 5330-5342.
276. Uhlen, M., Zhang, C., Lee, S., Sjöstedt, E., Fagerberg, L., Bidkhori, G., Benfeitas, R., Arif, M., Liu, Z., Edfors, F. and Sanli, K. (2017). A pathology atlas of the human cancer transcriptome. *Science*, *357*(6352), eaan2507.
277. Vaish, V., Rana, C., Piplani, H., Vaiphei, K. and Sanyal, S. N. (2014). Sulindac and celecoxib regulate cell cycle progression by p53/p21 up regulation to induce apoptosis during initial stages of experimental colorectal cancer. *Cell biochemistry and biophysics*, *68*(2), 301-319.
278. Valko, M., Rhodes, C., Moncol, J., Izakovic, M. M. and Mazur, M. (2006). Free radicals, metals and antioxidants in oxidative stress-induced cancer. *Chemico-biological interactions*, *160*(1), 1-40.
279. Vergara, D. A., Villegas, C. A., Pavicic, M. F., Fritz, M. A. and Ehrenfeld, I. P. (2014). Evaluation in vitro of cytotoxicity of dentinal desensitizing on human gingival fibroblasts. *Journal of Oral Research*, *4*(1), 12-18.
280. Verhoven, B., Schlegel, R. and Williamson, P. (1995). Mechanisms of phosphatidylserine exposure, a phagocyte recognition signal, on apoptotic T lymphocytes. *Journal of Experimental Medicine*, *182*(5), 1597-1601.

281. von Maltzahn, G., Park, J. H., Agrawal, A., Bandaru, N. K., Das, S. K., Sailor, M. J. and Bhatia, S. N. (2009). Computationally guided photothermal tumor therapy using long-circulating gold nanorod antennas. *Cancer research*, *69*(9), 3892-3900.
282. Walczak, H. (2011). TNF and ubiquitin at the crossroads of gene activation, cell death, inflammation, and cancer. *Immunological reviews*, *244*(1), 9-28.
283. Wan, J., Wang, J. H., Liu, T., Xie, Z., Yu, X. F. and Li, W. (2015). Surface chemistry but not aspect ratio mediates the biological toxicity of gold nanorods in vitro and in vivo. *Scientific reports*, *5*, 11398.
284. Wang, S., Lawson, R., Ray, P. C. and Yu, H. (2011). Toxic effects of gold nanoparticles on Salmonella typhimurium bacteria. *Toxicology and industrial health*, *27*(6), 547-554.
285. Wang, Y. and Huang, L. (2012). Multifunctional theranostic nanoparticles for brain tumors. *Molecular Therapy*, *20*(1), 10-11.
286. Wang, G., Wang, X., Yu, H., Wei, S., Willias, N., Holmes, D.L., Halfmann, R., Naidoo, J., Wang, L., Li, L. and Chen, S. (2013). Small-molecule activation of the TRAIL receptor DR5 in human cancer cells. *Nature chemical biology*, *9*(2), 84-89.
287. Wang, Y.H., Chen, S.P., Liao, A.H., Yang, Y.C., Lee, C.R., Wu, C.H., Wu, P.C., Liu, T.M., Wang, C.R.C. and Li, P.C. (2014). Synergistic delivery of gold nanorods using multifunctional microbubbles for enhanced plasmonic photothermal therapy. *Scientific reports*, *4*.
288. Wang, L., Hu, Y., Li, W., Wang, F., Lu, X., Han, X., Lv, J. and Chen, J. (2016). Identification of a peptide specifically targeting ovarian cancer by the screening of a phage display peptide library. *Oncology letters*, *11*(6), 4022-4026.
289. Ward, C. J., Tronndorf, R., Eustes, A. S., Auad, M. L. and Davis, E. W. (2014). Seed-Mediated growth of gold nanorods: limits of length to diameter ratio control. *Journal of Nanomaterials*, *2014*, 47.
290. Weissleder, R. (2001). A clearer vision for in vivo imaging. *Nature biotechnology*, *19*(4), 316-316.
291. Wiley, B., Sun, Y. and Xia, Y. (2007). Synthesis of silver nanostructures with controlled shapes and properties. *Accounts of Chemical Research*, *40*(10), 1067-1076.
292. Wicki, A., Witzigmann, D., Balasubramanian, V. and Huwyler, J. (2015). Nanomedicine in cancer therapy: challenges, opportunities, and clinical applications. *Journal of Controlled Release*, *200*, 138-157.
293. Wolff, A.C., Hammond, M.E.H., Hicks, D.G., Dowsett, M., McShane, L.M., Allison, K.H., Allred, D.C., Bartlett, J.M., Bilous, M., Fitzgibbons, P. and Hanna, W. (2013). Recommendations for human epidermal growth factor receptor 2 testing in breast cancer: American Society of Clinical Oncology/College of American Pathologists clinical practice guideline update. *Journal of clinical oncology*, *31*(31), 3997-4013.
294. World Health Organization. Cancer, Fact Sheet #297 2015. Available from: http://www.who.int/mediacentre/factsheets/fs297/en/ [last accessed 7 Apr 2015].
295. Wu, C. H., Liu, I. J., Lu, R. M. and Wu, H. C. (2016). Advancement and applications of peptide phage display technology in biomedical science. *Journal of biomedical science*, *23*(1), 8.
296. Xiang, D., Zheng, C., Zhou, S.F., Qiao, S., Tran, P.H.L., Pu, C., Li, Y., Kong, L., Kouzani, A.Z., Lin, J. and Liu, K. (2015). Superior performance of aptamer in tumor penetration over antibody: implication of aptamer-based theranostics in solid tumors. *Theranostics*, *5*(10), 1083.
297. Xiong, B., Cheng, J., Qiao, Y., Zhou, R., He, Y. and Yeung, E. S. (2011). Separation of nanorods by density gradient centrifugation. *Journal of Chromatography A*, *1218*(25), 3823-3829.
298. Xu, X., Smith, S., Urban, J. and Cui, Z. (2006). An in line non-invasive optical system to monitor pH in cell and tissue culture. *Medical engineering and physics*, *28*(5), 468-47.

299. Yah, C. S. (2013). The toxicity of Gold Nanoparticles in relation to their physiochemical properties. *Biomedical Research*, *24*(3).
300. Yang, J., Wu, J. C., Wu, Y. C., Wang, J. K. and Chen, C. C. (2005). Organic solvent dependence of plasma resonance of gold nanorods: A simple relationship. *Chemical physics letters*, *416*(4), 215-219.
301. Yang, C., Wang, H., Zhang, B., Chen, Y., Zhang, Y., Sun, X., Xiao, G., Nan, K., Ren, H. and Qin, S. (2016). LCL161 increases paclitaxel-induced apoptosis by degrading cIAP1 and cIAP2 in NSCLC. *Journal of Experimental and Clinical Cancer Research*, *35*(1), 158.
302. Yecies, D., Carlson, N. E., Deng, J. and Letai, A. (2010). Acquired resistance to ABT-737 in lymphoma cells that up-regulate MCL-1 and BFL-1. *Blood*, *115*(16), 3304-3313.
303. Yen, H. J., Hsu, S. H. and Tsai, C. L. (2009). Cytotoxicity and immunological response of gold and silver nanoparticles of different sizes. *Small*, *5*(13), 1553-1561.
304. Yu, M. K., Park, J. and Jon, S. (2012). Targeting strategies for multifunctional nanoparticles in cancer imaging and therapy. *Theranostics*, *2*(1), 3.
305. Yuan, J., Shaham, S., Ledoux, S., Ellis, H. M. and Horvitz, H. R. (1993). The C. elegans cell death gene ced-3 encodes a protein similar to mammalian interleukin-1β-converting enzyme. *Cell*, *75*(4), 641-652.
306. Zhang, Y., Hong, H. and Cai, W. (2011). Tumor-targeted drug delivery with aptamers. *Current medicinal chemistry*, *18*(27), 4185-4194.
307. Zhang, L., Yin, G., Yan, D., Wei, Y., Ma, C., Huang, Z., Liao, X., Yao, Y., Chen, X. and Hao, B. (2011). In vitro screening of ovarian tumor specific peptides from a phage display peptide library. *Biotechnology letters*, *33*(9), 1729-1735.
308. Zhang, Z., Wang, J., Nie, X., Wen, T., Ji, Y., Wu, X., Zhao, Y. and Chen, C. (2014). Near infrared laser-induced targeted cancer therapy using thermoresponsive polymer encapsulated gold nanorods. *Journal of the American Chemical Society*, *136*(20), 7317-7326.
309. Zharov, V. P., Galitovskaya, E. and Viegas, M. (2004, July). Photothermal guidance for selective photothermolysis with nanoparticles. In *Laser Interaction with Tissue and Cells Xv* (Vol. 5319, 291-301). International Society for Optics and Photonics.
310. Zharov, V. P., Galitovskaya, E. N., Johnson, C. and Kelly, T. (2005). Synergistic enhancement of selective nanophotothermolysis with gold nanoclusters: potential for cancer therapy. *Lasers in surgery and medicine*, *37*(3), 219-226.
311. Zheng, H., Tumin, D. and Qian, Z. (2013). Obesity and mortality risk: new findings from body mass index trajectories. *American journal of epidemiology*, *178*(11), 1591-1599.
312. Zhou, G., Wilson, G., Hebbard, L., Duan, W., Liddle, C., George, J. and Qiao, L. (2016). Aptamers: A promising chemical antibody for cancer therapy. *Oncotarget*, *7*(12), 13446.